1977

High-pressure Dielectric Properties Of Perovskite Ferroelectrics Related To The Earth's Mantle

Garry William Timco

NOTICE

The quality of this microfiche is heavily dependent upon the quality of the original thesis submitted for microfilming. Every effort has been made to ensure the highest quality of reproduction possible.

If pages are missing, contact the university which granted the degree.

Some pages may have indistinct print especially if the original pages were typed with a poor typewriter ribbon or if the university sent us a poor photocopy.

Previously copyrighted materials (journal articles, published tests, etc.) are not filmed.

Reproduction in full or in part of this film is governed by the Canadian Copyright Act, R.S.C. 1970, c. C-30. Please read the authorization forms which accompany this thesis.

THIS DISSERTATION
HAS BEEN MICROFILMED
EXACTLY AS RECEIVED

AVIS

La qualité de cette microfiche dépend grandement de la qualité de la thèse soumise au microfilmage. Nous avons tout fait pour assurer une qualité supérieure de reproduction.

S'il manque des pages, veuillez communiquer avec l'université qui a conféré le grade.

La qualité d'impression de certaines pages peut laisser à désirer, surtout si les pages originales ont été dactylographiées à l'aide d'un ruban usé ou si l'université nous a fait parvenir une photocopie de mauvaise qualité.

Les documents qui font déjà l'objet d'un droit d'auteur (articles de revue, examens publiés, etc.) ne sont pas microfilmés.

La reproduction, même partielle, de ce microfilm est soumise à la Loi canadienne sur le droit d'auteur, SRC 1970, c. C-30. Veuillez prendre connaissance des formules d'autorisation qui accompagnent cette thèse.

LA THÈSE A ÉTÉ
MICROFILMÉE TELLE QUE
NOUS L'AVONS REÇUE

HIGH PRESSURE DIELECTRIC PROPERTIES OF PEROVSKITE FERROELECTRICS RELATED TO THE EARTH'S MANTLE

by

Garry William John Timco
Department of Geophysics

Submitted in partial fulfillment
of the requirements for the degree of
Doctor of Philosophy

Faculty of Graduate Studies
The University of Western Ontario
London, Ontario
February, 1977

ABSTRACT

In light of the compelling evidence that minerals with the orthorhombic perovskite structure form a major part of the earth's mantle, one may anticipate that, for some of them, transitions into ferroelectric states may occur. These ferroelectric phases, however, would have to comply with high pressure conditions of constraint with deviatoric stresses and strains. These conditions are met in high pressure experiments when a solid-medium, such as pyrophyllite is used for the transmission of pressure. The present high pressure experiments were designed to deal, in particular, with the following two important questions: Firstly, would ferroelectric phenomena persist in the case of a perovskite crystal occurring as an inhomogeneous inclusion in a solid dielectric matrix subjected to pressure; that is, under the conditions that ferroelectrics would be likely to occur if they formed part of the earth's interior? Secondly, what are the effects of pressure on the properties of a polycrystalline aggregate of a ferroelectric material?

To answer these questions, two independent measuring techniques were designed and performed on several perovskite structured materials under high pressure constraint - single crystal and polycrystalline $BaTiO_3$, polycrystalline $Pb(Zr,Ti)O_3$ ceramics, and natural (non-ferroelectric) single crystals of $CaTiO_3$: (a) Determination of the ferroelectric-paraelectric transition temperatures, dielectric constant values and dissipation factors by means of a GR 1620 capacitance measuring assembly, and (b) hysteresis loop observations using a Sawyer-Tower circuit.

In answer to the first question, both types of experiments show that ferroelectric hysteresis in perovskites is not only possible, but remains extremely well behaved under conditions of deviatoric stress and strain. Moreover, both the experiments and the theoretical treatment of the problem indicate that existing ferroelectric states, occurring as elastic and dielectric inhomogeneities, can persist to much higher pressuresthan those expected for normal pressure-temperature conditions.

With regard to the second question, the high pressure experiments on polycrystalline $BaTiO_3$ and $Pb(Zr,Ti)O_3$ ceramics have detailed their behaviour in the pressure range to 55 kbar. Initial application of pressure results in a large decrease in the dielectric constant. Four of the five ceramic compounds investigated exhibit a linear decrease in the transition temperature with pressure ($dT^*/dp \sim -4.4^oC$/kbar, $BaTiO_3$; -4.6^oC/kbar, PZT-4; -4.2^oC/kbar, PZT-5H; -5.6^oC/kbar, PZT-8). In addition, graphs of the dielectric constant versus temperature under isobaric conditions indicate that, with increasing values of pressure, the dielectric peak height decreases and the peak width increases. For one ceramic (PZT-5A), the transition temperature decreases non-linearly with pressure and exhibits a point of inflection at ~30 kbar. The dielectric constant-temperature peak is extremely broad in this pressure region and with increasing pressure, 'sharpens' to a pressure independent shape above ~40 kbar. These results are discussed in terms of 90^o [redacted] in reorientation and the residual local microstresses in ferroelectric ceramic compacts.

ACKNOWLEDGEMENTS

I would like to extend my sincere thanks and appreciation to the following persons who helped me greatly throughout the course of this work:

Dr. H.H. Schloessin, my chief supervisor, for his excellent supervision and interesting ideas.

Connie Timco, my wife, for her unending patience, kindness and help at all times.

Drs. R.K. Chan and Z. Dvorak, for several interesting and informative discussions.

Drs. C.M. Carmichael and R. Clarke, for reading and commenting on my thesis.

My colleagues and fellow graduate students, for help too varied to mention.

Ms. Cathy Hawthorne, for her excellent typing of this thesis, as well as several manuscripts along the way.

Y. Ling, J. Forth, B. Price and J. Brunet, for technical assistance.

Mr. and Mrs. S.J. Timco, my parents, for their continual encouragement and help in so many ways.

I would also like to acknowledge with thanks financial assistance from the National Research Council of Canada.

TABLE OF CONTENTS

LIST OF FIGURES

LIST OF TABLES

LIST OF PHOTOGRAPHIC PLATES

LIST OF SYMBOLS

Symbol	
α	model parameter in distribution model
A	cation in perovskite lattice
A	area of crystal (or ceramic) face
B	cation in perovskite lattice
BT	barium titanate ($BaTiO_3$)
C	capacitance of sample
C_e	edge capacitance
C_x	measured capacitance
CT	calcium titanate ($CaTiO_3$)
d	diameter of crystal (or ceramic) face
D	dissipation factor of sample
D_x	measured dissipation factor
E	electric field
E_c	coercive field
ξ	energy (Chapter 3)
f	frequency
FE	ferroelectric(s); ferroelectricity
G	conductance
G_e	edge conductance
G_x	measured conductance
GR	General Radio
k	dielectric constant
k_3^f	free dielectric constant (Table 6T-1)

Symbol	
k_3^{cl}	clamped dielectric constant (Table 6T-1)
k_{max}	maximum dielectric constant
κ_p	planar coupling coefficient (Table 6T-1)
O	oxygen (anion) in perovskite lattice
p	pressure
P	polarization
P_r	remanent polarization
P_s	spontaneous polarization
PE	paraelectric (nonpolar) phase
PZT	Vernitron lead zirconate-titanate ceramic
ρ	density (Table 6T-1)
t	thickness of sample plate
$\tan\delta$	loss tangent or dissipation factor
T	temperature
T*	macroscopic transition temperature for ceramics
T_c	Curie temperature
T_c^o	Curie temperature at room pressure
x	mechanical strain
X	mechanical stress

CHAPTER I

GENERAL INTRODUCTION

With the growing list of reported ultra high pressure - temperature structural transformations to orthorhombic ABO_3 phases in several of the alleged mantle minerals, it appears that perovskites may form a major part of the earth's mantle (Bassett, 1976; Liu, 1976). Since a large number of solids which possess this structure are known to exhibit ferroelectric (FE) behaviour (Jona and Shirane, 1962), this raises the important question of whether any of the perovskite structured minerals in the earth's interior exist in ferroelectric states (Timco, 1974, 1975; Schloessin and Timco, 1977). This presents a new and rather exciting idea for solid-earth geophysicists. If present, their existence could be of considerable consequence since many of the physical properties of ferroelectrics, including their dielectric, elastic and piezoelectric properties are characterized by anomalous behaviour (Kanzig, 1957). This behaviour comes about as a result of the competition between the electronic polarizability and ionic dipole polarizability which causes a permanent asymmetrical shift in the ionic positions and brings about spontaneous dielectric polarization (the $4\pi/3$ catastrophe) (von Hippel, 1954). Consequently, FE may well play a role in shaping the physical behaviour and properties of the earth's mantle.

A first step in understanding the behaviour of a FE material in the earth's interior would be to study the general behaviour of perovskite ferroelectrics under high pressure - high temperature conditions. This

has been done for pressure conditions generated with fluid-media high pressure apparatus for several members of the perovskite family (see e.g. Samara, 1969, 1970). Certainly experiments of this type are extremely valuable since they elucidate ferroelectric behaviour in a straightforward, tractable experimental situation. That is, in these experiments the applied pressure is hydrostatic, since the fluid-media can readily flow to compensate for any deviatoric or shearing stresses present. However, for FE phases to exist in planetary interiors, they would have to comply with quasi-hydrostatic stress conditions with constraint by deviatoric stresses and strains. Exactly this type of environment is met in high pressure experiments when a solid medium is used for the transmission of pressure (Lees, 1966). Thus, in the case of solid-media, the FE material forms an elastically and dielectrically inhomogeneous inclusion (transforming inclusion) (Eshelby, 1956, 1957, 1961) in a non-ferroelectric matrix such that the ferroelectric transition occurring in the inclusion is accompanied by self-stressing. This distinction between the high pressure environments generated by the two types of pressure transmitting media is especially important for ferroelectric substances. This is so since FE properties are known to be extremely sensitive to the physical state of the crystal, i.e. whether or not it is free to develop its full strain upon transformation. A solid-medium provides an environment in which the applied stress is not truly hydrostatic since both deviatoric and shearing stresses may be present. Moreover, the solid provides a larger resistance to transformational strains and thereby 'physically constrains' the sample. It would seem that these are the very conditions which one would try to avoid if one is primarily concerned

with the analysis of the changes in dielectric properties with hydrostatic pressure. However, the case of a FE inclusion in a solid matrix subjected to high external stresses would seem to approximate closely to the state of stress and strain which would be encountered by a ferroelectric material in the earth's interior. Thus the prime objective of the present work was to investigate in detail the general high pressure behaviour of several perovskite structured materials constrained by solid media, with a particular emphasis on those which are ferroelectric. Two independent techniques were designed and applied to study FE properties under these pressure conditions: (a) Determination of the transition temperatures, dielectric constant values and dissipation factors by means of a (General Radio 1620 A) capacitance measuring assembly, and (b) hysteresis loop observations using a Sawyer-Tower (1930) circuit, which allowed the determination of the transition temperature as well as semi-quantitative information about polarization and coercivity. Since the reported transformations in the alleged mantle minerals to perovskite structures occur at pressures well above those available in solid-media high pressure devices, these materials could not be studied directly. Consequently, several isomorphic materials in the tetragonal modification were chosen for study instead. Those studied include barium titanate (both in single crystal and polycrystalline form), several ceramics of the lead zirconate-titanate $Pb(Zr,Ti)O_3$ system, and natural crystals of calcium titanate. A particular emphasis was placed on the polycrystalline (ceramic) form since FE materials, if present in the earth's interior, would most likely occur in polycrystalline assemblages. Since a solid-medium was employed for the transmission of pressure, the novel

approach of the inhomogeneous (transforming) inclusion in a solid matrix was chosen for the theoretical treatment of the problem.

CHAPTER II

PEROVSKITES AND FERROELECTRICITY

2.1 The Perovskite Structure

There are a large number of compounds which are members of the perovskite family - a term which is meant to include the ideal perovskite structure, itself, as well as the other structures which can be derived from it by small distortions and displacements of atoms (Megaw, 1957, 1973). The structure derives its name from the mineral perovskite (calcium titanate, $CaTiO_3$) in spite of the fact that $CaTiO_3$ does not actually have the ideal perovskite structure.

The perovskite structure is adopted by many oxide compounds which have the general formula ABO_3 where the valency of the A ion may range from 1+ to 3+, and that of the B ion from 3+ to 5+. This structure can be described by a cubic unit cell which contains a B atom at the centre of the cube, A atoms at the corners and O atoms at the centres of the cell faces (Figure 2.1). The A atoms are surrounded by twelve O atoms, whereas the B atoms are surrounded by six O atoms which are arranged at the corners of a regular octahedron. These octahedra are linked by their corners into a three-dimensional framework enclosing large holes which are occupied by the A atoms. Since the framework of linked BO_6 octahedra determine the dimensions of the structure, this places restrictions on the size of the A-cation which will fit into the hole between the octahedra. Ideally, the relationship between the radii should be

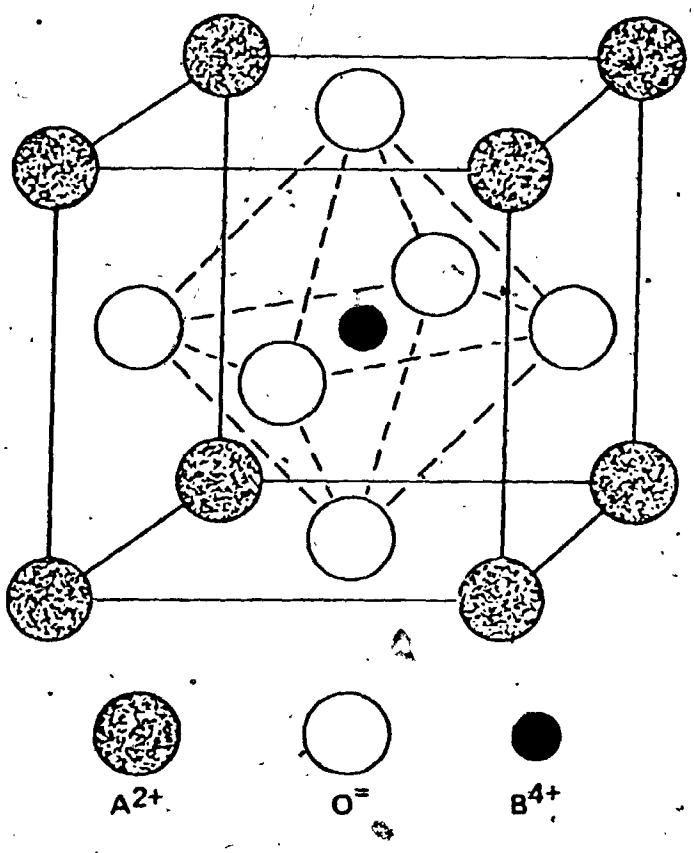

Figure 2.1 : The ideal perovskite structure ABO_3.

$$R_A + R_O = \sqrt{2}\ (R_B + R_O) \qquad (2.1)$$

However, since atomic radii vary with the state of ionization, a certain tolerance of fit may be expected such that

$$R_A + R_O = t\sqrt{2}\ (R_B + R_O) \qquad (2.2)$$

where t is a tolerance factor, usually between .85 and 1.05 for perovskites. This expression, the Goldschmidt Relationship (Megaw, 1957) provides a qualitative criterion for the existence of perovskites.

From symmetry considerations of the ideal cell, it is evident that a material with this centro-symmetric cubic structure cannot possess piezoelectric or ferroelectric behaviour. However, for several members of the perovskite family, the cubic phase transforms to either a tetragonal or orthorhombic phase when cooled through its characteristic transition temperature. For many perovskites, this transition to one of these lower symmetry states marks the onset of ferroelectric behaviour. Thus, a necessary but not sufficient condition for FE behaviour to be possible is that the crystal has either tetragonal or lower symmetry. Consequently, if the mantle perovskites exist in the cubic modification, ferroelectric behaviour is precluded. However, the fact that according to ultra-high pressure experimental results (Bassett, 1976; Liu, 1976) the orthorhombic phase of the perovskite structure is predominant keeps open the possibility of ferroelectric behaviour in the mantle.

2.2 The Earth's Mantle: Evidence for Perovskite Structures

In recent years, seismological investigations of the earth's interior have provided valuable information on the physical nature of the mantle. In general, these investigations have indicated that the earth's mantle may be subdivided into three well-defined regions: (1) the upper mantle, which extends from below the crust to a depth of ~400 km. This region is characterized by regional variations in velocity distributions and a low velocity zone; (2) the transition zone between 400 and 1,000 km which is characterized by high velocity gradients, particularly in two depth intervals of 400 and 650 km; and (3) the lower mantle, which extends from 1,000 to 2,900 km, and is characterized by moderate and relatively uniform increases in velocity with depth. The region from 400 to 2,900 km is sometimes also referred to as the deep mantle (Ringwood, 1975). It is generally believed that under the pressure and temperature conditions which exist in the earth's mantle between 400 to 900 km, the major minerals of olivine $(Mg,Fe)_2SiO_4$ and pyroxene $(Mg,Fe)SiO_3$ composition become unstable and transform into new assemblages of close-packed phases. These solid-solid transformations and the resulting changes in the elastic properties and densities of the materials could then explain the observed changes in seismic properties in this region (Ringwood, 1975).

The methods and techniques for investigating and/or determining the possible phase transformations in the mantle may be divided into two groups - indirect methods and direct methods (Ringwood, 1975):

The indirect methods are those which allow one to define certain physical and thermodynamical conditions under which structure transfor-

mations become possible. For example, in the case of high pressure polymorphs of existing ionic compounds, these should satisfy the conditions that the high pressure polymorph is denser than the low pressure phase, and that the radius ratios of compressed 'effective' radii of the constituent ions are consistent with the geometrical packing arrangement of the new structure. Using this approach, for example, Ringwood (1962) first predicted that enstatite $MgSiO_3$ would transform to a perovskite structure under the pressure-temperature conditions corresponding to those of the lower mantle.

The direct methods of investigation are those concerned with high pressure-temperature experimental studies on the physical properties of solid materials. These may be either dynamic (i.e. short duration shock wave) or static in nature. In general, the static high pressure studies in this area may be subdivided into two distinct pressure ranges. In the pressure region below ~100 kbar, several types of high pressure devices have been widely used to study the physical properties of earth materials, including the piston-cylinder apparatus, belt apparatus and multi-anvil apparatus (Hall, 1964). Since the maximum pressure attainable with these high pressure devices corresponds to a depth of ~300 km, these types of studies are somewhat limited in the sense that the presses are incapable of producing the pressures which correspond to those of the transition zone. Nevertheless, by studying isomorphs of the alleged mantle minerals which have lower solid-solid transformation pressures (e.g. germanates as models for silicates), these types of studies have yielded valuable information on the possible phase transitions and physical properties of the mantle. For the pressure range up to ~300 kbar, a

diamond anvil high pressure apparatus with pulsed laser heating is employed. This method allows the direct determination of high pressure structures from the x-ray diffraction pattern of a powdered sample which is compressed between two diamond anvils and heated to temperatures up to ~2,000°C. Experiments with this technique have provided firm evidence that many of the major and most abundant forms of accepted mantle minerals transform to an ABO_3 perovskite structure under ultra high pressure-temperature conditions.

Following Ringwood's (1962) prediction that $MgSiO_3$ might transform into a perovskite structure in the deep mantle, Ringwood and Major (1967), in their experimental studies on the germanium isomorph of calcium rich solid solutions observed that $CaGeO_3$ transformed into a perovskite structure at ~100 kbar and 1000°C. Subsequently, Ringwood and Major (1971) found that the perovskite-type solid solutions were formed in silicates in the system $CaTiO_3$ - $CaSiO_3$ for pressures greater than ~100 kbar. This work demonstrated the important finding that octahedral Si^{4+} can enter the B site of a perovskite lattice. According to Ming and Bassett (1974), the ferromagnesium olivines and pyroxenes dissociate into their constituent oxides at pressures of 150-250 kbar and temperatures of 1000-2000°C. However, they recombine to form orthorhombic perovskite structures at higher pressures with temperatures of 1000-2000°C (Bassett, 1976). From studies of phase transformations of pyrope garnet ($Mg_3Al_2Si_3O_{12}$), the perovskite structure of pure $MgSiO_3$ was eventually obtained by Liu (1974) under static pressure and temperature conditions corresponding to those of the lower mantle (p>300 kbar, T>800°C). Liu has also shown that both forsterite Mg_2SiO_4 and enstatite

$MgSiO_3$ assume as post-oxide phases the orthorhombic perovskite structure of $MgSiO_3$ with a certain admixture of MgO (Liu, 1975a). In addition, Liu (1975b) has found that ilmenite $(Fe,Mg)TiO_3$ transforms into a perovskite structure at 140 kbar and 1400°C. The smallest specific volume recorded so far for a perovskite structure was observed by Reid and Ringwood (1975) for $ScAlO_3$, which is representative of the orthorhombic perovskite modification. Finally, Liu (1976) has found that ferromagnesium silicate olivines $(Mg,Fe)_2SiO_4$, pyroxenes $(Mg,Fe)SiO_3$ and garnets $(Mg,Fe)_3Al_2Si_3O_{12}$ with $Mg/(Mg+Fe) \gtrsim .3$ when compressed to pressures above 250 kbar and heated to temperatures of 1000°C, transform to high pressure phases having the orthorhombic perovskite structure.

The results of the direct static high pressure experiments as well as those from the indirect methods and shock wave experiments have been used by Ringwood (1975) to predict the possible mineralogy with depth for a predominantly olivine-pyroxene composition mantle (Figure 2.2). From this figure it is evident that perovskite type structures may dominate in a major part of the earth's lower mantle.

2.3 Ferroelectricity in Perovskite Structures

Although there are many different mechanisms that will lead to a large spontaneous or co-operative dielectric polarization, one predominant mechanism is that found in perovskite structured materials. For these materials, a net permanent electric moment of the octahedron can result by a unilateral displacement of the positive B ion against its negative oxygen surrounding. This leads to a high dielectric constant in most crystals which contain the TiO_6 constellation. With proper

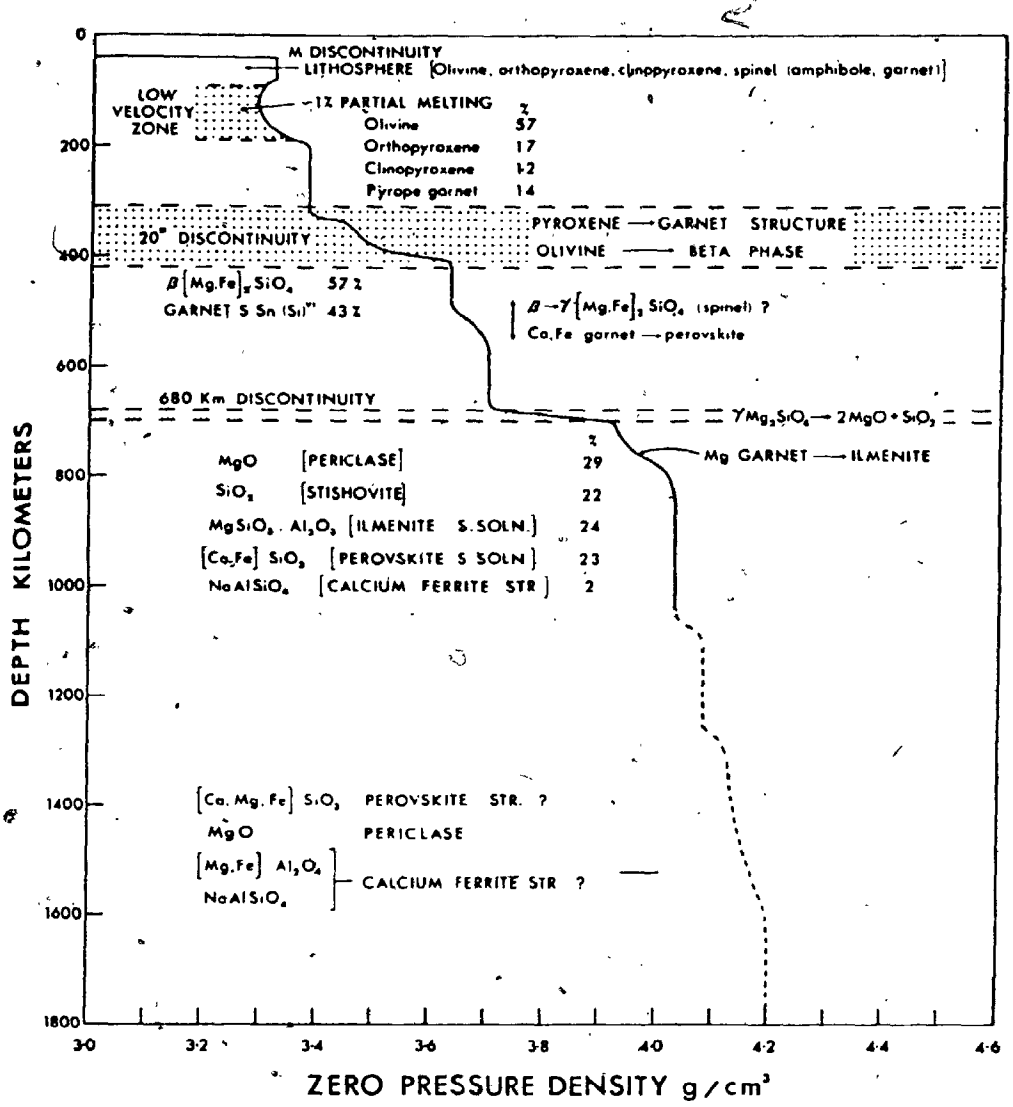

Figure 2.2 : Possible mineral assemblages and corresponding zero-pressure densities for a model mantle (after Ringwood, 1975).

coupling of the moments as described below, FE behaviour is possible.

In the cubic phase above the Curie temperature, the B ions have their equilibrium position in the centre of the octahedra, and the permanent dipole moments cancel one another. However, strong fluctuations of the net moments around the zero value occur by thermal vibrations of the ions about their equilibrium positions. Since the oxygen octahedra and their moments are coupled by common oxygen ions, any displacement unbalances two of the neighbouring B ions. This tends to push all of the B ions in the same direction (Figure 2.3). If the B_1 ion moves towards the O_1 ion, the dipole moment $B_1 - O_1$ becomes stronger and the moment $B_1 - O_2$ becomes weaker. Consequently, O_1 moves towards B_1 and O_2 away from it, with the result that B_2 and B_3 follow the movement of B_1. The side ions B_4 and B_5, as well as their counterparts above and below the plane of figure follow suit, since the coupled oxygen ions O_3 and O_4 tend to move downwards, repelled by O_1. This forms a type of positive feedback coupling. At the Curie temperature the tendency to bring the vibrations of neighbouring ions into ordered phase relations prevail against the random agitation, and the equilibrium position of the critical ions shift to one side. Thus, a polar axis is created. This description originally put forward by von Hippel (1954) indicates that the perovskite structure of adjacent oxygen octahedra is particularly favourable for the existence of ferroelectric behaviour.

In 1960, a mathematical theory which successfully explains the FE behaviour in perovskites was proposed by Cochran (1960, 1961). Essentially the theory is based on the argument that for a crystal which is wholly or partly ionic, the lattice vibrations are accompanied by

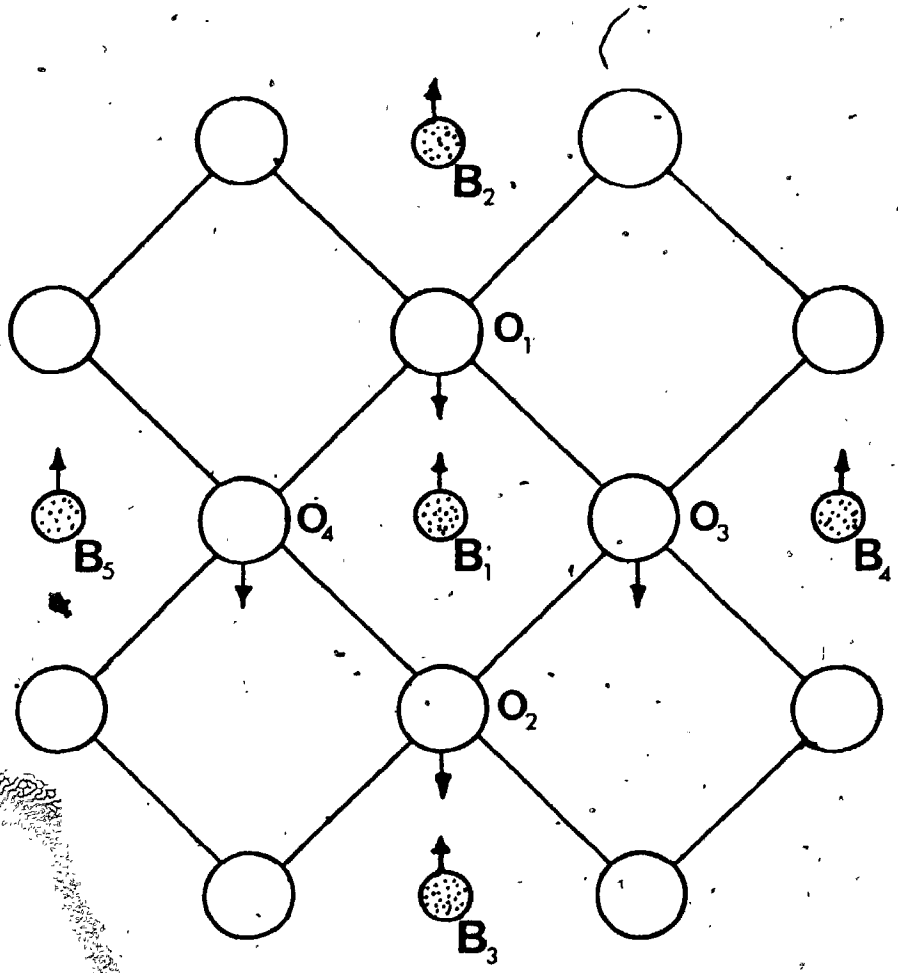

Figure 2.3 : Schematic representation of the feedback coupling and displacement of ions for ferroelectric behaviour in perovskites (after von Hippel, 1954).

polarization oscillations of equal frequency. These oscillations create a local field which interacts with the ions through long range Coulomb forces. If, for one particular mode of vibration, these long range forces have the same magnitude but differ in sign from the short range repulsive forces, the total restoring force is very small and the crystal becomes unstable for this mode (the "soft-mode"). From the authors viewpoint, the best description of this theory was presented by Professor A. von Hippel in his opening remarks to the Second International Conference on Ferroelectricity held in Japan in 1969. Professor von Hippel (1970) states: "Cochran has given the long-range force concept new respectability by the assumption that a transversal optical mode ω_T softens and moves at the Curie temperature toward zero:

$$\frac{\omega_T^2}{\omega_0^2} = \gamma(T - T_C) \qquad (2.3)$$

and such an effect has in principle been observed. Cochran's postulate is based on an ionic diatomic lattice model (introduced by Born and Huang) and its various refinements, visualizing the following physical situation: An optical phonon mode - of wavelength long in comparison to the atomic distances - causes a displacement of a positive versus negative partial Bravais lattice and thus an atomic polarization proportional to that displacement. This atomic polarization produces an instantaneous electronic polarization. Atomic and electronic polarization, acting in feedback according to

$$E' = E + 4\pi w P \qquad (2.4)$$

(where E' is the local field, E is the applied field, $w(=\frac{1}{3})$ is the Lorentz factor, and P is the polarization), increase the polarization and thus lower the original mechanical resonance frequency ω_0 to ω_T. Instead of the applied field, a long-range self-created internal field has been invoked as the cause of the transition. And that statement is couched frequently in such a formidable mathematical language that no experimentalist dares to disagree".

2.4 Basic Properties of Ferroelectrics

When an external electric field, E, is applied across a dielectric crystal, the crystal becomes electrically polarized. The polarization values which are measured for normal dielectrics upon application of the field E are in most cases quite small. Therefore, the effects that this polarization has on the physical properties of the crystal are usually inconsequential. There are however, a rather large but limited number of crystalline dielectrics which exhibit polarization values which are orders of magnitude larger than those observed in most crystals. In fact, a normal dielectric (such as the alkali halides) could theoretically obtain polarization values equivalent to that found in these crystals only with electric fields on the order of 10^5 to 10^8 V/cm (Jona and Shirane, 1962). Those materials which exhibit such large polarization effects are called ferroelectrics and, compared to normal dielectrics, they have several important and distinguishing features. In this section, the basic properties of FE materials will be briefly summarized. Several excellent texts on the subject (Kanzig, 1957; Megaw, 1957, Jona and Shirane, 1962; Burfoot, 1967) can be consulted for more detail.

The name ferroelectricity came about from the formal similarity of the ferroelectric effect with that of ferromagnetism. This similarity, however, is purely phenomenological. Just as in the case of a ferromagnetic material which exhibits a spontaneous magnetization and hysteresis effects between the magnetization and the magnetic field, a ferroelectric material exhibits spontaneous electric polarization, P_S, and hysteresis effects between the polarization and the electric field. That is, ferroelectrics are materials which possess a spontaneous electric polarization, the direction of which can be reversed by applying a suitable electric field. By definition, it is this switching process or reversibility of the dipoles by a field that constitutes ferroelectricity. In general, the direction of P_S may be along one unique axis of the crystal, or along several that are crystallographically equivalent in the non-polar phase. Since FE crystals exhibit dielectric hysteresis, the electric polarization is not solely determined by the electric field. Thus, FE are characterized by dielectric hysteresis loops. These are non-linear polarization (P) - electric field (E) plots as shown schematically in Figure 2.4. There are, in general, three characteristic values of the FE crystal which may be obtained directly from the hysteresis loop: P_s, the spontaneous polarization (obtained by a linear extrapolation of the saturated portion of the loop to the E = 0 axis); P_r, the remanent polarization (value of P at the E = 0 axis); and E_c, the coercive field (minimum value of E required to bring the polarization to zero). Clearly, if the applied E field is less than E_c, no hysteresis loop will be evident.

In addition to the dipole reversibility, there are several other features and characteristics of FE that are important but are ancillary.

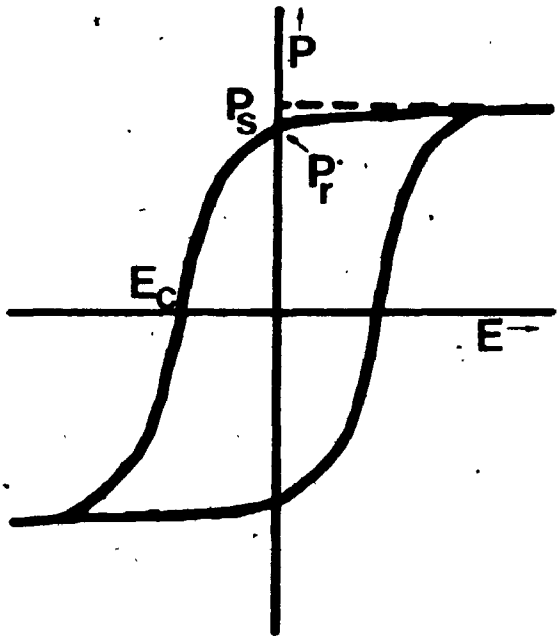

Figure 2.4 : Typical ferroelectric hysteresis loop showing the spontaneous polarization (P_s); remanent polarization (P_r); and the coercive field (E_c).

Basically, these may be summarized as follows:

(1) All FE must belong to a crystal class whose symmetry allows both piezo- and pyroelectric behaviour in the FE phase, i.e. one of the polar classes. This occurs in ten of the thirty-two crystal classes.

(2) Usually a FE crystal is not uniformly polarized in one direction, but is comprised of a number of domains. Each individual domain contains a large number of dipoles which are all aligned in the same direction. Individual domains are separated by a domain wall. In the tetragonal phase of a perovskite, for example, the domain pattern may be quite complex since it is possible for adjacent domains to be polarized at angles of either 90^{o} or 180^{o} from one another. In this case the polar axis of a domain may either be perpendicular to the plane of the crystal (c-domain) or in the plane of the crystal (a-domain). Consequently, when an electric field is applied to a FE crystal, the corresponding change of the macroscopic dipole moment of the crystal occurs through the nucleation and growth of the domains that are favourably oriented with respect to the applied field.

(3) Most ferroelectrics lose their FE properties above a characteristic transition temperature (the Curie Temperature, T_c). The higher temperature phase is called the paraelectric (or non-polar) phase and is characterized by the loss of P_s and a linear P-E plot.

(4) In the temperature region near the transition, the dielectric constant, k, becomes extremely large ($k \sim 10^3$-10^5) and exhibits a maximum at the transition temperature (the Curie point). These values for the dielectric constant are orders of magnitude greater than that for a normal dielectric ($k \sim 4.5$, quartz SiO_2, Cady, 1964; $k \sim 9.8$,

periclase MgO, Mott and Gurney, 1964; k ~ 5.6, halite NaCl, Mott and Gurney, 1964).

(5) In most ferroelectrics, the temperature dependence of the dielectric constant above the transition temperature can be fairly accurately described by the Curie-Weiss law

$$k = C/(T - T_o) \qquad (2.5)$$

where C is the Curie constant, and T_o is the Curie-Weiss temperature.

(6) The transition from the FE to paraelectric phase is, in all cases, either a first or second order transition. A first order transition involves a volume change and a discrete change in the polarization at the transition temperature. For a second order transition, the polarization goes continuously to zero with no discrete volume change at the transition. There is, however, a discrete change in the specific heat and thermal expansion coefficients for the crystal.

As a consequence of the anomalous dielectric properties of ferroelectrics, many of the other fundamental parameters of the crystal including its elastic, electro-optic and piezoelectric properties exhibit anomalous behaviour (Kanzig, 1957). It is precisely this feature which makes important the consideration of FE phases in the earth's interior.

2.5 Possible Implications of Ferroelectric Phases in the Earth or Planetary Interiors

The implications of FE phases with respect to the physical properties and mechanisms in the earth's and planetary interiors still await detailed assessment. However, at this time one may anticipate

some of the ways that the spontaneous polarization and strain which are associated with FE phases may appreciably affect the physical characteristics of the earth's mantle.

Obviously, the extremely high dielectric constant values (10^3 - 10^4 typical) associated with ferroelectrics especially in the neighbourhood of a transition would influence the electrical behaviour of the mantle. Since electromagnetic radiation is attenuated more in a material with a high dielectric constant (von Hippel, 1954), it seems reasonable to infer that a ferroelectric layer would screen and attenuate any electromagnetic radiation passing through it. Furthermore, FE structures in the lower mantle would affect the core-mantle coupling, and, since FE phases would occur in an environment of materials with different elastic and dielectric properties, the spontaneous polarization would be associated with induced space charge distributions. These, in non-equilibrium would produce electrical currents. Moreover, the space charges would influence both the nature and rate of diffusion of charged particles in the mantle. Since the refractive index (n) of a material is related to the high frequency dielectric constant (k_∞) by $k_\infty = n^2$, the refractive index of a perovskite material would also be high. Ringwood and Major (1971), for example, observed small inclusions of high refractive index in their high pressure-temperature experimental studies on $CaSiO_3$. They ascribed these inclusions to the observed perovskite solid solutions. This high refractive index could be expected to influence the radiative part of the heat transfer in the mantle, which is given by (see, for example, Stacey, 1969)

$$K_r = \frac{16}{3} \frac{n^2}{\eta} \sigma T^3 \qquad (2.6)$$

where K_r is the radiative thermal conductivity, n is the extinction coefficient, σ is Stefan's constant and T is the temperature. Thus, due to the high refractive index, this could be expected to be high in a FE phase near its Curie temperature. However, a simultaneous increase in the extinction coefficient is likely to offset at least part of this effect. Because of the inherent coupling between dielectric polarization and spontaneous strain ('dielastic polarization'), which finds expression in the piezoelectric, electrostrictive and elastic coefficients, any FE structure present in the earth's interior would exhibit elastic anomalies and affect elastic wave propagation. It seems not implausible that the 20° seismic discontinuity may be related to the exsolution of perovskite structures observed by Ringwood and Major (1967, 1971) at pressures indicated for the depth of the discontinuity (~300-400 km).

The steep rise in the electrical conductivity by 4-6 orders of magnitude between 400-900 km depth in the earth's mantle (Stacey, 1969) is too large to be accounted for by a gradual change in activation energy with temperature and pressure for an extrinsic conduction mechanism (Dvorak and Schloessin, 1973); it requires a major change in the conduction mechanism. It is possible that this change can be attributed to the increasing fraction of minerals assuming the spinel structure. On the other hand, the calculated pressures for this depth interval are compatible with the pressures which are required to produce perovskites in the laboratory. Recently, Schloessin and Timco (1977) have suggested that, if many of the perovskite structures reside at or near their transition temperature in this region, their presence could explain this large conductivity increase as being due to the high admittance

values and increases in conductivity by 2-5 orders of magnitude which have been found to attend the FE transition in typical cases.

One may speculate that FE phenomena may be predominant in the giant as well as the terrestrial planets. For these, however, the soft-mode vibrations observed for perovskite ferroelectrics would probably not be the mechanism responsible for the FE behaviour. In the giant planets, dielectric polarization could occur as a result of at least three different mechanisms: 1) proton motion in hydrogen bonded structures and hydrogen bonds exhibiting double-well potentials, 2) order-disorder transitions of non-symmetrical radicals such as NH_4^+, glycine and NO_3 and 3) transitions in numerous methylammonium-metal alums. For example, as a tentative explanation of their experimental observations, Costantino and Daniels (1975) recently suggested the existence of a pressure induced FE state in the δ-phase of solid methane (at $p \sim 4$ kbar for $T \sim 18$ K).

Schloessin and Timco (1977) have suggested that the sporadic but often intense radio bursts from Jupiter (Burke, 1961; Gallet, 1961) could possibly be explained by large stress induced FE depolarization pulses, probably of tidal origin due to Io and Jupiter V. Electrical pulses with peak powers of several hundred kilowatts of microsecond duration have been produced in the laboratory (Lysne and Percival, 1975) by shock or impact depolarization of FE samples. Similar pulses are associated with depolarization by decompression causing ferroelectric-antiferroelectric transitions (Gonard et al, 1972). The apparent angular diameters of the active source regions on Jupiter have been determined to be smaller than 3 second of arc. Consequently, the energies which

have been calculated (Burke, 1961; Gallet, 1961) on the basis of very inefficient energy conversion ratios between radio and thermal emissions, have led to the conclusion that the bursts, if thermal in origin, must be attributed to mechanisms which dominate the local thermal balance. The difficult problem of finding suitable heat sources, however, could be resolved if the bursts were caused by FE phenomena constituting highly efficient converters from mechanical into electrical energy. If a correlation between bursts and the motion of the inner satellites could be firmly established, these radio bursts might be explained as caused, or triggered off by the conversion of the tidal energy.

CHAPTER III

THE FERROELECTRIC INCLUSION

3.1 The Transforming Inclusion

J.D. Eshelby in a series of papers (Eshelby, 1956, 1957, 1961) developed a general theoretical treatment to describe the properties of the inhomogeneous, transforming inclusion in a solid matrix. Basically, the transformation problem can be formulated as follows: A region (the inclusion) within an isotropic elastic solid (the matrix) undergoes a spontaneous change of form which, but for the presence of the matrix would be some prescribed, homogeneous strain. Because of the surrounding material, the strain will be modified and stresses will be present both inside and outside the region. This problem becomes more complex if the inclusion has elastic properties which differ from those of the matrix. If, then, an external stress is applied to the matrix, the inclusion becomes misfitting (inhomogeneous) due to the compressibility contrast between the matrix and inclusion. Although this general theory was developed by Eshelby before the widespread use of solid-media for pressure transmission in high pressure research, it would seem that the problem of the inhomogeneous inclusion is exactly that encountered in a solid-medium high pressure apparatus. Consequently, Eshelby's theory is eminently suited to describe, in general, the situation of a sample (i.e. the inclusion) in a solid high pressure cell (i.e. the matrix), and, in particular, the behaviour of a ferroelectric transforming inclusion in a solid matrix subjected to pressure.

3.2 Thermodynamic Theory of Ferroelectrics

A quantitative thermodynamic account of the FE phase transition with the condition that along the FE-PE phase boundary the change in free energy of the system is zero ($\Delta G_{PE \rightarrow FE} = 0$) is usually determined for a system which consists of either an isolated 'free' (i.e constant stress) or 'clamped' (i.e. constant strain) crystal. In this theory (see, for example, Devonshire, 1954) the energy of the system is expressed as the sum of the individual energy components comprised of the elastic, piezoelectric, electrostrictive and electric energies of the crystal. The stable state of the system corresponds to that where the total free energy is a minimum. In the case of the free or clamped crystal, the shift in transition temperature with pressure can be determined from either the Clausius-Clapeyron or Ehrenfest relations (Samara, 1969) depending on whether the transition is of first or second order. However for the case of a FE phase forming part of a multi-component system as realized in the present high pressure experiments, this treatment is often insufficient (Schloessin and Timco, 1975, 1976; Timco and Schloessin, 1975a). In this case the energy of formation for the FE phase has to be established for the whole system and is dependent upon the sample, the material of the high pressure cell, and the loading device. Moreover, the reference phase which is usually taken as that of the highest crystal symmetry (i.e. the paraelectric phase) is no longer simply determined by the FE material. In this case, since the inclusion is accompanied by self-stressing, the reference phase will be dependent not only on the sample, but also on both the properties and sequence of the stress and temperature application to the system as a

whole. Since this situation has many features in common with that of the inhomogeneous, transforming inclusion, one can take advantage of the extensive theoretical work of Eshelby (1956, 1957, 1961) in dealing with this problem.

3.3 The Transforming Ferroelectric Inclusion

Suppose we introduce a FE crystal to fit snugly into the cavity in a high pressure cell at a temperature above the Curie temperature. The crystal and matrix are both stress free. We now isothermally apply a pressure X_i^A to the matrix. If the compressibility of the matrix and inclusion are the same, this pressure will produce a strain x_j^A in the inclusion. Clearly however, if there is a difference in compressibility between the matrix and inclusion, the crystal will become a misfitting inclusion. This misfit will induce surface tractions (X_i^S) which will be taken up by a layer of body force spread over the interface between matrix and inclusion. When this layer of body force is relaxed, each element on the surface of the inclusion will move through a displacement u_j^M. Thus, the energy will be determined by the energy due to the applied external pressure, ξ_A, and the energy due to the inclusion:

$$\xi_m = \xi_A + \xi_{Inc} \tag{3.1}$$

where

$$\xi_A = \frac{1}{2} \int X_i^A x_j^A \, dv \tag{3.2}$$

The energy ξ_{Inc} due to the presence of the inclusion consists of a term ξ_∞ which assumes that the stress field generated by the inclusion (X_i^S) falls off to boundaries at infinity (i.e. as if the matrix were infinite

in extent), and an image term ξ_{im} which takes into account the stress and strain required to annul the strain produced by the inclusion at the finite boundaries of the matrix. Thus,

$$\xi_{Inc} = \xi_{\infty} + \xi_{im}$$

$$= -\frac{1}{2}\int X_i^S (x_j^M - x_j^S)dv - \frac{1}{2}\int X_i^{im} x_j^S \, dv \qquad (3.3)$$

The energy ξ_m due to the applied load and the presence of the inclusion is thus

$$\xi_m = \xi_A + \xi_{Inc}$$

$$= \frac{1}{2}\int X_i^A x_j^A \, dv - \frac{1}{2}\int X_i^S (x_j^M - x_j^S)dv - \frac{1}{2}\int X_i^{im} x_j^S \, dv \qquad (3.4)$$

We have carried the question here only so far as showing that ξ_{Inc} is a significant additional elastic energy term which enters the Gibbs free energy calculation. Thus, this constitutes a major distinction between the isolated crystal and the crystal constrained by a matrix.

Next, we decrease the temperature to just below the paraelectric-ferroelectric transition temperature for normal (hydrostatic) pressure conditions. As we have seen, any change in the inclusion affects the energy of the total system. Thus, whether or not the PE→FE transition will take place will depend on the energy balance not in the inclusion alone, but in the total system including the loading device.

In the event of a ferroelectric transformation, there will be displacements u_j^F as a result of the spontaneous strain. However, depending on the relative contrast in compressibility between the matrix

and inclusion, this displacement may or may not be the same as that for the free crystal u_j^T. Clearly, in the case of a hard matrix, the full spontaneous transformation strain for the free crystal may be prevented from developing. Thus, this will produce self-stressing and a further misfit of the inclusion in the matrix. The energy associated with this misfit will then be

$$\xi_{inc}^t = -\frac{1}{2}\int X_i^T(x_j^F - x_j^T)dv \tag{3.5}$$

Since the transformation occurs in the presence of the external load, the work done by the surface tractions X_i^A on the body as the surface displacements change from x_j^A to $x_j^A + x_j^F$ is the interaction energy ξ_{int} of the inclusion with the applied stress field. Thus, in the event of a transformation, the change in the energy of the whole system (inclusion plus matrix plus loading device) is

$$\Delta\xi_{tot} = \xi_{inc}^t + \xi_{int} \tag{3.6}$$

where

$$\xi_{int} = -\int X_i^A\, x_j^T\, dv \tag{3.7}$$

Thus we may write

$$\xi_{tot} = \xi_o + \xi_A + \xi_{Inc} + \xi_{inc}^t + \xi_{int} \tag{3.8}$$

where ξ_o is the potential energy of the loading mechanism in the absence of the inclusion. In equation (3.8), the first two terms depend only on the elastic field due to the load, and the third and fourth terms depend only on the fields due to inclusion. The last term, however, depends

upon both of these fields.

Apart from the elastic energy terms, the total free energy change associated with the paraelectric-ferroelectric transition must also include the contributions from all of the other energy terms including electric, electrostrictive and piezoelectric. Then the total free energy change $\Delta G_{PE \rightarrow FE}$ as a result of the changes in crystal structure and dielectric properties can be determined. If $\Delta G_{PE \rightarrow FE} < 0$, the transformation is energetically possible. Crucial to the difference between the transition processes in the free crystal and the crystal forming an inhomogeneous inclusion are, therefore, the elastic terms, the energy due to the presence of the inclusion and the interaction energy with the applied stress field. This suggests that with pressure application to a matrix plus inclusion, some FE transitions may be suppressed. However, there is also the possibility that suitable matching of the stress with elastic constant differences between matrix and inclusion could set the conditions necessary for ferroelectric states lying just outside the stability field of the free crystal.

CHAPTER IV

EXPERIMENTAL

4.1 Generation of Pressure

In these experiments the pressure was generated with a cubic (hexahedral) press (Hall, 1964) which consists of six hydraulic rams self-suspended by tie bars which are in an octahedral arrangement. Two such presses were used - (1) a 200 ton capacity press (Photo P.1) which is capable of producing a pressure of 55 kbar with an anvil size of 1.27 cm (½ inch), and (2) a 1,000 ton capacity press (Photo P.2) which is capable of producing a pressure of 60 kbar with an anvil size of 2.54 cm (1 inch). All dielectric constant measurements were performed with the latter, whereas the hysteresis loop studies on the barium titanate single crystals were performed with the former.

The use of this type of press requires that a solid be used as a pressure transmittimg medium. Pyrophyllite $Al_4(Si_8O_{20})(OH_4)$, a fine-grained naturally occurring hydrous aluminum silicate (unfired lava, American Lava Corp.) was used for this purpose. The pyrophyllite was milled cubical in shape such that its edge length was 25% larger than that of the anvil face. Consequently, with the mutual advance of the six anvils, the pyrophyllite transmits the pressure uniformly over the central region of the cube. In addition, the excess material along the cube edges extrudes between the anvil heads and forms self-sealing gaskets in this region (see Figure 4.1). Since pyrophyllite is electrically

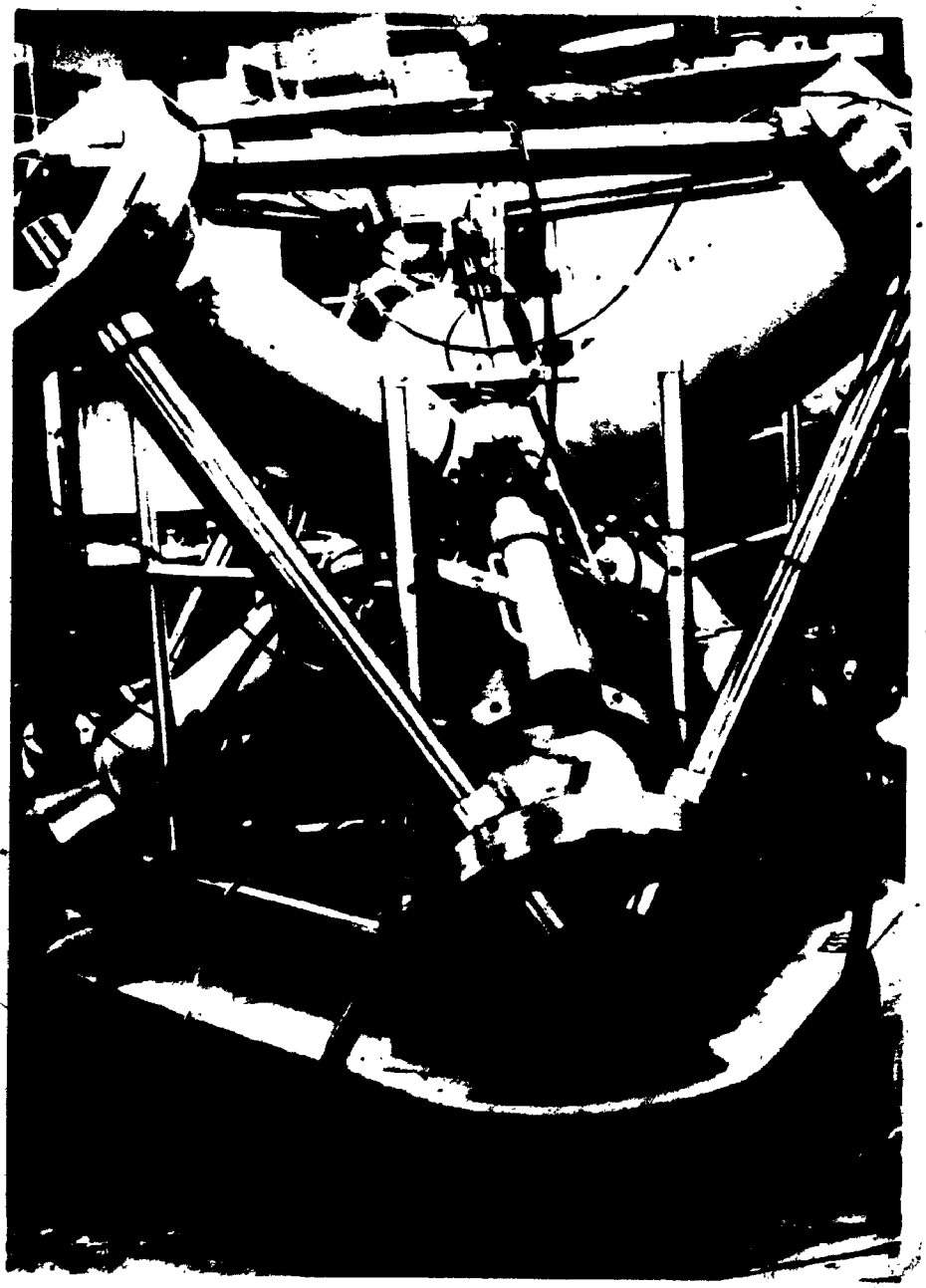

Photo P.1 : 200-ton capacity cubic press.

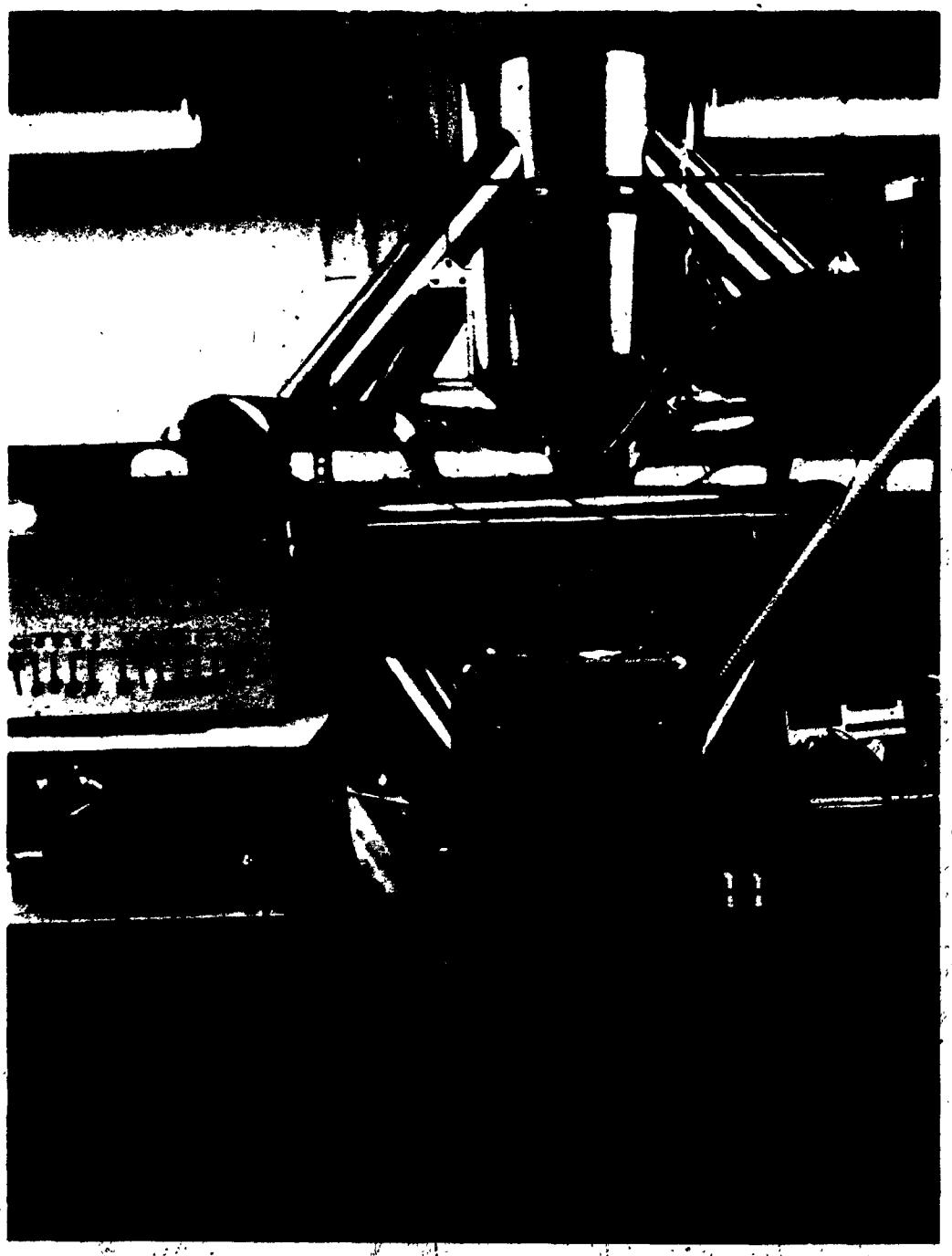

Photo P.2 : 1,000-ton capacity cubic press. The GR 1620-A capacitance measuring assembly is shown at left.

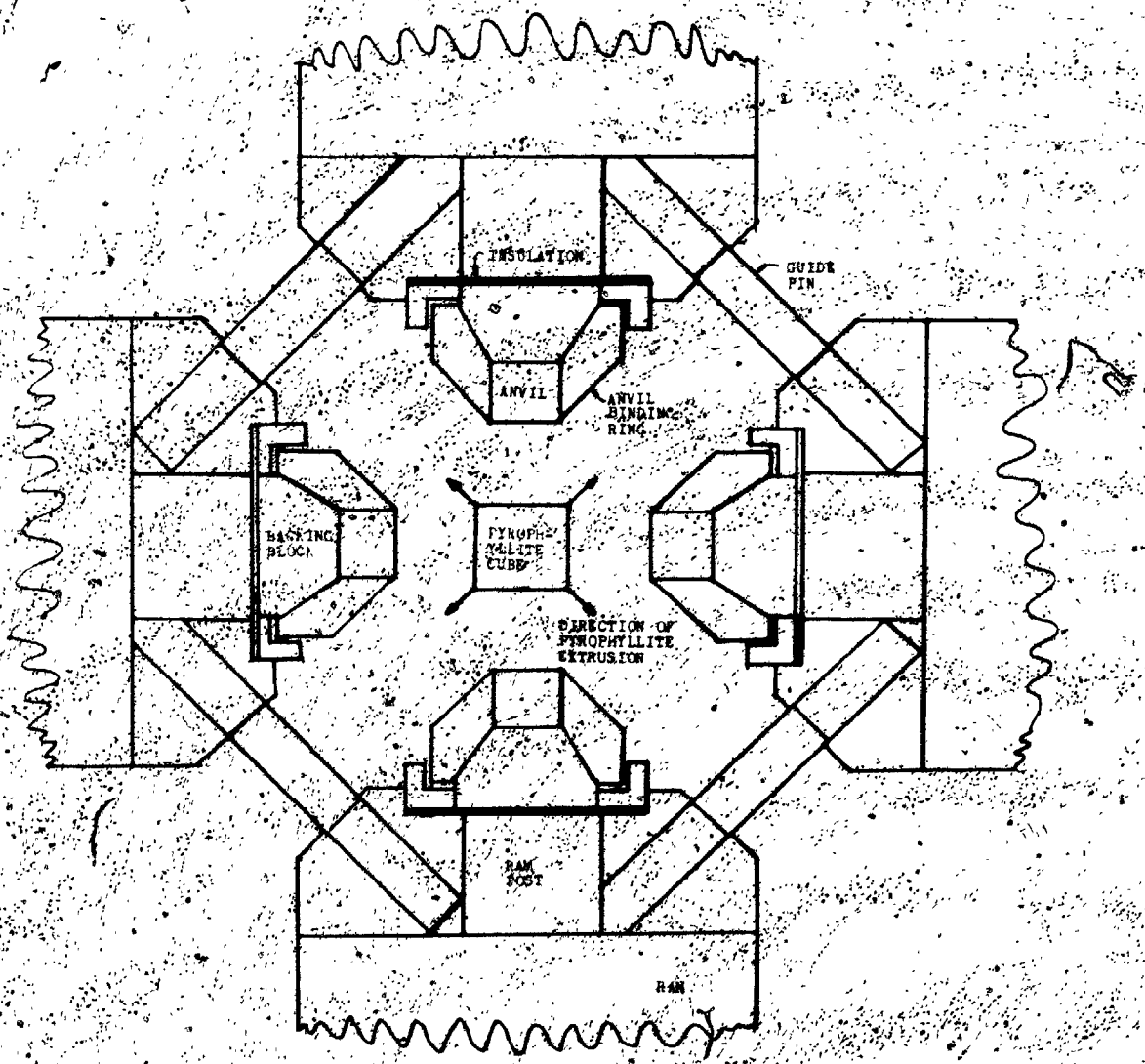

Figure 4.1 Schematic cross section through cubic press showing four of the six anvils. All parts are made of hardened steel except the anvils which are tungsten carbide/cobalt inserts.

insulating, and since each anvil is electrically insulated from the main body of the press by large backing insulation (Figure 4.1), the anvils are electrically isolated from one another. This allows one to use each of them for independent electrical connections.

The pressure was controlled by means of varying the hydraulic oil pressure in the system by means of either electric or manual pumps. Conversion of this pressure to sample cell pressure was based on runs containing silver nitrate, bismuth and barium. The $AgNO_3$ I-II transition at 9.8 kbar, the Bi I-II and II-III transitions at 25.4 and 27.0 kbar, and the Ba II-III transition at 59.6 kbar (Kennedy and La Mori, 1962), all determined by electrical resistivity changes were taken as the fixed points. A comparison of several calibration runs indicates that the estimates of the mean sample cell pressures determined in this way are accurate and reproducible to better than $\pm$ 2 kbar. For all of the experimental runs on the perovskite samples, care was taken to ensure that the sample under study was small and positioned at the exact centroid of the high pressure apparatus. This was done to ensure the smallest stress differences, estimated to be within about 1 kbar for mean sample cell pressures above 20 kbar (Lees and McCartney, 1968).

4.2 Sample Cell Arrangement

The basic arrangement of the high pressure sample cell is shown in Figure 4.2. This figure shows the pyrophyllite cube housing the sample in its centre, with heater wires and a thermocouple arranged about it.

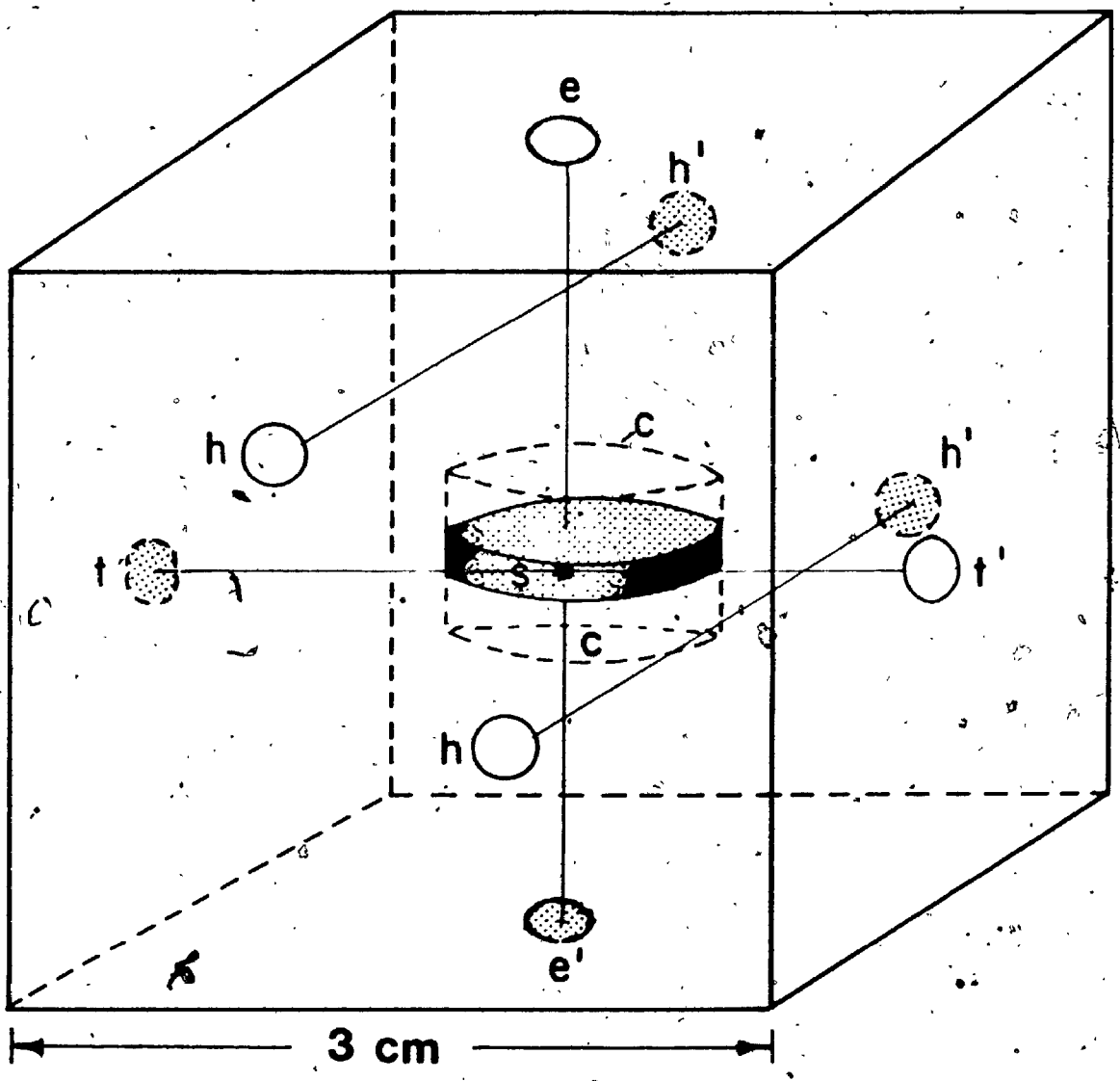

Figure 4.2 : Schematic representation of the experimental arrangement in the pyrophyllite cube: ee' electrodes, tt' thermocouple, hh' heater wires, s sample, c ceresine envelope (used only in single crystal studies).

The samples investigated in this study were obtained from various sources. The barium titanate ($BaTiO_3$) and lead zirconate titanate ($Pb(Zr,Ti)O_3$) ceramics were obtained from the Vernitron Corp. (Bedford, Ohio, U.S.A.). These were disc shaped of ~.6 cm diameter and .20-.25 cm thickness. The barium titanate single crystals were obtained through the courtesy of the Harshaw Chemical Company (Solon, Ohio, U.S.A.), and the calcium titanate ($CaTiO_3$) single crystals were obtained from Ward's Scientific (Toronto, Ont., Canada). In all cases, silver paint electrodes were applied to the disc faces and a .025 cm Pt wire was taken from each electrode to opposite sides of the cube for contact with the anvil faces (ee', Figure 4.2). The silver paint assures good contact with the crystal and ensures that the applied potential is impressed across the crystal. Due to the irregular shape of the $BaTiO_3$ and $CaTiO_3$ single crystals and their consequent misfit in the cylindrical cavity in the pyrophyllite cube, they were surrounded by ceresine wax in the high pressure cell. This provided a completely fitting medium of both high ductility and high resistivity ($\sim 10^{18}$ Ω-cm).

The temperature of the sample was raised by passing AC currents through four .05 cm diameter platinum wires which were inserted into four holes drilled through the pyrophyllite cube between opposite faces (hh', Figure 4.2). The current and voltage across these wires were measured on two Advance digital multimeters DMM2, and these values were related to the thermocouple readings as an independent check on the reproducibility of the thermocouples performance.

The temperature was measured by inserting a .025 cm Pt/Pt 10% Rh thermocouple .15-.20 cm from the edge of the crystal. The two ends were

brought out at the two remaining cube faces (tt', Figure 4.2). The resulting emf values were measured with either a Kipp and Zonen BD5 Micrograph Recorder or a Keithley 160B Digital Multimeter and were corrected for both room temperature and the slight pressure effects on the thermocouple (Bundy, 1961).

In the present high pressure experiments, the placement of a thermocouple in the pressure cell was a convenient and reasonably accurate means of estimating the temperature of the sample. With this technique, however, there are several factors which limit the accuracy of measurement of the absolute temperature. First of all, physical necessity dictates that the thermocouple bead cannot occupy the (central) position in the pressure cell where the sample sits. Thus, the bead must be slightly offset to a position .15-.20 cm from the edge of the sample. Clearly then, if large temperature gradients exist in the cube, the temperature at the thermocouple bead may or may not accurately represent the sample temperature. To check for the existence of temperature gradients in the central portion of a pyrophyllite cube in the 1000 ton capacity press, a separate experiment was performed in which a thermocouple was inserted into the high pressure cell such that its bead occupied the central portion of the cube (i.e. the sample position). In addition, heater wires and the (off-centre) thermocouple were placed in their usual position in the high pressure cell (see Figure 4.2). The results of this experiment indicate that throughout the temperature range from room temperature to 250°C, both thermocouples were in reasonable agreement (i.e. there was little temperature gradient over this region of the cube). The maximum temperature difference determined by this procedure was ~4%

in the higher temperature region. Secondly, since the ends of the thermocouple terminate on anvil faces, which in turn are connected to the measuring device by electrical leads, several metal-metal junctions are present in the thermocouple circuit. Consequently, one must assume that these extraneous junctions are symmetrical about the thermocouple bead, such that any emf generated by one junction will be cancelled by the emf from the corresponding junction on the other side. This is a reasonable assumption since the influence of these junctions at room temperature can be easily accounted for, and moreover, they should be relatively insensitive to changes in temperature in the high pressure cell. It is estimated that this effect will influence the accuracy of the measurement of the absolute temperature by less than 1%. Thirdly, the fact that cold-junctions cannot be used as a reference point for the ends of the thermocouple may introduce some error. In reality, the reference temperature of the thermocouple-anvil junction (which is assumed constant) "floats" above room temperature due to the heat generated in the pressure cell. For the relatively low temperatures (<300^{o}C) used in the present experiments, however, this reference temperature should not change by more than 5^{o}C. Finally, since the corrections for the pressure effects on the couple are known only for hydrostatic conditions (Bundy, 1961), the additional corrections for the non-hydrostatic stress components in solid-media devices cannot be accounted for. Certainly however, this correction should be very small (<½%).

The problems mentioned above primarily limit the accuracy of the absolute temperature, but have much less of an effect on the relative temperature differences. These are estimated to be accurate to ± .5^{o}C.

The error in the absolute temperature, however, may amount to more than 6%, especially in the higher temperature region.

In all of the experimental runs, the results were obtained isobarically, the temperature being raised and lowered slowly with sufficient allowance for system equilibrium (typically 1.5-2 minutes after a change in temperature). All dielectric measurements were performed with a measuring frequency of 1 or 10 kHz and a field strength of less than 10 V/cm. In calculating the dielectric constant from the measured capacitance, the corrections for the dimensional change in the sample were neglected; i.e. the cell constant of the disc was assumed to remain constant. Although this assumption is not strictly valid, this approach is one commonly taken in these types of high pressure experiments since the detailed compressibility of the ceramic specimens is not known. Nevertheless, the assumption is a reasonable one since the compressibility of the perovskite specimens should be relatively small. This is so since the perovskite lattice has extremely close atomic packing, the ceramic specimens are of high theoretical density and there was little dimensional change in the sample when measured after the high pressure run. At most, it is estimated that this will effect the absolute value of k by ~4% over the entire pressure range to 55 kbar. It would seem, however, that this is of little consequence in light of the extremely large changes encountered in k due to the FE-PE phase transition.

4.3 Capacitance Measurements

Measurements of the capacitance and dissipation factor (see Appendix A) were performed with a General Radio (GR) 1620-A capacitance

measuring assembly which consists of a GR-1615 bridge, GR-1311 generator and GR-1232-AP tuned amplifier and null detector. The GR-1615 bridge is an inductively coupled ratio arms bridge similar to that described in the literature by Cole and Gross (1949) and Mungall and Morris (1963). The bridge is designed in such a way that two transformer secondary windings make up the ratio arms of the bridge, whilst the standard capacitor, $C_{st.}$, and the unknown capacitor, C_x, form the other two arms of a conventional four-arm bridge. These features are shown schematically in Figure 4.3. The beauty of this system lies in the fact that any stray capacitances in the measuring circuit from high potential to ground (C_H) are electrically reflected across the windings of the ratio arms, and therefore, they do not affect the conditions for the bridge balance. Similarly, capacitances from low potential to ground (C_L) shunt the detector thereby affecting only the bridge sensitivity. These important features combined with the very high accuracy of the bridge ($>\pm$ .1%) make it particularly suitable for high pressure research.

To date, only three investigations have dealt with the measurement of the capacitance of materials in solid-media high pressure devices ($SrTiO_3$, Samara and Giardini, 1965; $NaNO_3$, Barnett et al, 1969; $BaTiO_3$, Clarke, 1976). In all of these cases, the electrical leads from the crystal electrodes to the capacitance bridge were brought out through the pyrophyllite gaskets. Experimentally, however, it is much more convenient to use two anvil faces as connections to the electrodes. Consequently, an experimental method for measuring the dielectric properties of small samples surrounded by solid-media was devised with this feature in mind.

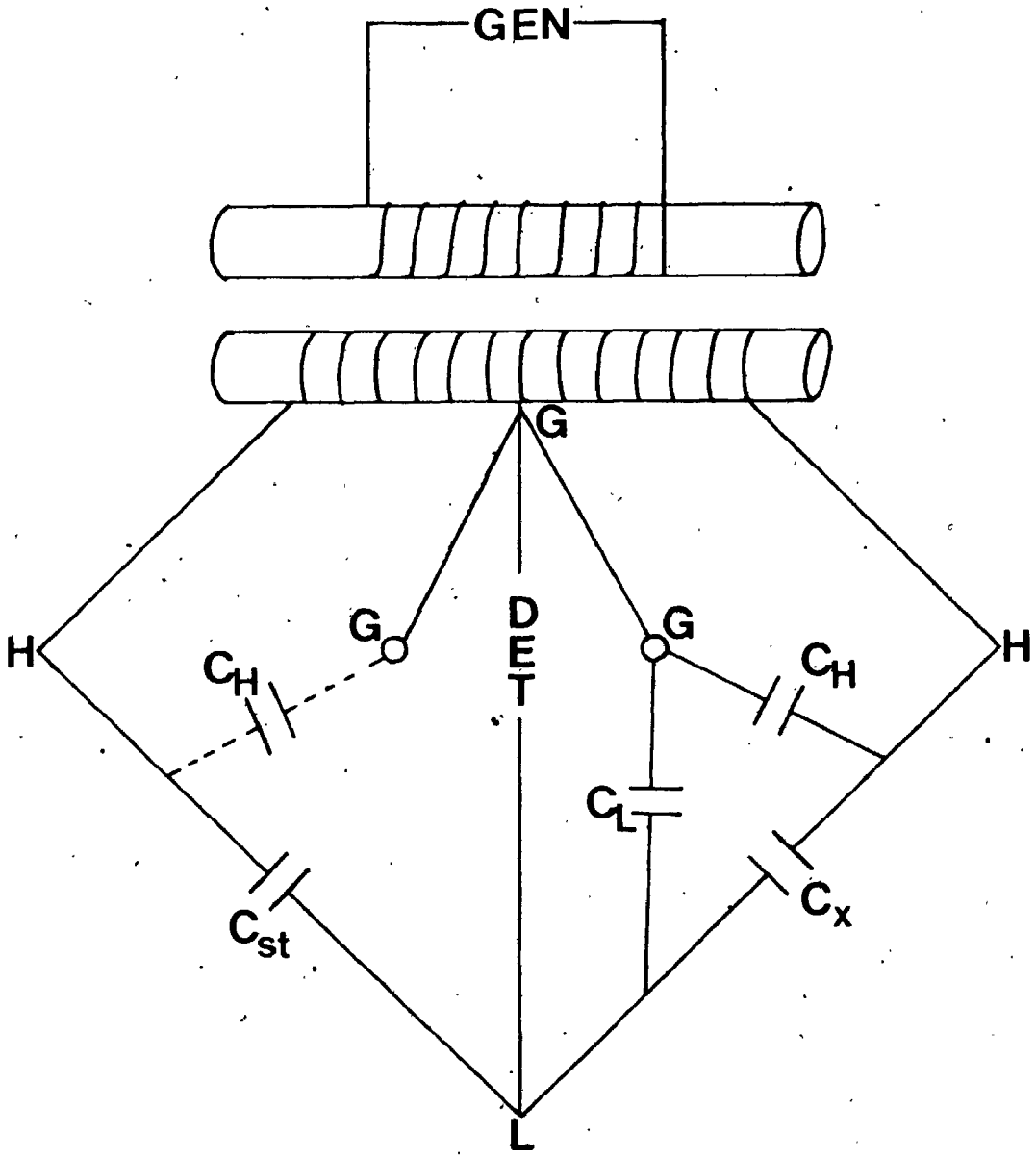

Figure 4.3 : Schematic representation of a capacitance bridge with transformer ratio arms.

In designing an experimental technique to measure dielectric properties under pressure, it is necessary to make use of the features of the capacitance bridge in order to be able to make accurate measurements. One need consider, for example, the experimental problems involved. First of all, the sample under study must necessarily be connected to the bridge by long leads - one of which must be completely shielded. Furthermore, the sample must be completely embedded in pyrophyllite and, for convenience, opposite anvils must be used as connections for the sample electrodes. Unavoidably all of these contribute stray capacitances to the measuring circuit as shown in Figure 4.4. This figure gives a two dimensional cross section of the sample in the pyrophyllite cube under pressure, and indicates all of the stray capacitances and electrical leakage paths present. These include: (A) the capacitance along the length of the connecting co-axial cable; (B) the capacitance from one electrode-anvil to ground; (C) the capacitance from the other electrode-anvil to ground; (D) the symmetrical sets of capacitance formed by the pyrophyllite gaskets between anvils; (E) the edge capacitance due to the fringing of the electric field in the volume of pyrophyllite containing the sample; (F) the electrical leakage paths through the gaskets, and (G) the electrical leakage paths through the pyrophyllite surrounding the sample. All of these must either be eliminated from the measuring circuit (that is, so that they do not affect the bridge balance conditions) or else be accounted for in the measured values.

The capacitance along the length of the co-axial cable (A, Figure 4.4) falls into the first category since all capacitances from low potential to ground shunt the detector and therefore do not affect the bridge

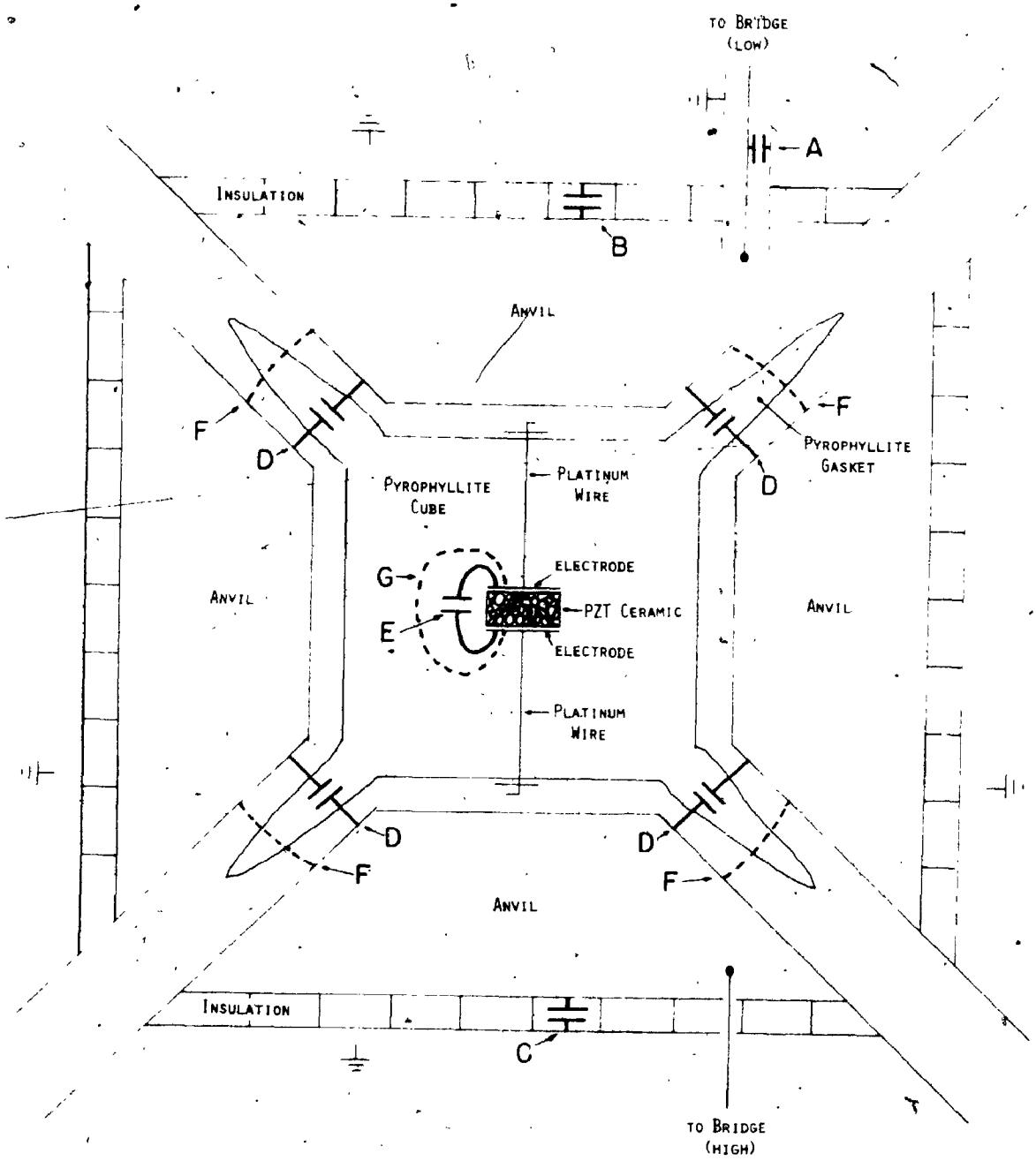

Figure 4.4 : .Schematic cross-sectional view through the sample cell and tungsten carbide anvils showing stray capacitances (A,B,C,D,E,) and electrical leakage paths (F,G).

balance. Similarly, if the main body of the high pressure apparatus (rams, tie-bars, etc.) is grounded, the capacitance from one anvil-electrode across the backing insulation (B, Figure 4.4) is eliminated. In a like manner, the capacitance from the other anvil-electrode across its backing insulation is electrically reflected in the transformer windings, and therefore it also does not affect the balance conditions. Clearly, proper grounding is crucial in this case. That is, both the shield of the co-axial cable and the main body of the press must be grounded to the same potential as the ground of the capacitance bridge. If this is not done, the large capacitance (~1.4 nf) across each of the anvils backing insulation (B, C, Figure 4.4) is placed in parallel with the sample. Since these capacitances are more than ten times larger than that of the samples, they would mask the sample capacitance. Proper grounding eliminates this effect by producing a three-terminal, two-electrode arrangement. This was confirmed experimentally by comparing the values obtained using this grounding technique with those obtained by by-passing these large capacitances by bringing the electrical leads directly out through the pyrophyllite gaskets (see Appendix B).

The remaining stray capacitances (D, E, Figure 4.4) and electrical leakage paths (F, G, Figure 4.4) shunt the sample and therefore cannot be eliminated from the measuring circuit. Consequently a method was devised to account for their effect.

These were taken into account by employing an equivalent circuit in which the sample was represented by a capacitance, C, in parallel with a conductance, G, which represents the samples loss. The total stray (edge) capacitance shunting the sample (D, E, Figure 4.4) was

accounted for by a capacitor, C_e, and all conductance paths (F, G, Figure 4.4) were represented by a conductance, G_e, both of which are in parallel with the sample. This is shown in Figure 4.5a.

In measurement, the capacitance bridge readout is given in terms of one apparent capacitance, C_x, in parallel with one apparent conductance, G_x, as shown in Figure 4.5b. It can be shown that the sample capacitance, C, in terms of the measured capacitance, C_x, is

$$C = C_x - C_e \tag{4.1}$$

and that the sample conductance, G, in terms of the measured conductance, G_x, is

$$G = G_x - G_e \tag{4.2}$$

Furthermore, the sample dissipation factor, D, can be calculated from the measured dissipation, D_x, by

$$D = D_x \frac{(1 - (G_e/G_x))}{(1 - (C_e/C_x))} \tag{4.3}$$

To estimate C_e and G_e, a separate experiment was performed measuring the dielectric properties of an a-cut quartz tablet, a low dielectric constant ($k = 4.5$, Cady, 1964), low loss ($\rho \sim 10^{14}$ Ω-cm, Cady, 1964) material. The results of this experiment (Appendix C) and equations (4.1) - (4.3) were applied to the measured C_x, D_x values in all of the other experiments in order to correct for the edge effects. Figure 4.6 shows the effect of this correction on both the capacitance and dissipation factor measured at 1 kHz for one of the PZT samples

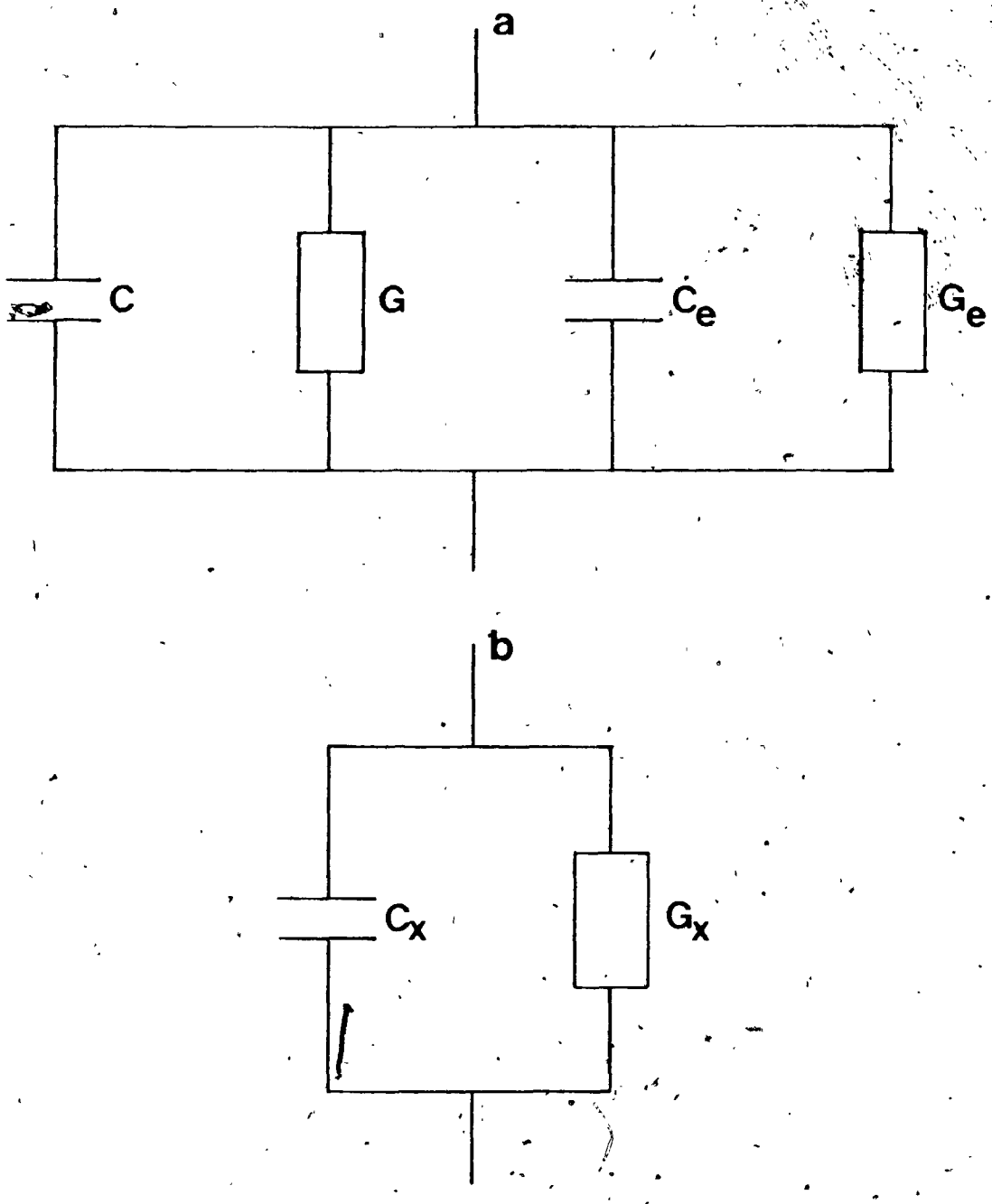

Figure 4.5 : Equivalent circuit used in accounting for edge effects: a - sample capacitance (C), sample conductance (G), edge capacitance (C_e), edge conductance (G_e); b - measured capacitance (C_x), measured conductance (G_x).

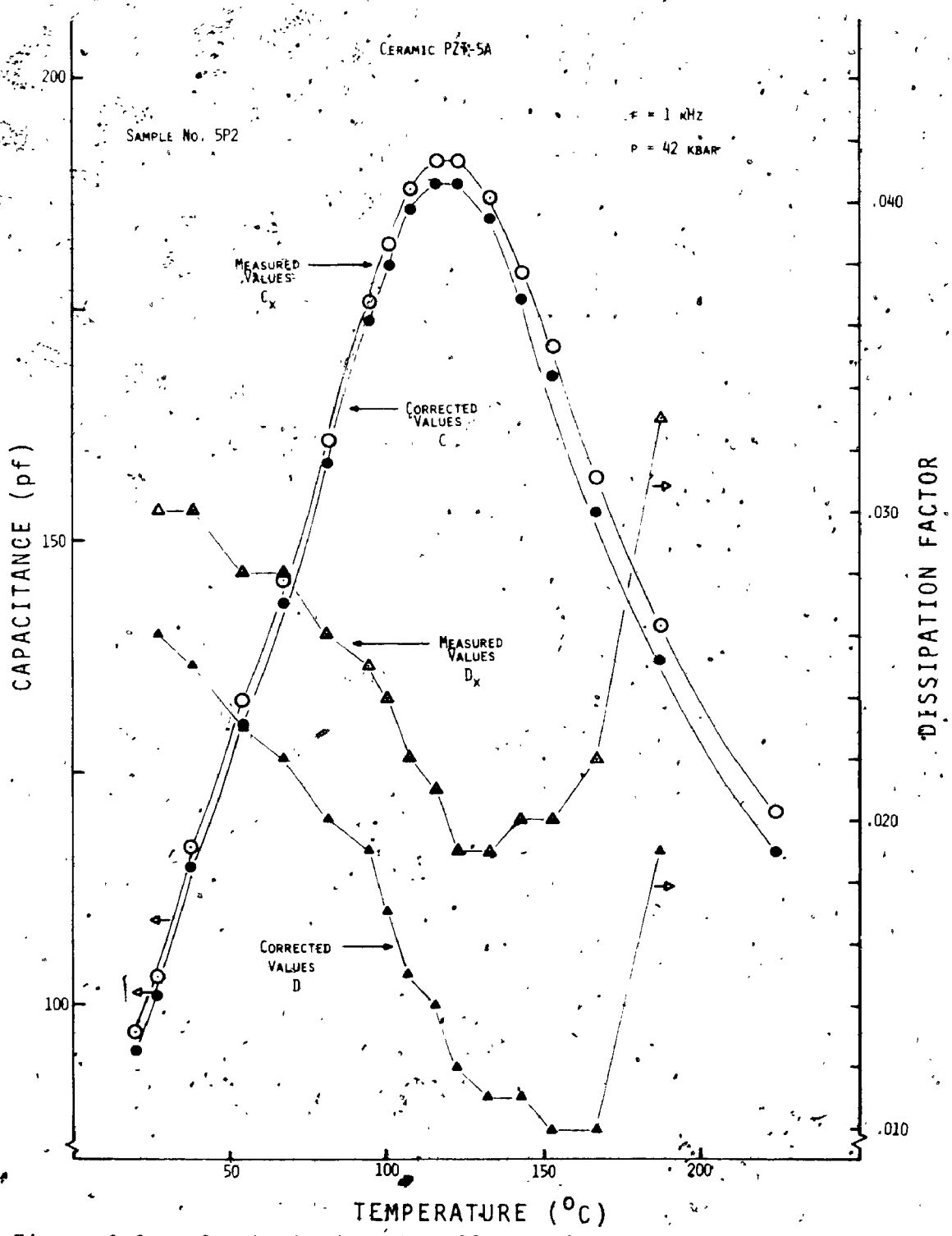

Figure 4.6 : Graph showing the effects of the edge correction on the capacitance and dissipation factor values for one $Pb(Zr,Ti)O_3$ sample for a measuring frequency of 1 kHz.

investigated. In this case the edge capacitance is ~4% of C_x, and the edge effects account for typically .010 of the measured D_x values. With a 10 kHz measuring frequency, however, the edge corrections are substantially less. Figure 4.7 shows the edge corrections for both the capacitance and dissipation factor measured at 10 kHz for the same PZT sample shown in Figure 4.6. With this measuring frequency, the impairing effects of the pyrophyllite on the capacitance values amount to less than 2%, and on absolute dissipation values by ~.002. Consequently, unless otherwise stated, all measurements were made with a measuring frequency of 10 kHz. The observed, large frequency dependence of the edge corrections is attributed to the strong frequency dependence of the dielectric properties of pyrophyllite (Timco et.al., 1976a, 1976b, Appendix D). It is estimated that this correction procedure yields capacitance values accurate to within ~1% and dissipation factor values to ~10%. Note that prior to and during the experiments, several precautions were taken to reduce and/or maintain controlled edge conditions, including drying the assembled pyrophyllite cube in a vacuum oven, storing the dried cubes in a desiccator, coating the anvil side faces with a thin layer of oil to reduce G_e (F, Figure 4.4) and maintaining a relatively low room humidity.

4.4 Hysteresis Loop Observation

The ferroelectric hysteresis loops were displayed on the screen of an Advance OS1000 oscilloscope by means of a Sawyer-Tower (1930) circuit (see Figure 4.8). This circuit basically consists of two capacitors in series - C_c the crystal capacitance and C_r the reference

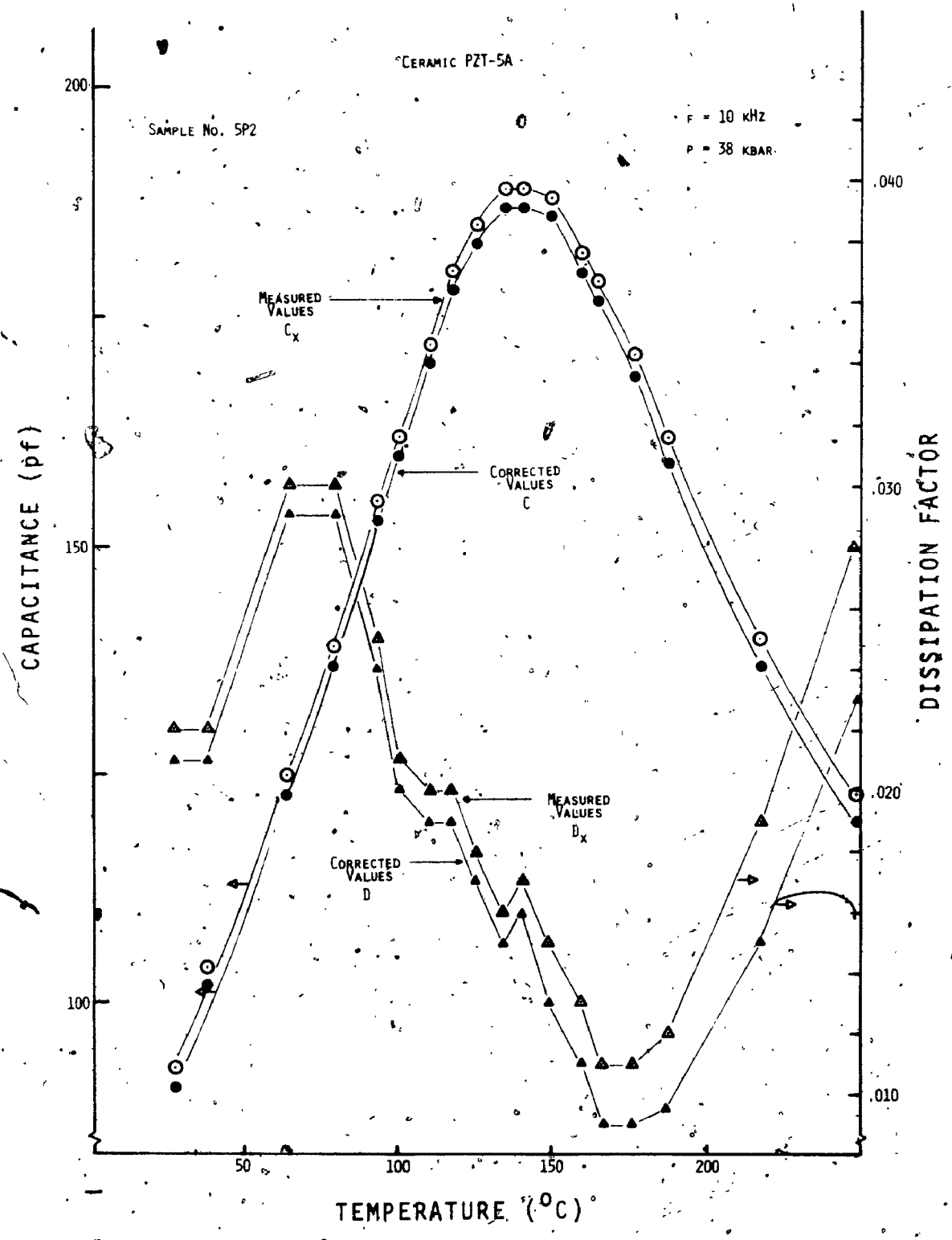

Figure 4.7 : Graph showing the effects of the edge correction on the capacitance and dissipation factor values for one $Pb(Zr,Ti)O_3$ sample for a measuring frequency of 10 kHz.

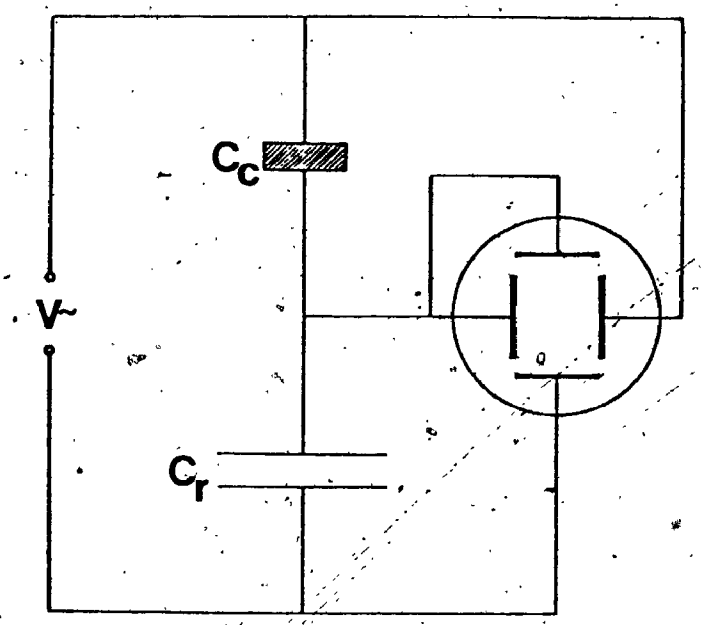

Figure 4.8: Schematic representation of the Sawyer-Tower circuit for the observation of ferroelectric hysteresis loops.

capacitor chosen such that $C_r >> C_c$. In this case, the impedance across C_c is very high and, since the charge Q must be the same on each capacitor, the vertical sweep on the oscilloscope is approximately proportional to the polarization P in the crystal. If the vertical scale sensitivity on the oscilloscope is S (= V_c/y) volts/cm, where V_c is the instantaneous voltage across C_r and y is the deflection of the electron beam (in cm.), then the polarization P is given by

$$P \approx \frac{C_r V_c}{A} = \frac{C_r S y}{A} \qquad (4.4)$$

where A is the area of the crystal plate. In these experiments, sixty cycle voltage was applied by feeding the output of a variac into a 5:1 step-up transformer, thus producing maximum voltages of ~600 volts (E ~ 6000 V/cm) across the crystal. A 1:1 floating transformer was also included in the circuit for safety. Most readings were taken with $C_r \sim 2$ μf and a .1 MΩ potentiometer was used to limit the x-deflection on the oscilloscope.

CHAPTER V

POLYCRYSTALLINE AND SINGLE CRYSTAL BARIUM TITANATE

5.1. Introduction

Barium titanate ($BaTiO_3$) is, to date, probably the most extensively studied ferroelectric material. There are several reasons for this. First of all, from the viewpoint of a solid state physicist, the relatively simple perovskite structure of barium titanate affords a means whereby one can get a good understanding of FE behaviour. Secondly, it is of great practical importance since it is chemically and mechanically very stable, its room pressure Curie temperature is above room temperature ($T_c^o \sim 115 - 120^oC$), it has a relatively wide temperature range of stability, and it can easily be prepared in the form of polycrystalline samples.

The specific dielectric properties of single crystal $BaTiO_3$ were first detailed by Merz in 1949. He found that the dielectric constant - temperature curve exhibits a series of large peaks at temperatures of $\sim 120^oC$, 0^oC and -90^oC. These are due to a series of polymorphic phase transitions which barium titanate undergoes with changes in temperature (Kay and Vousden, 1949). Upon cooling from high temperature, the cubic (paraelectric) phase elongates along a cube edge [100] to form a tetragonal phase at $\sim 120^oC$. This transition marks the onset of FE behaviour. Upon further cooling, the tetragonal phase transforms at 0^oC to an orthorhombic phase. In this transition, the cube elongates along a

face diagonal [110] rather than an edge. At even lower temperatures ($-90^{o}C$), a rhombohedral cell elongated along the body diagonal [111] is formed. In each temperature interval, the direction of the ferroelectric dipole is parallel to the elongation of the unit cell.

To date, the effects of hydrostatic pressure on both single crystal and ceramic barium titanate (BT) have been well investigated, with, however large quantitative discrepancies in the findings. Merz (1950) investigated the change in the FE-PE transition temperature, T_C, with pressure to 4 kbar and found that it decreases linearly ($dT_C/dp = -5.8^{o}C/kbar$) to ~2.5 kbar, whereupon it increases with pressure. Klimowski (1962) measured the pressure (to ~13 kbar) and temperature ($22-180^{o}C$) dependence on the dielectric constant of $BaTiO_3$ single crystals, and found that T_C decreases non-linearly with an initial slope of $-4.3^{o}C/kbar$. Leonidova and Polandov (1962) found a sudden drop in the permittivity of a $BaTiO_3$ single crystal at a pressure of ~11 kbar and room temperature. Minomura et al (1964) carried out pressure investigations to 13 kbar in the temperature range of $-20^{o}C$ to $140^{o}C$, and found that the Curie temperature decreases at a rate of $-6.3^{o}C/kbar$. Leonidova and Volk (1966) determined that the Curie temperature decreases non-linearly with pressure to 8.5 kbar such that $-dT_C/dp$ increases with increasing pressure. Samara (1966) carried out the most detailed investigation of the combined effects of pressure (to 25 kbar) and temperature ($20 - 150^{o}C$) on the polarization, dielectric constant, dielectric loss and the Curie temperature for both single crystal and ceramic specimens. He found that T_C decreases linearly with increasing pressure, but at a rate which varied from -4.6 to $-5.9^{o}C/kbar$ for different samples.

Polandov et al (1967) measured the pressure dependence of the Curie point to 10 kbar and found that it decreases linearly with pressure at a rate of $-4.8^{o}C$/kbar. In 1970, Minomura et al reported that to pressures of ~5 kbar, the cubic-tetragonal, tetragonal-orthorhombic and orthorhombic-rhombohedral transition temperatures decrease with increasing pressure. In 1971, Samara reported on the pressure dependence of both the orthorhombic-rhombohedral and tetragonal-orthorhombic phase boundaries. Finally, most recently, Clarke (1976) measured the pressure (to 50 kbar) and temperature ($-20^{o}C$ to $150^{o}C$) dependence of the dielectric properties of a $BaTiO_3$ single crystal in a solid tetrahedral high pressure cell and obtained a dT_C/dp value of $-4^{o}C$/kbar. In addition, Clarke determined the Curie critical region to be 34 kbar and $15^{o}C$.

Samara's (1966) results on the effects of pressure on the temperature dependence of the dielectric constant of both single crystal and polycrystalline barium titanate show distinctly different behaviour. For both types of samples, the large characteristic peak in k is observed at the transition temperature. However, whereas for the single crystal, the values of k in the vicinity of the Curie temperature (i.e. k_{max}) increase by 60-70% over 15 kbar, the values of k_{max} for the ceramic decrease by over 50% for the same pressure interval. Samara explains the increase in k_{max} for the crystal as evidence that with increasing pressure, the first order cubic-tetragonal transition in BT acquires the characteristics of a second order transition. Samara (1971) predicted the Curie critical region for $BaTiO_3$ to fall in the range of ~30-40 kbar. This has recently been confirmed by Clarke (1976). The

large decrease in k_{max} measured on the polycrystalline specimens, on the other hand, has so far not found a very satisfactory explanation. Samara (1966) tentatively explained it as being due to either the influence of the internal microstresses in the ceramic, or a possible anomalous behaviour in the pressure dependence of the a-axis dielectric constant. However, later experiments by Samara (1971) have shown that the pressure dependence of k_a for $BaTiO_3$ is normal.

In the present experiments, the effects of pressure on the dielectric constant, dissipation factor, FE-PE transition temperature and remanent polarization of polycrystalline ceramics have been investigated in detail. In addition, the effects of pressure on the hysteresis loop of single crystal barium titanate at room temperature have also been studied.

5.2 High Pressure Behaviour of $BaTiO_3$ Ceramics

Figure 5.1 shows the temperature dependence of the dielectric constant, k,* at various pressures for one sample of ceramic barium titanate. All of the samples investigated showed similar behaviour, including one which was surrounded in a ceresine envelope in the high pressure cell (Figure 5.2). From these figures it is evident that, at constant pressure, the dielectric constant exhibits a maximum in its

*In this thesis the dielectric constant, k, of a material is defined as the ratio of the dielectric permittivity of the material (ε) to the dielectric permittivity of free space (ε_0), i.e. $k = \varepsilon/\varepsilon_0$. This quantity is also sometimes called the relative dielectric constant or dielectric coefficient, and is equivalent to the dielectric permittivity ε in cgs units (since $\varepsilon_0 = 1$ in this system).

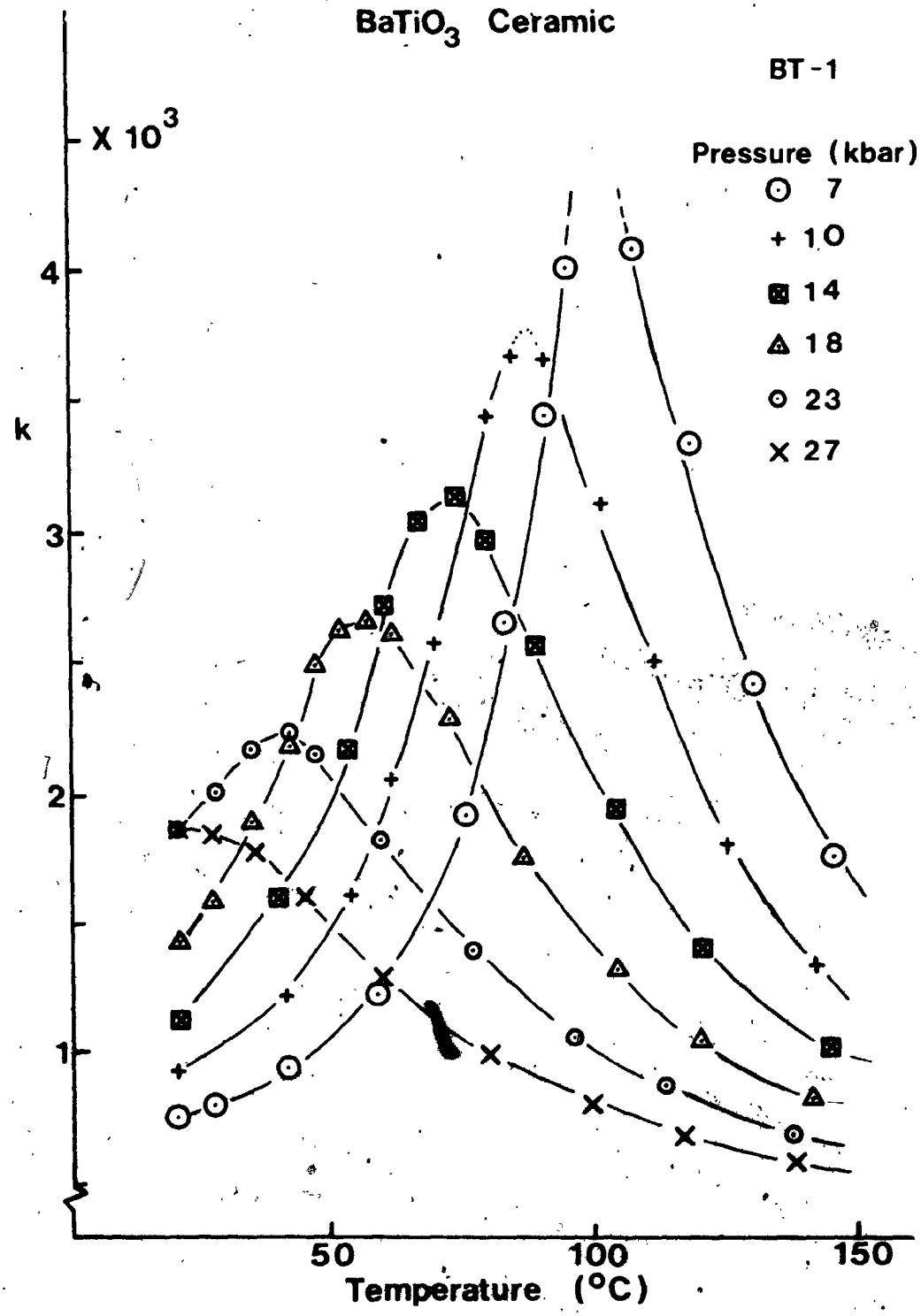

Figure 5.1 : Graph of the temperature dependence of the dielectric constant, k, at various pressures for one of $BaTiO_3$ ceramics (BT-1) in a pyrophyllite matrix.

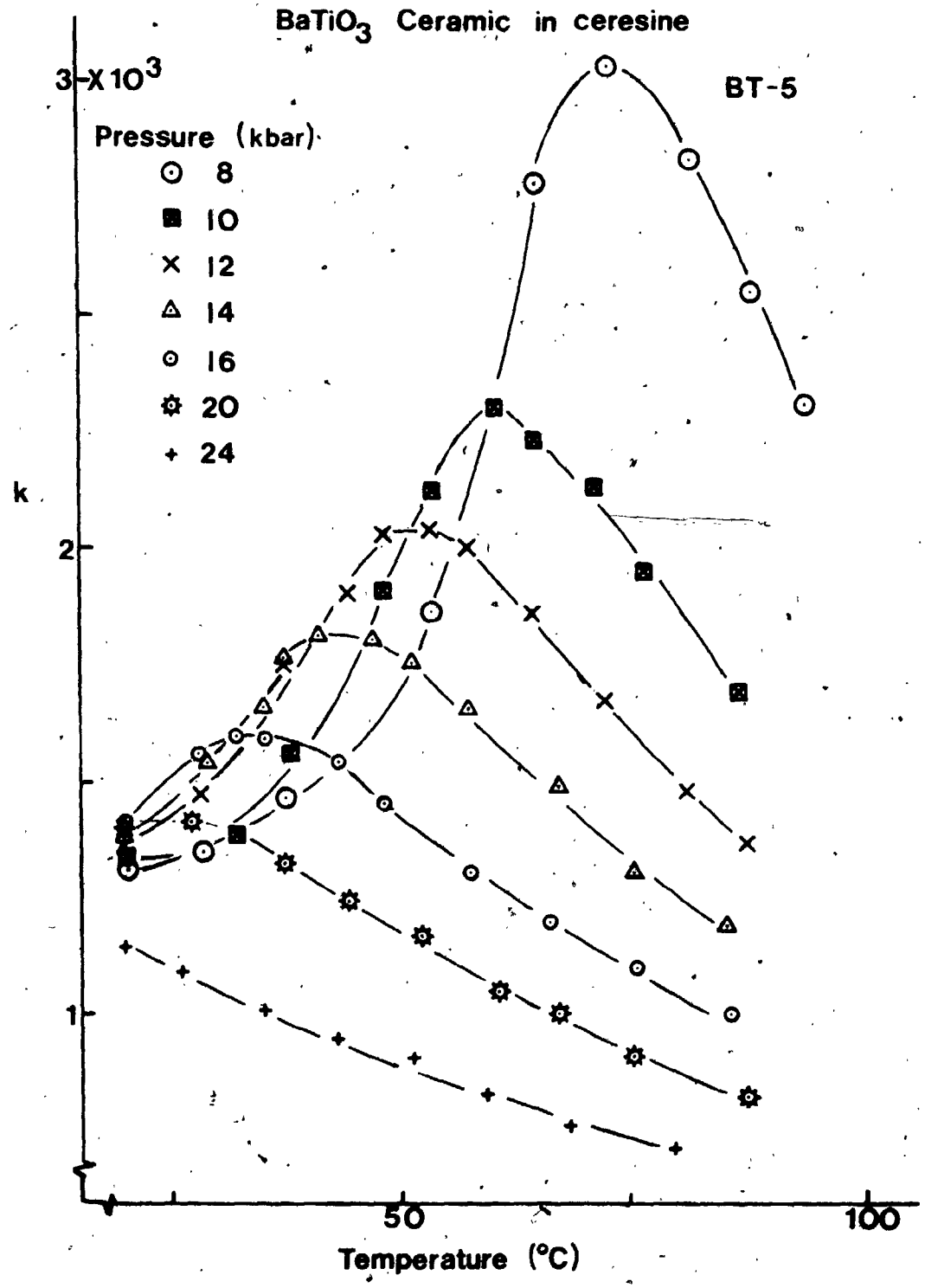

Figure 5.2 : Graph of the temperature dependence of the dielectric constant, k, at various pressures for a $BaTiO_3$ ceramic (BT-5) in ceresine.

variation with temperature. This behaviour is the same as the room pressure behaviour of a FE ceramic with free boundaries; namely, the dielectric constant exhibits a maximum on going through the FE-PE transition (von Hippel, 1954). It appears, therefore, that a polycrystalline FE material which is under high pressure conditions perhaps very similar to those of a planetary interior maintains the peak which is characteristic of a FE transition. In this case, the transition temperature is defined as the temperature of maximum dielectric constant, T*. As evidenced in Figures 5.1 and 5.2, this temperature decreases with increasing pressure.

Although the peaks in the k-T curves remain prominent throughout the investigated pressure range, the general shape of the curves is altered by pressure. Thus, it is important to note that the maximum value of the dielectric constant, k_{max}, decreases with increasing pressure, and the half-width of the k-T distribution curve increases with pressure. Evidently, this 'peak broadening' is not entirely restricted to ceramic samples forming inhomogeneous inclusions since Samara (1966) observed similar behaviour for $BaTiO_3$ ceramics in a fluid-medium press. It would seem, therefore, that this behaviour is characteristic of $BaTiO_3$ in a polycrystalline form. Thus, in seeking an explanation for this behaviour, one must examine the physical make-up of a ceramic material.

In any discussion of polycrystalline ceramic compacts of randomly orientated, anisotropic grains, one must bear in mind that each grain in the compact is subjected to a very complex field of local residual microstresses with, at room pressure, a net zero vector sum of all of the

stresses in the compact. These are an artifact of the sintering and cooling procedures since, in a sintered compact, the boundaries of neighbouring grains are under mutual constraint. Thus, upon cooling following sintering, the full thermal contractive strains are prevented. Moreover, neighbouring grains may be partially joined by welding stresses such that the volume adjacent to the contact for one is under compression, whereas the other is under tension. Furthermore, on cooling through the transition temperature, the paraelectric cubic phase transforms into a tetragonal ferroelectric phase with the polar axis assuming any one of the original cube-edge directions. The developing strain involves an outward movement of the crystal faces perpendicular to the tetragonal c-axis, while those parallel to the c-axis move inward. If the individual grains were not constrained, the full strain would develop, thereby resulting in a stress-free sample. In a polycrystalline compact, however, this motion is impeded by neighbouring grains. Consequently, this modified strain results in stressed grains. This stress may be partially relaxed, however, by 90^{0} domain wall motion which results in a twinned structure. In this case, the polar directions of the domains are distributed over the three original cube-edge directions in such a way as to minimize the energy involved with the spontaneous polarization and the attendant dimensional change (Le Chatelier's principle).

A quantitative estimate of the stresses developed in the direction of the FE-axis and in the plane perpendicular to it has been given for the case of an isolated grain in a BT ceramic (Buessem et al, 1966). Although this calculation demonstrates the significance of constraint, it does not provide an assessment of the effects of alternating

compressive and tensile strains averaged over all grains. An account of the distributions of grain size, shape and orientation is far more complicated and requires the combined application of theories for the elastic, plastic and dielectric properties of inhomogeneous substances. Thus, unlike the case of a single crystal, it is difficult to characterize the dielectric properties of a ceramic, especially its pressure and temperature variations, in relation to a unique, well-defined reference state.

Since each grain in the ceramic has a stress dependent transition temperature, the internal stress distribution for the compact will determine the particular shape of the dielectric constant - temperature curve. The concept of an internal stress distribution in the ceramic can be combined with a suitable model for the dielectric behaviour of each grain to qualitatively explain the experimentally observed high pressure peak broadening (Figures 5.1, 5.2). One such approach is that originally conceived by Diamond (1961) and recently extended by Martirena and Burfoot (1974a, 1974b). This model is based on the idea that the FE grains are mono-domains and that the transition temperatures, T_C, for different grains have values which follow a Gaussian distribution of width α about some conveniently chosen temperature. Each grain is assumed to have a constant value for its dielectric constant below T_C, whereas above T_C the Curie-Weiss law is assumed to hold. Adopting this model, Martirena and Burfoot (1974b) have shown that with increasing values of α the dielectric constant - temperature curve broadens. This is the behaviour which is observed experimentally (Figures 5.1, 5.2). This suggests, then, the value of the α parameter in the distribution model increases with increasing pressure. An explanation for this may be sought in examining the

level and distribution of the internal residual microstresses in the compact. That is, since stresses affect the value of T_C, one would expect the values of α to vary with the range and number of positive and negative microstresses which deviate from the mean value. If this model were correct, it would give us some insight into the pressure variation of the residual microstresses in ceramic compacts. From the experimental results (Figure 5.1, 5.2), one would have to conclude that in a polycrystalline aggregate, both the magnitude and range of the residual microstresses increase with increasing pressure.

Figure 5.3 shows the isobaric changes of the dissipation factor, D, for the same sample and under the same experimental conditions as that shown in Figure 5.1. In general, with increasing pressure at constant temperature, D decreases. However, with increasing temperature at constant pressure, the D values exhibit a slight maximum, then decrease to a constant value of ~.004. This temperature dependence agrees well with that measured on $BaTiO_3$ ceramics at room pressure by Westphal (reported by von Hippel, 1954). Thus, pressure does not alter the general characteristics of the isobaric D-T curves, but it shifts them towards lower temperatures. This corresponds to the observed shift in T* with pressure. The reason for the lower loss in the paraelectric phase may be sought in the fact that, above the transition, there is no pre-existing domain pattern to overcome. Thus, since the dielectric losses are almost entirely domain wall losses (Jaffe et al, 1971), a decrease in the dissipation factor is expected at the transition.

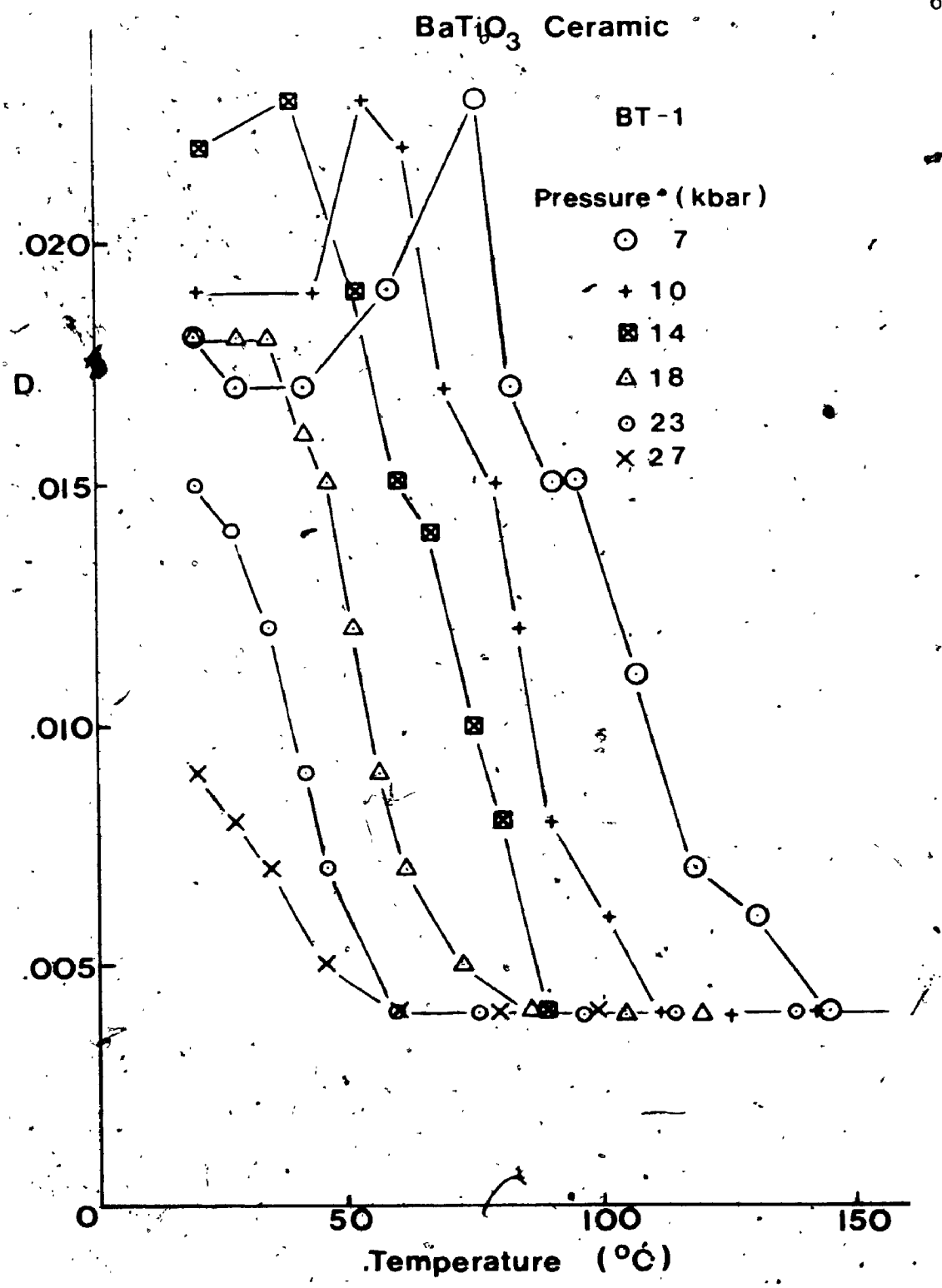

Figure 5.3 : Graph of the isobaric variation of the dissipation factor, D, with temperature for the $BaTiO_3$ ceramic shown in figure 5.1 (BT-1).

To supplement the dielectric measurements of barium titanate ceramics, a number of experimental runs were performed in which the remanent polarization, P_r, and coercive field, E_c, were measured as a function of temperature and pressure. In this case, the polarization and coercive field were obtained from the FE hysteresis loop of the $BaTiO_3$ sample. These were displayed on the screen of an oscilloscope by means of a Sawyer-Tower circuit (see section 4.4). The results of these experiments are presented in Figures 5.4 and 5.5.

Figure 5.4 shows the effect of pressure on the general shape and behaviour of the FE hysteresis loop of a barium titante ceramic sample embedded in a pyrophyllite matrix subjected to a large external pressure. This figure shows a series of hysteresis loops which are photographic records of the oscilloscope screen. From this figure it is evident that with increasing pressure, the FE hysteresis loop closes, and for a pressure of ~20 kbar at room temperature, the FE hysteresis is evidently lost. It is interesting to note that for all pressures, the loop retains its symmetry characteristics.

Figure 5.5 shows the temperature dependence of the remanent polarization, P_r, of a $BaTiO_3$ ceramic for various isobaric conditions. In all cases, the polarization tends to zero with increasing temperature as the transition temperature is approached. It is known that in this relatively low pressure region, the FE-PE transition for BT is a first order transition (Samara, 1971). This should involve a distinct discontinuity in the spontaneous polarization at the transition temperature. A sudden drop of the value of polarization has been observed on measure-

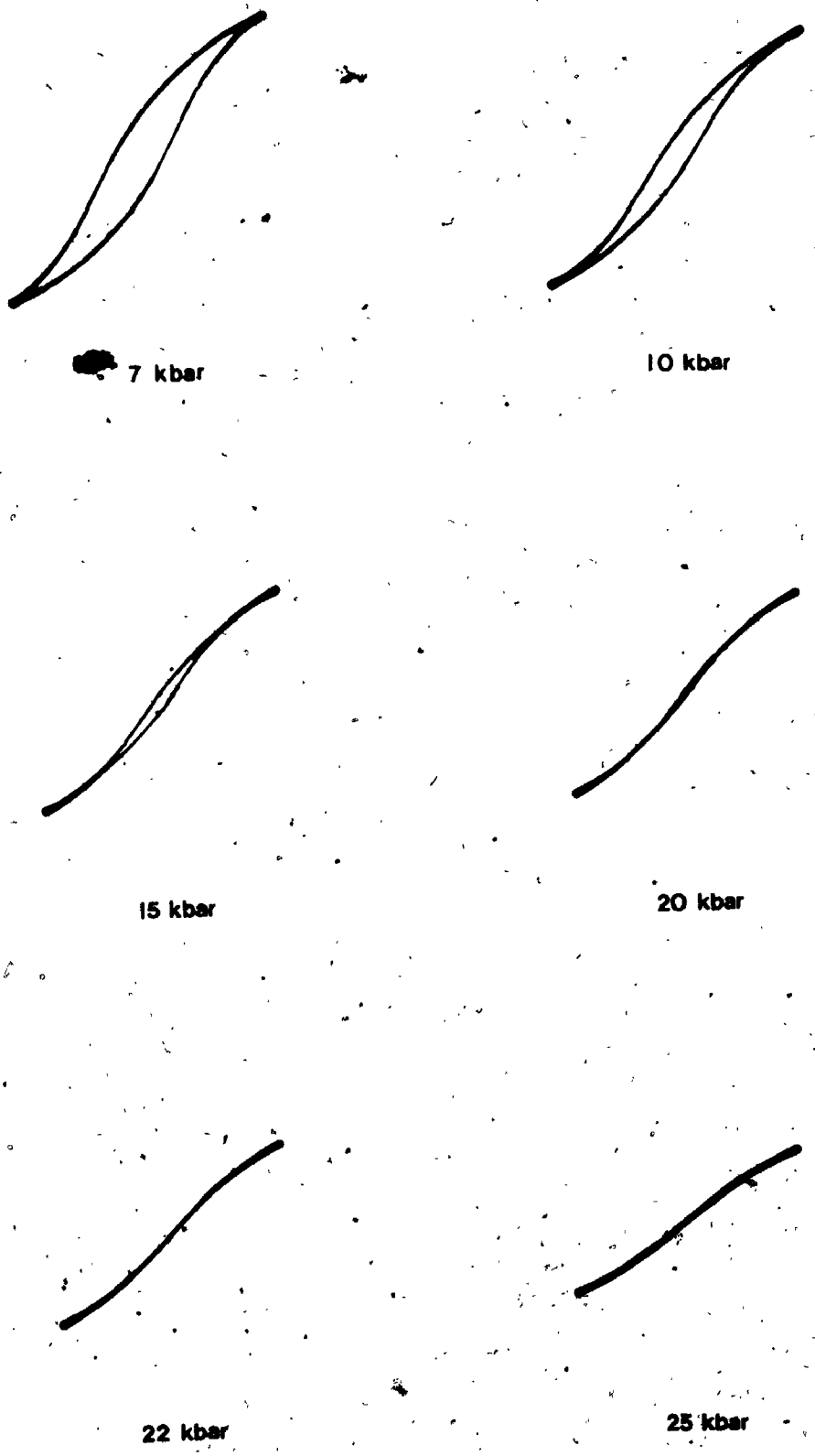

Figure 5.4 : Photographic records of the FE hysteresis loops of $BaTiO_3$ ceramic (BT-3) at room temperature and various pressures.

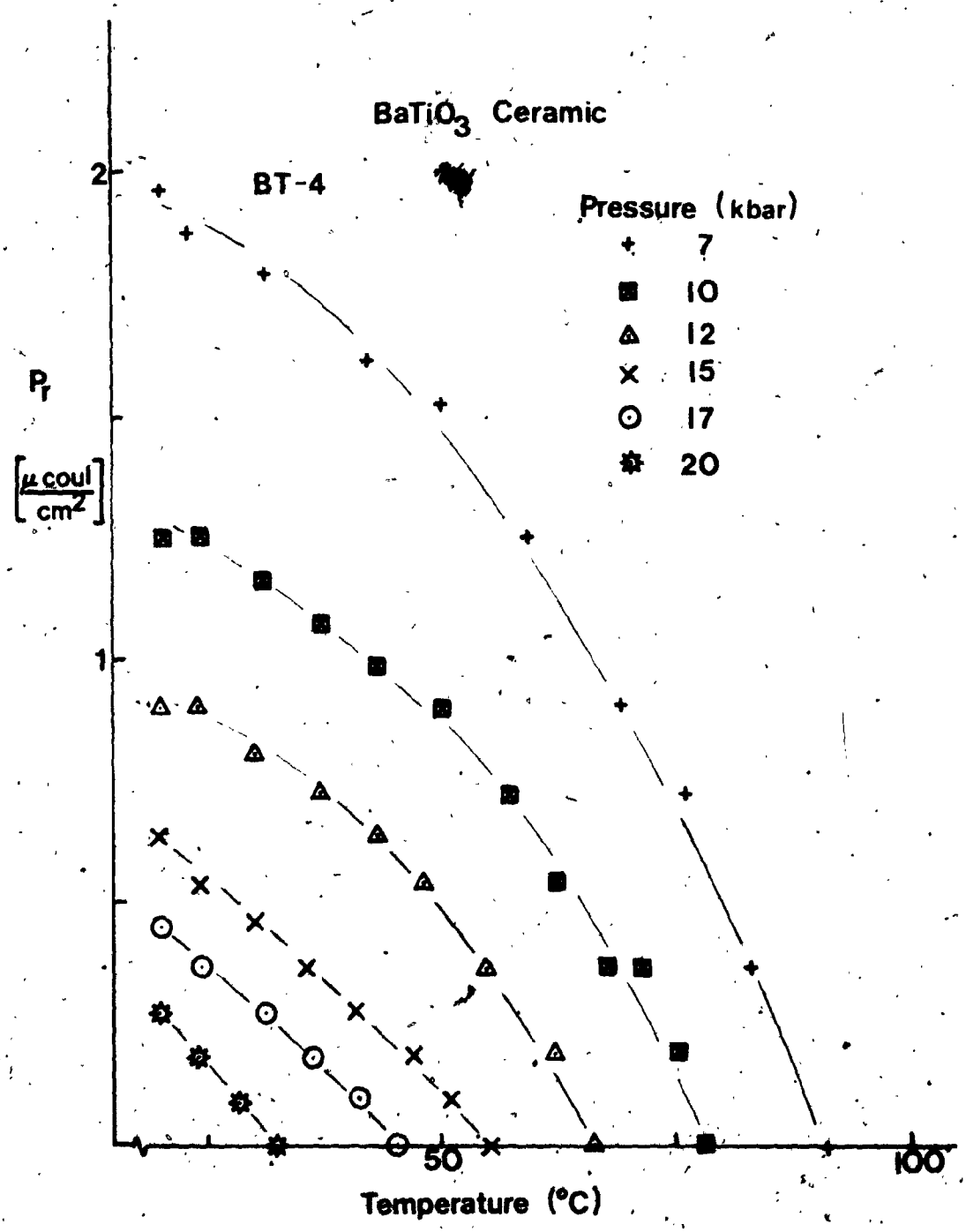

Figure 5.5 : Graph of the isobaric changes in remanent polarization, P_r, with temperature for $BaTiO_3$ ceramic BT-4.

ments made on BT single crystals under fluid-media pressure conditions (Samara, 1966). In the case of polycrystalline BT in a solid pressure medium, however, it is evident that the polarization goes continuously to zero with no sharp or apparent discontinuity. This behaviour is reasonable for ceramic specimens since individual grains in the aggregate are under different stress-strain conditions. Consequently, the sharp discontinuity is obliterated by the broad distribution in T_C and corresponding P_S values.

5.3 The p-T Stability Field of $BaTiO_3$ Ceramics under Constraint

To obtain values for the transition temperature for the FE-PE transition for various pressure settings, the polarization-temperature curves (as in Figure 5.5) were extrapolated to the P = 0 axis. These temperature values were then plotted as a function of pressure to obtain the phase diagram shown in Figure 5.6. Included in this figure is the phase boundary determined by Samara (1966) for hydrostatic pressure conditions. For the present hysteresis loop observations, the transition temperature was taken as the temperature at which the hysteresis loop closes, i.e. $P_r = 0$. It is estimated that this temperature can be determined to an accuracy of $\pm 2^{o}C$.

In addition to the values of the transition points obtained by hysteresis loop observations (Samples No. BT-3, BT-4), those obtained by dielectric constant measurements of BT ceramics (Sample No. BT-1, BT-2, BT-5) are also indicated in Figure 5.6. In this case, the transition temperature for each pressure profile was taken as the temperature of maximum dielectric constant along that profile. These values

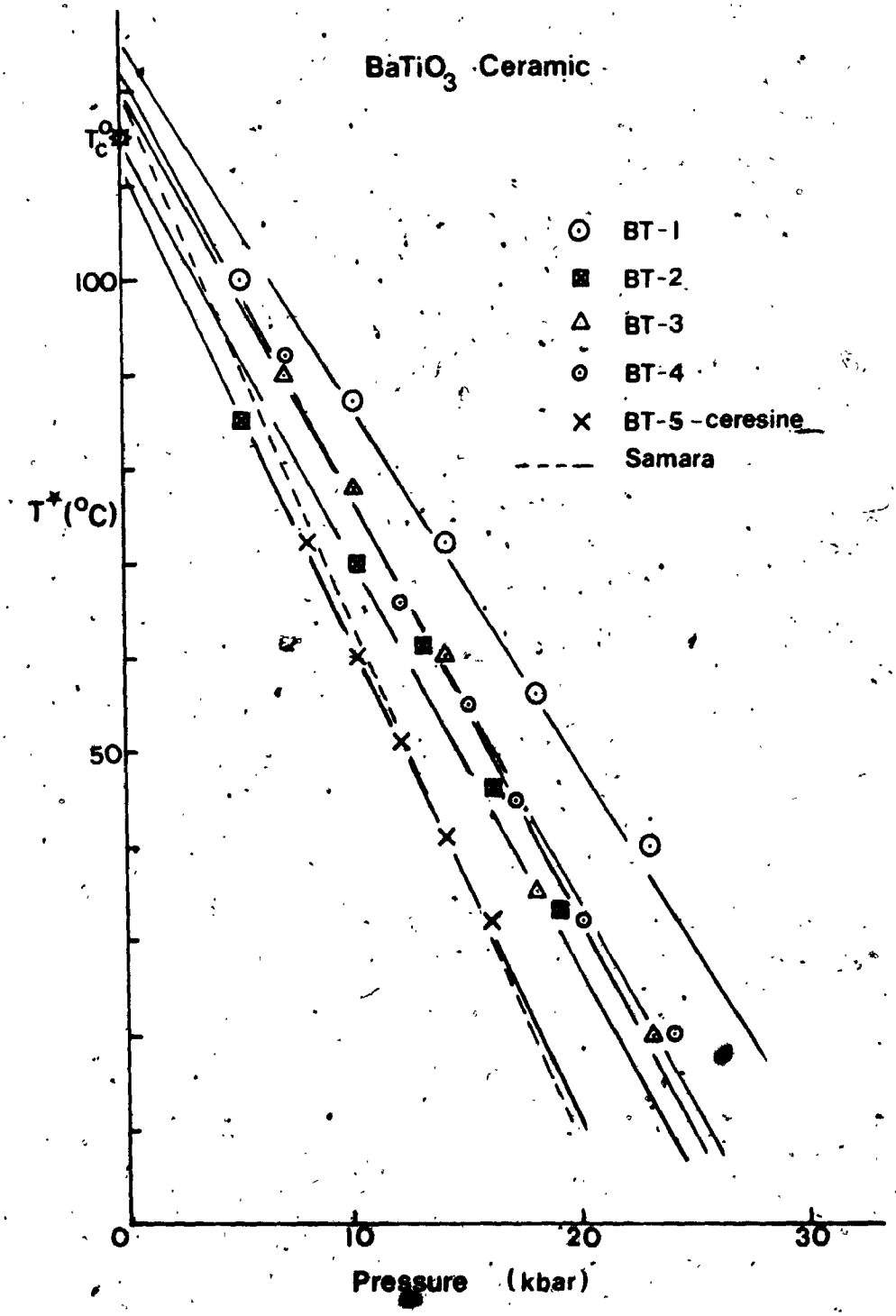

Figure 5.6 : Graph of the change in T* with pressure for each of the $BaTiO_3$ ceramics investigated. Included in the figure is Samara's (1966) phase boundary determined for hydrostatic pressure conditions.

are estimated to be accurate to $\pm$ 5^{o}C. This large an uncertainty is due to the relatively flat nature of these curves about the transition, especially in the higher pressure region. Nevertheless, this accuracy is sufficient to determine the general behaviour of the transition temperature with pressure.

In Figure 5.6, the variation of the FE-PE transition temperature for BT ceramics as inhomogeneous inclusions is shown as a function of pressure for all of the BT ceramic samples investigated. The transition points obtained by the two independent techniques used in the present experiments are in good agreement with one another. Within experimental accuracy, the transition temperature decreases linearly with pressure. The small differences in the temperature values extrapolated to zero pressure could reflect the inherent difficulties in measurement of absolute temperature in solid-media high pressure devices (Hall, 1964). These difficulties, however, should have little effect on the relative temperature values. A linear regression analysis on the data indicates that the transition temperature changes with pressure at a rate of -3.8^{o}C/kbar (#BT-1), -4.3^{o}C/kbar (#BT-2), -4.6^{o}C/kbar (#BT-3), -4.3^{o}C/kbar (#BT-4) and -5.0^{o}C/kbar (#BT-5). These values are listed in Table 5T-1. A similar spread in dT*/dp values has also been observed for BT single crystals and ceramics (-4.6 to -5.9^{o}C/kbar, Samara, 1966, 1969), PZT-4 ceramics (-4.4 to -4.8^{o}C/kbar, Timco and Schloessin, 1975b, 1976a) and PZT-5H ceramics (-3.9 to -4.6^{o}C/kbar, Timco and Schloessin, 1976b, 1976c). This variation from sample to sample may be partly due to the presence of impurities, domain structure and small deviations from hydrostatic stress conditions realized by the sample (Samara, 1966).

Table 5T-1

Ceramic	Sample No.	(dT*/dp) (^{o}C/kbar)	Determined by
$BaTiO_3$	BT-1	-3.8	k-T curves
$BaTiO_3$	BT-2	-4.3	k-T curves
$BaTiO_3$	BT-3	-4.6	P_r-T curves
$BaTiO_3$	BT-4	-4.3	P_r-T curves
$BaTiO_3$ (in ceresine)	BT-5	-5.0	k-T curves
$BaTiO_3$	Average	-4.4	

From Figure 5.6 it is evident that, as predicted in Chapter 3, the elastic incompatability between the matrix and inclusion influences the stability field of the FE phase of the ceramic specimen. It is evident that the results obtained on the ceramic in the ceresine envelope ($dT^*/dp = -5.0^oC/kbar$; BT-5) are in better agreement with Samara's (1966) hydrostatic results on BT ceramics ($dT^*/dp = -5.1^oC/kbar$) than those obtained on samples constrained by a pyrophyllite matrix ($-3.8^oC/kbar$, BT-1; $-4.3^oC/kbar$, BT-2; $-4.6^oC/kbar$, BT-3; $-4.3^oC/kbar$, BT-4). Presumably the mechanically softer ceresine provides less of a constraint and acts to modify the stress differences, thereby providing a greater degree of hydrostaticity. In any event, it is clear that the stability field for a polycrystalline aggregate constrained as an inhomogeneous inclusion under high pressure conditions is extended to pressures above those for an isolated free BT ceramic under pressure.

One can view the observed decrease of the phase boundary with pressure (Figure 5.6) in terms of the lattice strains involved with the transformation. At the PE-FE transition, the cubic unit cell elongates along the c-axis and contracts along the a-axes with a resulting net increase (~1%) of the unit cell volume. Since pressure favours the smaller volume, a decrease in the transition temperature with pressure is expected and observed.

One can make use of the apparent difference in dT^*/dp values between the 'free' hydrostatic case (Samara, 1966) and the 'constrained', quasi-hydrostatic case to estimate numerically part of the difference in elastic strain energy between them (Chapter 3). In doing so, one is able to obtain a reasonable estimate of the deviatoric stresses in a solid-

medium high pressure apparatus. It should be emphasized at the outset, however, that due to the complexity of the problem, several simplifications and assumptions must necessarily be made. Nevertheless, in calculating this energy, several informative features on the nature of the phase transition under constraint are revealed.

From equation (3.6), the change in the elastic energy of the system in the case of high pressure constraint is given by

$$\Delta\xi_{tot} = \xi^{t}_{inc} + \xi_{int}$$

$$= \xi^{t}_{inc} - \int X^{A}_{i}\, x^{T}_{j}\, dv \qquad (5.1)$$

where ξ^{t}_{inc} is defined in equation (3.5), X^{A}_{i} is the applied stress and x^{T}_{j} is the stress-free transformational strain. If one considers that the applied stress field is primarily hydrostatic (X^{h}_{i}) with small deviatoric stresses (X^{d}_{i}) superimposed, equation (5.1) becomes

$$\Delta\xi_{tot} = \xi^{t}_{inc} - \int X^{h}_{i}\, x^{T}_{j}\, dv + \xi_{d} \qquad (5.2)$$

where ξ_{d} is

$$\xi_{d} = -\int X^{d}_{i}\, x^{T}_{j}\, dv \qquad (5.3)$$

It is clear that there is no analogous term to ξ_{d} in the change in elastic energy for a sample in a hydrostatic pressure system. It is this term ξ_{d} which can be calculated. Thus, the problem at hand involves determining the strain of the FE→PE transition, and the attendant deviatoric stress field generated by an elastic (plastic) incompatability between the matrix and inclusion.

To determine the volume strain upon transformation, one must necessarily use the values for the FE-PE transformation in a free single crystal. This tacitly implies that at the transition, the ceramic as a whole behaves in a generalized manner similar to a single crystal. Kay and Vousden (1949) have determined that at the FE-PE transition, the dimensions of the unit cell change such that the length of the c-axis decreases from 4.022 Å to 4.009 Å; whereas the length of the a-axes increase from 4.0045 Å to 4.009 Å. Thus, at the transition the stress-free transformational strain ($x_1^T = x_2^T = .0045/4.009$; $x_3^T = -0.13/4.009$) results in a decrease in the volume of the unit cell of $(\Delta V)_f = -.064$ Å^3.

To estimate the deviatoric stresses, it would seem reasonable to treat the situation in terms of any differences in transformational volume strain between the two cases. For a first order transition, the discontinuous volume change (ΔV) is related to the change in transition temperature with pressure by the Clausius-Clapeyron equation (see, for example, Samara, 1969)

$$\frac{\Delta T}{\Delta p} = T_c^o \frac{\Delta V}{Q} \qquad (5.4)$$

where T_c^o is the room pressure transition temperature and Q is the latent heat of the transformation. If one assumes that T_c^o and Q are the same for both the free and constrained cases, then the difference in the observed dT^*/dp values for the two cases (Figure 5.6) can be attributed solely to the difference in elastic strain. Thus, it follows that

$$(\Delta V)_c = (\Delta V)_f \left[\frac{(\Delta T/\Delta p)_c}{(\Delta T/\Delta p)_f} \right] \qquad (5.5)$$

where the subscripts f and c represent the free and constrained cases respectively. Using the average $(dT^*/dp)_c$ value determined for a pyrophyllite matrix (-4.3°C/kbar), and Samara's (1966) result of $(dT^*/dp)_f$ = -5.1°C/kbar, the volume change at the FE-PE transition for the case of constraint is calculated to be $(\Delta V)_c$ = -.054 $\AA^3$ /unit cell. Thus, this net volume change is smaller than that for the free case by $(\Delta V')$ = .010 $\AA^3$/ unit cell.

One can view this situation as being caused by a deviatoric stress which is determined by the shape of the FE inclusion and the orientation of its axis of polarization. In reality, this stress field may be quite complex. For the purpose of this calculation, however, one can consider the stress field acting on a single crystal which would produce the differential volume change $(\Delta V')$ as a result of the phase transition. It is known that the spontaneous strains which are associated with the FE transition may be characterized by a shape parameter (c/a-1) whose temperature dependence is closely related to the P_s^2 - T curve (Megaw, 1973). The experimental observation that the p-T stability field is extended in the case of constraint (Figure 5.6) would suggest that constraint increases the c/a ratio of $BaTiO_3$, thereby maintaining the deviations from isotropy to higher pressures. It seems reasonable to interpret this situation as the result of a compressive deviatoric stress acting in the a, b plane of the crystal. As such, the problem is now reduced to finding the value for a planar stress X_1^d which would result in a volume decrease of -.010 $\AA^3$/unit cell. In this case, the strain x_1' in terms of the deviatoric stresses is given by (see, for example, Cady, 1964)

$$x_1' = S_{11} X_1^d + S_{12} X_2^d + S_{13} X_3^d \qquad (5.6)$$

where S_{11}, S_{12} and S_{13} are the elastic compliances. Now, if one assumes that $X_1^d = X_2^d$ and $X_3^d = 0$, and that the strain is taken up in the a, b plane only, equation (5.6) becomes

$$X_1^d = \frac{1}{S_{11} + S_{12}} x_1' \qquad (5.7)$$

Thus, using $S_{11} = 8.33 \times 10^{-13}$ cm^2/dyne and $S_{12} = -2.68 \times 10^{-13}$ cm^2/dyne (Jona and Shirane, 1962), this deviatoric stress is calculated to be $-.14 \times 10^9$ dynes/cm^2 (.14 kbar).

Then the energy ξ_d (equation 5.3) associated with the PE-FE transition in the case of constraint is

$$\xi_d = -\sum X_i^d x_j^T \qquad (5.8)$$

$$= -4 X_1^d x_1^T - 2 X_1^d x_3^T$$

$$= 1.1 \text{ J/mole}$$

Thus, this energy represents part of the elastic energy change on transformation from the PE→FE state for the case of BT under constraint. As previously pointed out, this elastic energy term is unique to the case of constraint. It should be re-emphasized, however, that in addition to this term, the contributions from all of the other energy terms are required in order to calculate the total free energy change associated with the transition.

It is of interest to note that as demonstrated in the above calculation, a (planar) deviatoric stress of magnitude ~.14 kbar

perpendicular to the axis of the sample disc can explain the observed extension in the p-T diagram for the FE phase (Figure 5.6). Although the estimate of the magnitude of this field is undoubtedly too small, a deviatoric stress field of this type seems reasonable. For example, Lees and McCartney (1968), from their experiments on the piezoresistance effect in n-type silicon determined the same type of deviatoric stress field in a multi-anvil tetrahedral-type press. In their case, they estimate the stress differences to be on the order of 1 kbar. In addition, Forsbergh (1954) determined experimentally that a two-dimensional stress perpendicular to the c-axis of a BT single crystal results in an increase in the transition temperature of the sample. Forsbergh found that the increase in T_C varies quadratically with the two-dimensional pressure according to

$$T_C = T_C^o + 3.1 \times 10^{-5} p^2 \qquad (5.9)$$

where p is the oil pressure in atmospheres. It seems reasonable to conclude, therefore, that a sample which experiences such a two-dimensional stress superimposed as a deviatoric stress on hydrostatic pressure conditions (i.e. the present case) would have a higher transition temperature than that of a sample under the same mean value of hydrostatic pressure alone (i.e. Samara's case). Then, the p-T stability field of the FE phase would be extended as observed (Figure 5.6). As such, it would seem reasonable to anticipate that for stress differences in solid-media on the order of the yield strength of the matrix (~1-2 kbar), the stability field for a single crystal may be greatly extended.

5.4 Single Crystal Hysteresis Loop Studies

Having observed that perovskites in polycrystalline form not only exhibit FE hysteresis under constrained, high pressure conditions, but remain extremely well behaved, it is of interest to detail the high pressure behaviour of BT in single crystal form under similar stress-strain conditions. In particular, the basic question of the existence of a FE hysteresis loop for a perovskite-structure single crystal in a matrix needs to be established. Previously it has been shown that FE hysteresis is possible in soft, hydrogen bonded, order-disorder type ferroelectrics (tri-glycine sulphate) which are constrained by a matrix under pressure (Timco, 1974, 1975; Timco and Schloessin, 1974). However, no evidence exists for a displacive-type transformation under the same conditions. To this end, several experiments were performed on single crystal specimens of barium titanate.

For these experiments, small irregular shaped fragments, usually triangular shaped thin wedges (edge length ~.3 cm; thickness ~.03 cm) were broken from a larger mother crystal which had a "butterfly wing" morphology. These fragments were electroded with silver paint and placed in a ceresine envelope in the high pressure cell. It was found that if the initial pressure application was sudden (i.e. if the hydraulic rams were advanced by means of an electric pump), the electrical connection to the crystal would be severed. Consequently, it was necessary to advance the rams manually by means of a hand pump. Of the five experiments attempted, FE hysteresis was observed in two of them.

2 3

OF/DE

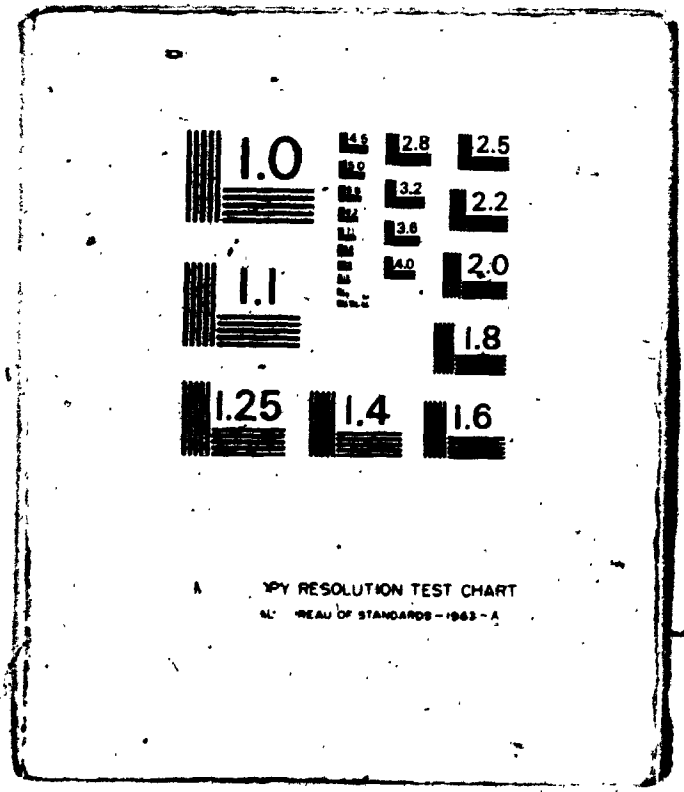
1.0
1.1
1.25
1.4
1.6
2.8
2.5
3.2
2.2
3.6
2.0
4.0
1.8
RESOLUTION TEST CHART
BUREAU OF STANDARDS-1963-A

Figure 5.7 shows a photographic record of a FE hysteresis loop for single crystal barium titanate (#B4C) under a pressure of 4 kbar in a solid-medium high pressure apparatus. It is evident that FE hysteresis is indeed attainable in single crystal perovskites constrained under high pressure conditions. At this point it should be emphasized, however, that both the degree of clamping and the exact nature of the applied stress will affect the existence or non-existence of any ferroelectric behaviour. It has been shown, for example, that FE hysteresis in Rochelle salt, a soft, hydrogen-bonded FE is not possible under conditions where switching in FE tri-glycine sulphate is still observable (Timco, 1974, 1975). Moreover, recent experiments by Clarke (1976) have indicated that it is not possible to reverse the spontaneous polarization of a BT crystal embedded in an epoxy cylinder under pressure. This suggests that for FE behaviour to be possible, there is a critical coupling between the elastic compatibility of a FE crystal with its surrounding medium.

Figure 5.8 shows photographic records of the effect of increasing pressure at room temperature on the general shape and overall behaviour of $BaTiO_3$ crystal B4C. This represents the second pressure profile on this crystal. It is evident that the polarization increases slightly with pressure, then decreases, passing through a broad maximum in the pressure range around 25 kbar. For this run, the hysteresis loop remains prominent to the highest pressure investigated (49 kbar). This general behaviour was not observed on the initial profile on this sample. In this case, the polarization was seen to increase sharply with initial loading of the press, then decrease slightly, followed by a further

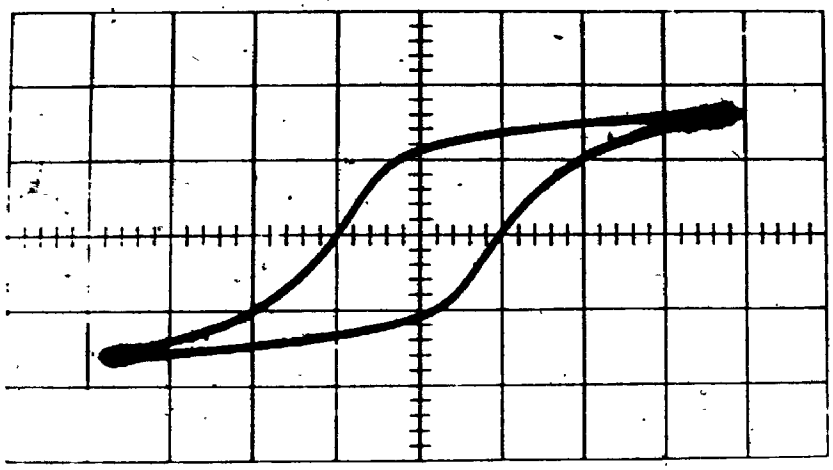

Figure 5.7 : Photographic record of the FE hysteresis loop of $BaTiO_3$ single crystal B4C at p=4kbar.

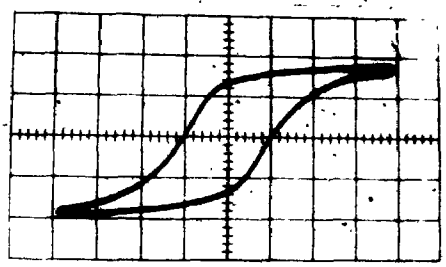

4 kbar

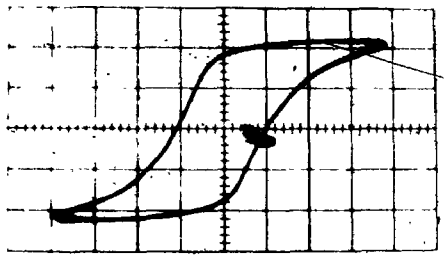

17 kbar

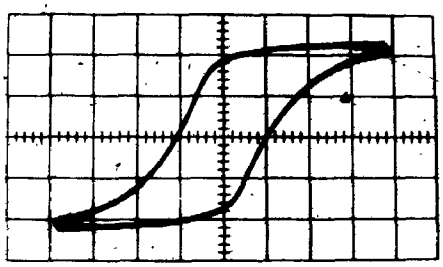

25 kbar

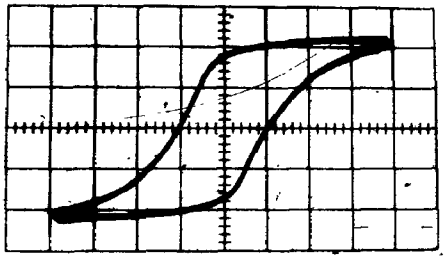

34 kbar

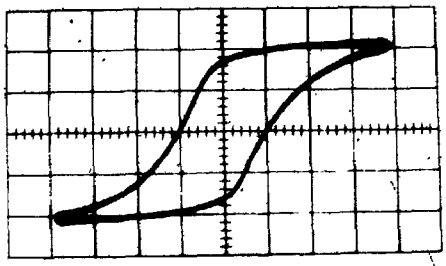

42 kbar

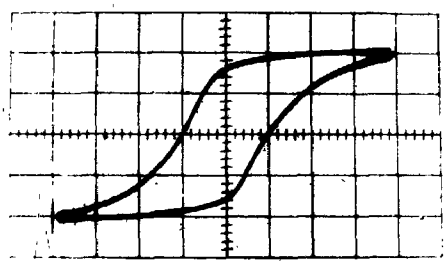

49 kbar

Figure 5.8 : Photograph records of the FE hysteresis loops of $BaTiO_3$ single crystal B4C at room temperature for increasing pressure.

increase to a relatively pressure independent shape in the region of 15 to 26 kbar. Above this pressure, the polarization decreased, and the loop disappeared at a pressure of ~40 kbar. Although no photographic records were taken on this profile, the relative polarization and coercive field values were recorded from the oscilloscope screen. These values are shown for all samples in Figures 5.9 and 5.10 respectively.

Figure 5.11 shows the response of crystal B4C to the release of pressure after the second pressure profile for this sample. Clearly the behaviour shown in this figure is not the reverse of that obtained on increasing pressure (Figure 5.8). In this case, the polarization decreased with decreasing pressure to ~9 kbar whereupon it slightly increased. For all pressure profiles for crystal B4C, the hysteresis loop remained both symmetrical and non-distorted.

Figure 5.12 shows the behaviour of the FE hysteresis loop of another $BaTiO_3$ crystal (#B5C) with increasing pressure on the first pressure profile for this sample. In this case, both the polarization and coercive field decreased with increasing pressure until the eventual closure of the loop at ~45 kbar. With release of pressure, the loop did not recover, even after two days at a pressure of 4 kbar. Consequently, no further profiles were obtained for this sample.

It is evident from examination of Figures 5.8 to 5.12 that the general high pressure behaviour of BT single crystals not only differ from sample to sample, but also for different pressure profiles. In addition, as evidenced on the first run of #B4C, the behaviour may be erratic along any one individual profile. These differences may be ascribed to the deviations from hydrostatic pressure conditions realized

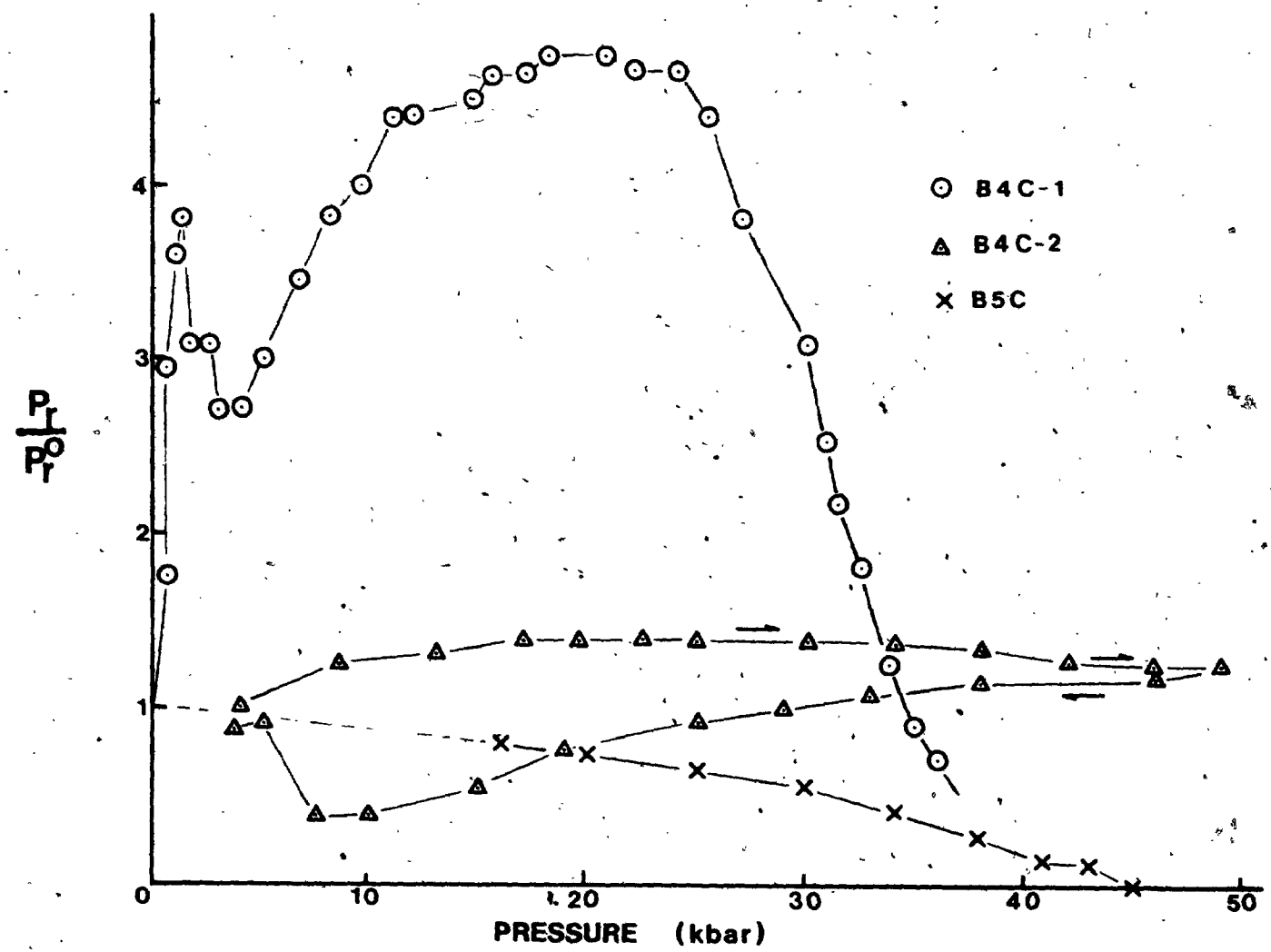

Figure 5.9 : Graph of the relative change in remanent polarization for $BaTiO_3$ single crystals B4C (first and second runs) and B5C at room temperature.

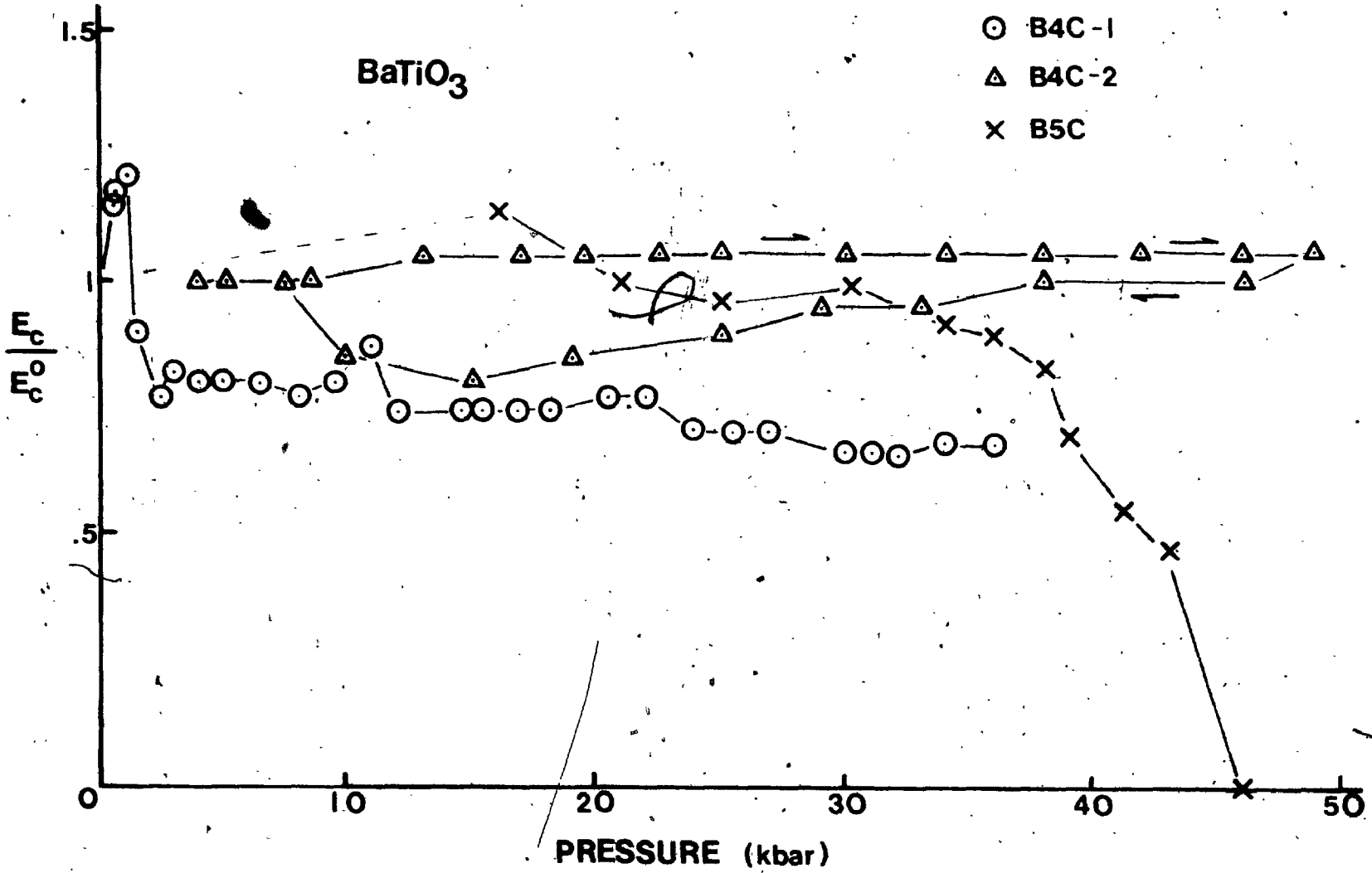

Figure 5.10 : Graph of the relative change in coercive field for $BaTiO_3$ single crystals B4C (first and second runs) and B5C at room temperature.

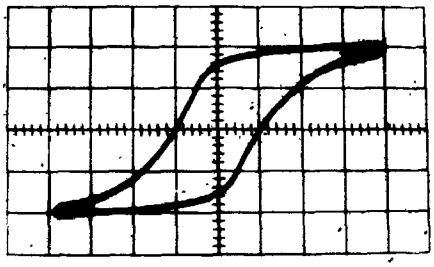

46 kbar

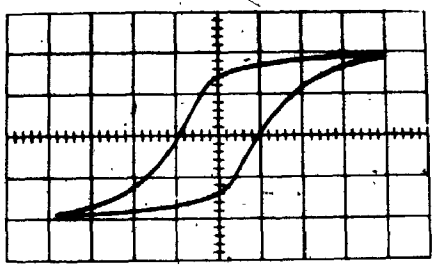

33 kbar

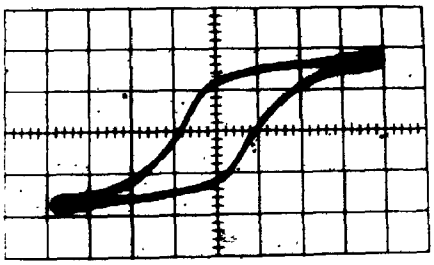

25 kbar

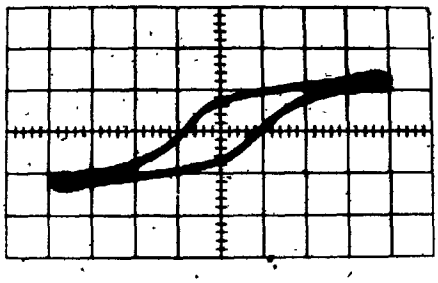

15 kbar

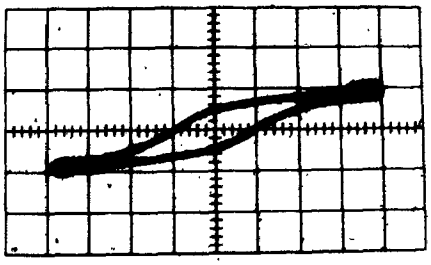

8 kbar

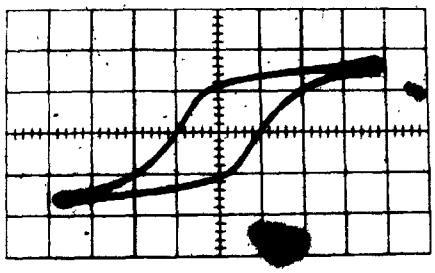

4 kbar

Figure 5.11: Photographic records of the FE hysteresis loops of $BaTiO_3$ single crystals B4C at room temperature for decreasing pressure.

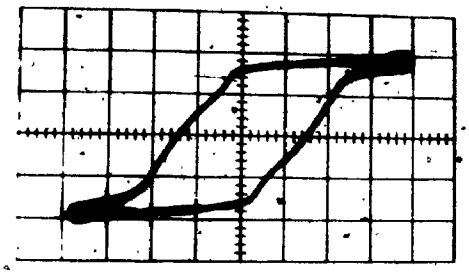

16 kbar

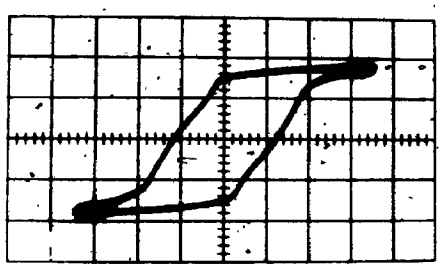

21 kbar

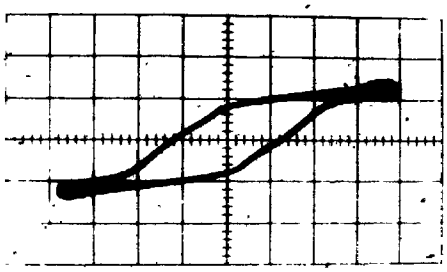

34 kbar

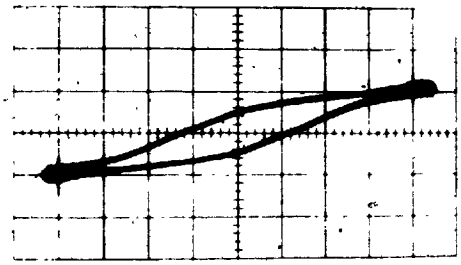

38 kbar

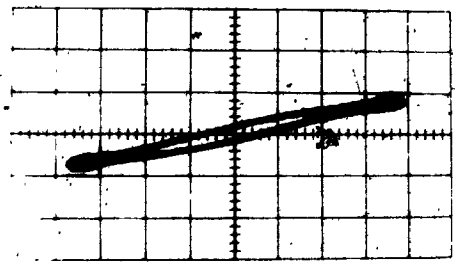

43 kbar

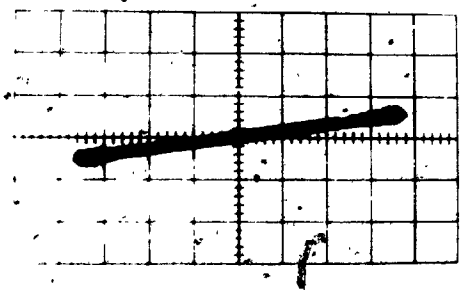

49 kbar

Figure 5.12 : Photographic records of the FE hysteresis loops of $BaTiO_3$ single crystal B5C at room temperature for increasing pressure.

by the sample. It would seem that for these irregular shaped, thin wedge specimens, the attending deviatoric stress field would be far more severe than that for a disc shaped polycrystalline specimen. The general high pressure behaviour of these crystals (Figure 5.9) as well as the apparent distortions of the FE hysteresis loop of sample no. B5C (Figure 5.12) would attest to this. A much more startling feature than this, however, is the persistence of the FE behaviour to very much higher pressures than anticipated. That is, high pressure studies on BT single crystals under (fluid-media) hydrostatic systems (Samara, 1966, 1969) have indicated that the FE-PE transition temperature decreases with increasing pressure. Therefore in the case of an isolated free crystal of $BaTiO_3$ at purely hydrostatic pressure conditions, the FE transition would be displaced below room temperature for a pressure of ~18 kbar (Samara, 1966). Because of this, the FE hysteresis loop would no longer be observable at room temperature for pressures above that value. In the case of constraint, however, the FE hysteresis loops for single crystal specimens persist to very much higher pressures-up to 49 kbar! This result is striking evidence for the conclusion reached on theoretical grounds (Chapter 3) that the properties of a composite system may be far more complex than that of the isolated case. In particular, it is apparent that the FE state in a crystal which constitutes an inhomogeneity can have a drastically modified stability field. A similar, but not as pronounced a modification in the p-T stability field has also been observed and discussed in detail for BT ceramic specimens (section 5.3).

5.5 General Discussion

The existence of the FE hysteresis loop for both BT single crystals and ceramics has significant consequence when interpreted in terms of FE phases forming in planetary interiors. Under the test conditions, at the 10-50 kbar level, both matrix and inclusion are in the fully plastic range, and sample pressures are very close to hydrostatic. The deviatoric stresses associated with the misfit between the transforming inclusion and matrix, therefore, should be of the same order of magnitude as those likely to be encountered by minerals undergoing FE phase transitions in the earth's mantle. It would seem, therefore, that the testing conditions were indeed very similar to the actual conditions under which a FE phase would form in a planetary interior. Clearly, the results show that FE hysteresis is possible under these types of conditions.

The results of the experiments further suggest that the behaviour and existence (or non-existence) of a FE material will strongly depend not only on the dielectric and elastic compatibility contrast between the FE inclusion and its surrounding medium, but also on the nature and physical form of the material. As such, a FE phase may form or be extended into a p-T region in a planetary interior which, based upon our experience with FE materials under hydrostatic pressure conditions would be outside the 'ordinary' ferroelectric stability range of the material.

CHAPTER VI

POLYCRYSTALLINE LEAD ZIRCONATE-TITANATE

6.1 General Properties of the $Pb(Zr,Ti)O_3$ System

In 1954, Jaffe and co-workers found that solid solution ceramics which are based on the lead zirconate-titanate system (Figure 6.1; Sawaguchi, 1953) exhibit strong piezoelectric properties when they are cooled in a large electric field (i.e. when they are electrically poled). Since then, the detailed physical properties of these ceramics, including their relative polarization, dielectric constant, piezoelectric constants and elastic compliances have been thoroughly studied in order to determine their suitability as piezoelectric transducers. One important finding of this research was that even slight amounts of chemical additives could drastically alter the physical characteristics of the ceramic. For example, substitution of a penta-valent ion in the B-site of the lattice (donor doping) would greatly enhance the dielectric constant of the ceramic. On the other hand, subsitution of a tri-valent ion in the B-site (acceptor doping) would result in a decrease in both the dielectric constant of the ceramic, and its sensitivity to external stresses (Jaffe et al, 1971). As such, ceramics based on the $Pb(Zr,Ti)O_3$ system are now being marketed with specific chemical additives which are designed to enhance various physical properties. Currently, these compounds are the dominant transducer materials in the frequency range to a few MHz.

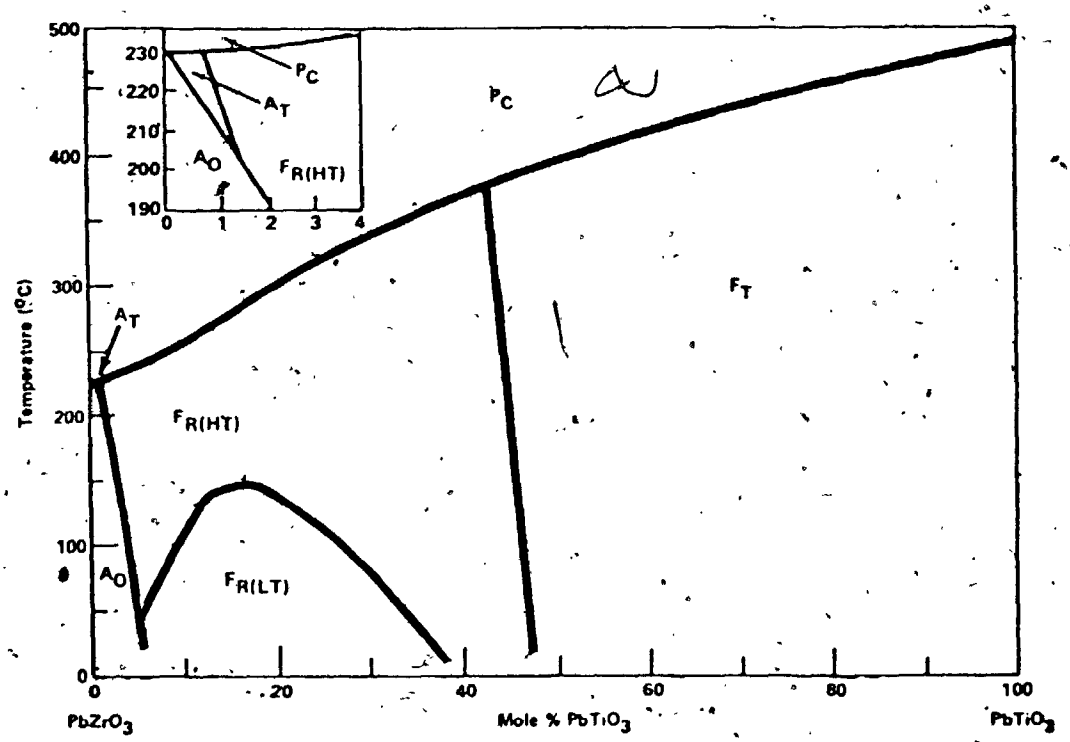

Figure 6.1 : $PbZrO_3$-$PbTiO_3$ phase diagram showing the stability regions for the paraelectric phase (P_C-cubic), ferroelectric phases (F_T-tetragonal, F_R-rhombohedral) and anti-ferroelectric phases (A_T-tetragonal, A_O-orthorhombic), (after Sawaguchi, 1953; Jaffe et al, 1971).

The $Pb(Zr,Ti)O_3$ system was chosen for study in the present experiments for several reasons. First of all, the Curie temperatures of these ceramics (typically ~300°C) are much higher than that of barium titanate. This, therefore invites utilization of the full pressure range (up to ~55 kbar) available with the cubic press. Secondly, these zirconate-titanates provide a system of materials whose high pressure behaviour has not been previously investigated, and thirdly, they are readily available in various solid solution compositions. This in itself makes the system attractive to geophysicists since many of the abundant mineral systems of the earth's mantle $(Mg,Fe)_2SiO_4$ olivines and $(Mg,Fe)SiO_3$ pyroxenes occur in this form. Thus, although this system is much more complex, both chemically and physically than the basic barium titanate system, it presents a case perhaps very similar to perovskite structures in the earth's mantle. One disadvantage of this system, however, lies in the fact that the exact chemical compositions are known (to the author) for only two of the four ceramics investigated. This, combined with the unknown details of manufacture for each ceramic limits the detailed interpretation of the experimental results.

In the present study, four different chemically altered compositions of the basic PZT system were investigated. Basically, these ceramics may be divided into three distinct groups: 1) unmodified (isovalent substituted) ceramics (PZT-4), 2) donor-doped ceramics (PZT-5A, PZT-5H) and 3) acceptor doped ceramics (PZT-8). The numbers after the designation PZT are simply labels attached to these ceramics by the manufacturer. These ceramics all possess the perovskite ABO_3 structure and are just on the tetragonal side of the tetragonal-rhombohedral phase

boundary (Figure 6.1) (Berlincourt, 1971). They are solid solutions of typically 96-98% theoretical density with grain sizes on the order of 2-8 μ. The domain sizes, however, may be as small as .1 μ. A comparison of some of the pertinent physical properties of these ceramics are presented in Table 6T-1. Note that the values listed in this table are 'typical' values for these ceramics, and standard tolerances are ± 20% of these values. A detailed list of the physical properties of PZT ceramics can readily be found elsewhere (Berlincourt, 1971; Jaffe et al, 1971).

To date, relatively few investigations have dealt with the change in transition temperature with pressure for these PZT-type compounds. Previously investigated systems include PZT-5A to 2.8 kbar (Burfoot and Martirena, 1972; Martirena and Burfoot, 1974a, 1974b), PZT 65/35 to 20 kbar (Lysne and Bartel, 1975), PZT-4 to 56 kbar (Timco and Schloessin, 1975b, 1976a) and PZT-5A and PZT-5H to 56 kbar (Timco and Schloessin, 1976b, 1976c). However, several pressure investigations in the region ≤3 kbar have detailed both the piezoelectric and dielectric properties for temperatures well below the transition (Berlincourt and Krueger, 1959; Brown, 1961; Brown and McMahon, 1962; Nishi and Brown, 1964; Krueger, 1967; Wilhelm and McLaren, 1973). All of these studies, except those of Timco and Schloessin (1975b, 1976a, 1976b, 1976c) used fluid-media for the transmission of pressure.

6.2 Initial Application of Pressure

Figure 6.2 shows the relative change in capacitance upon initial loading of the press for one sample each of PZT-4, PZT-5A, PZT-5H and

Table 6T-1

	PZT-4	PZT-5A	PZT-5H	PZT-8
k_3^f	1,300	1,700	3,400	1,000
k_3^{cl}	.635	830	1,730	580
D	.004	.02	.02	-
κ_p	.58	.60	.65	.51
ρ $(kg\text{-}m^{-3})$	7,500	7,750	7,500	7,600
$T_c^o(^oC)$	325	365	195	300

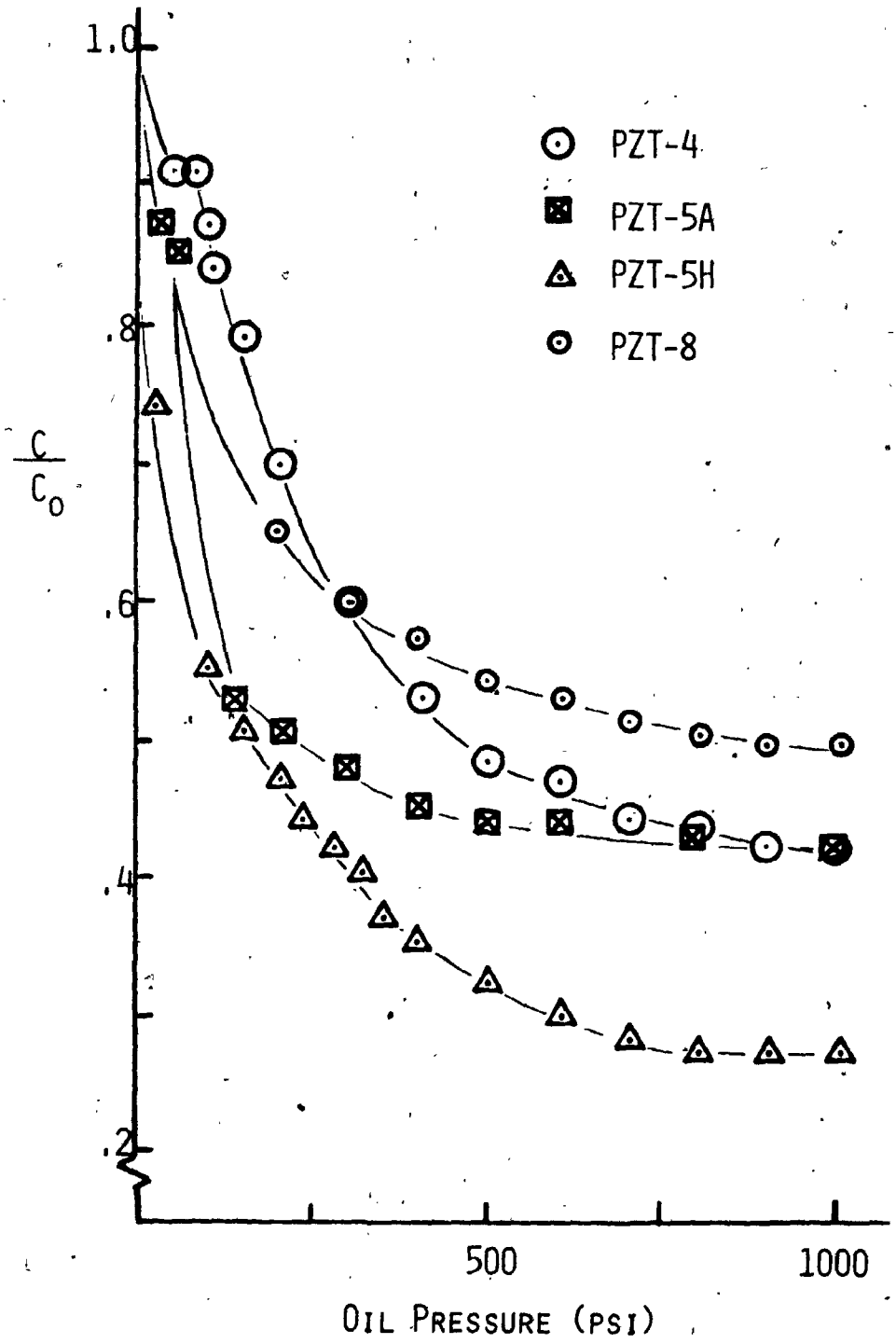

Figure 6.2 : Graph showing the relative change in capacitance of ceramics PZT-4, PZT-5A, PZT-5H and PZT-8 versus hydraulic oil pressure during initial loading of the press. An oil pressure of 800 psi in the rams corresponds to an estimated central cell pressure of 10 kbar.

PZT-8. The striking feature of this graph is that, in the pressure range 0-10 kbar, the capacitance values drop to less than one-half of the original (room pressure) value. This non-reversible decrease in the dielectric constant in the low pressure region was observed in every experiment for all of the PZT and BT ceramics.

This type of behaviour is markedly different than that found in fluid-media hydrostatic systems where dielectric constant values are reported to initially increase with hydrostatic pressure (Nishi and Brown, 1964; Berlincourt, 1971; Burfoot and Martirena, 1972; Wilhelm and McLaren, 1973). Brown (1961) however, using a two-dimensional stress perpendicular to the c-axis, also observed a striking decrease similar to that shown in Figure 6.2. He found that for PZT-4, application of a stress of ~4 kbar resulted in a decrease in the dielectric constant from ~1,400 at p = 0 kbar to ~700 at p ~4 kbar. Moreover, his experiments indicate that this decrease is relatively insensitive to the ratio of the applied principal stresses. Brown explains this behaviour by suggesting that as the stress is increased, the FE domains would redistribute until most of the domains become aligned with their c-axis normal to the stress axis. Since the c-axis dielectric constant is much lower than that of the a-axis (Tsuzuki et al, 1974), this domain re-alignment should result in a decrease in the dielectric constant tending towards a limiting value.

Brown's experimental findings, combined with the results of experiments performed in fluid-media hydrostatic systems confirm that, in the low pressure region (say 0-10 kbar) in the cubic press, the stress experienced by the sample is far from hydrostatic. Previous experiments, using solid-media in a tetrahedral press, have also indicated that the

largest deviatoric stresses occur in this low pressure region (Lees and McCartney, 1968). In the present experiments, the dielectric constant markedly decreases with initial pressure generation, especially at pressures below ~2 kbar (Figure 6.2). Now, according to Krueger (1967) and Berlincourt (1971), a two-dimensional planar stress perpendicular to the c-axis causes k to decrease, whereas a compressive stress along the c-axis causes k to increase. It is thought possible that such a planar stress situation may arise from the sample geometry, i.e. from the stress raising properties of a thin cylindrical disc on first loading. If this were the case, the decrease in dielectric constant might be accounted for by preferential domain wall alignment in the plane of the disc for as long as the overall stress in the pyrophyllite matrix is too low to be immediately relaxed by plastic flow. Then, one might expect more of a change in the ceramics which have comparatively high domain wall mobility, i.e. the donor doped 5 series (Gerson, 1960; Jaffe et al, 1971). This is observed experimentally (Figure 6.2). The apparent leveling off to a constant k value in the 3-10 kbar range (Figure 6.2) may then be attributed to either domain re-orientation saturation, or to a decrease in the deviatoric (planar) stresses present. More than likely, it is some combination of the two.

From the foregoing discussion, it is evident that values of the dielectric constant of a PZT sample measured in either a fluid-medium or a solid-medium press which are at the same pressure-temperature conditions (say 20 kbar and room temperature) are not comparable in value. One would expect, however, that the large decrease in the dielectric constant which is confined to the initial unsettled stage of pressuri-

zation in the solid-media experiments, will have little or no effect on the transition temperature of the sample once the matrix has reached a fully plastic state.

The large initial change in the measured capacitance is somewhat reminiscent of a similar change in capacitance between the "free" and "clamped" state of the crystal (Burfoot, 1967). Usually, clamping is the result of applying a sufficiently high measuring frequency to a piezoelectric material such that the inertia of the crystal prevents the full response of the strain to the applied electric field. As such, the dielectric constant drops to approximately one-half of its (low frequency) value. The crystal is effectively clamped for frequencies of two times its piezoelectric resonance frequency. Clearly this is not the case in the present experiments. Another form of clamping, however, is physical clamping (Cady, 1964; Burfoot, 1967). In this case, the crystal may be regarded as having its boundaries firmly attached to a medium of infinite rigidity which prevents all alterations in strain. In the present experiments, this form of clamping could come about as a result of two different mechanisms. First of all, although individual grains in the ceramic specimens are under mutual constraint at room pressure, one would expect that when subjected to pressure, closure of any pore spaces in the ceramic would further inhibit FE deformation strains. This alone, however, could not account for the decrease in k since a similar pore closure would occur under fluid-media hydrostatic conditions. A second type of clamping would come about in the form of the whole ceramic being constrained by the solid pyrophyllite matrix. Clearly, this effect would not occur in a fluid-medium apparatus. At first glance this latter

explanation seems rather attractive. However, this type of clamping can never be totally effective in practice since the pyrophyllite is not of (relative) infinite rigidity. Furthermore, the fact that the lower capacitance value is retained when the sample is removed from the pyrophyllite cell after the high pressure run, suggests that this explanation is not correct. Thus, although physical clamping may be partially responsible for the large drop in the dielectric constant, the presence of deviatoric stresses during the initial unsettled stages of pressurization is the more likely cause.

Using the experimental results, one can set up a very simple model to estimate the relative number of 90^{o} domains which re-orientate when subjected to a planar stress. To do this, a method is required to calculate the dielectric constant in terms of both the relative number of domains aligned in any one direction (n_i) and the anisotropic dielectric coefficients (k_i) of the grains. For an isotropic ceramic sample, the simplest approach is to assume that each of the three principle directions (a, b, c) intersect the same relative number of 90^{o} domains. Then if one assumes a linear combination of the form

$$k = n_1 k_1 + n_2 k_2 + n_3 k_3 \qquad (6.1)$$

and the anisotropic dielectric coefficients values determined for PZT single crystals by Tsuzuki et al (1974), ($k_1 = k_2 \sim 2{,}000$; $k_3 \sim 200$), one obtains a calculated macroscopic dielectric constant value of ~1400. This is in surprisingly good agreement with that measured for the isovalent substituted ceramic specimens (PZT-4) at room pressure and temperature ($k \sim 1300$). Now, after the initial pressure excursion in a

solid-medium apparatus, this value drops to a limiting value of typically ~600 for PZT-4. Using this value for k in equation (6.1), it can be shown that for this large a decrease in k, 90^{o} domain re-orientation in the c-direction would have to be ~78% complete. This amount of re-orientation, however, is unexpectedly high in view of the fact that for electrically poled samples, the domain re-orientation is only about 44% complete (Berlincourt and Krueger, 1959). Moreover, such a large domain re-orientation should lead to a substantial increase in the axial polarization values for these ceramics. This, however, was not observed in any of the hysteresis loop studies on BT ceramics. Moreover, high pressure experiments by Berlincourt and Krueger (1959) have also indicated that lateral stresses on BT and PZT ceramics cause only very slight changes in the polarization. In addition, they found that even though the remanent strain indicated that more domains were aligned with the axial (c) direction, the total polarization of these ceramics decreased along this direction. Certainly it would seem that although domain re-orientation plays a large role in accounting for the decrease in the dielectric constant when the ceramic is subjected to a two-dimensional stress, this situation is much more complex. In fact, if domain re-orientation alone caused the large initial decrease, this change in the dielectric constant should, at least to some extent, be reversible. This, however, was not the case.

Although the internal mechanism in the ceramics which is responsible for the decrease in k appears to be much more complicated than just a simple domain re-alignment, there can remain little doubt that deviatoric stresses are responsible for initiating this phenomena. It would

seem, therefore, that some type of depolarization mechanism which is caused by the deviatoric stresses may be responsible for the degradation of the electrical properties of these ceramics. In this respect it is of interest to note that recent studies on the effects of axial shock loading on the electromechanical response of various PZT compounds (Cutchen, 1966; Lysne, 1975; Lysne and Bartel, 1975; Lysne and Percival, 1975) have shown that dielectric breakdown may occur in shock loaded FE ceramics. This breakdown takes the form of a rapid and non-reproducible degradation of the electrical response (Lysne, 1975). In these experiments, Cutchen (1966) attributes this behaviour to the fact that the moving shock front may liberate charge carriers which would then either be accelerated into the stressed regions (where a process of depoling may take place), or else be carried at the shock front. Although shock conditions obviously do not occur in the present experiments, a similar type of depolarization mechanism which is related to the anisotropic stress experienced by the sample may occur. This, however, requires experimental confirmation, and thus, there is no certainty on this point.

Since the interesting behaviour of the large decrease in the measured capacitance with initial loading of the press (Figure 6.2) has not been previously reported, considerable effort was spent in analyzing this observation. To investigate the influence of the elastic contrast between the matrix and inclusion on this behaviour, two further experiments were performed. For one, a PZT-4 ceramic disc (of diameter ~.6 cm) was enveloped in ceresine and placed in the centre of a pyrophyllite cube which had an inner hole diameter of ~1.1 cm. The dielectric response of this arrangement with pressure is shown in Figure 6.3. In this case,

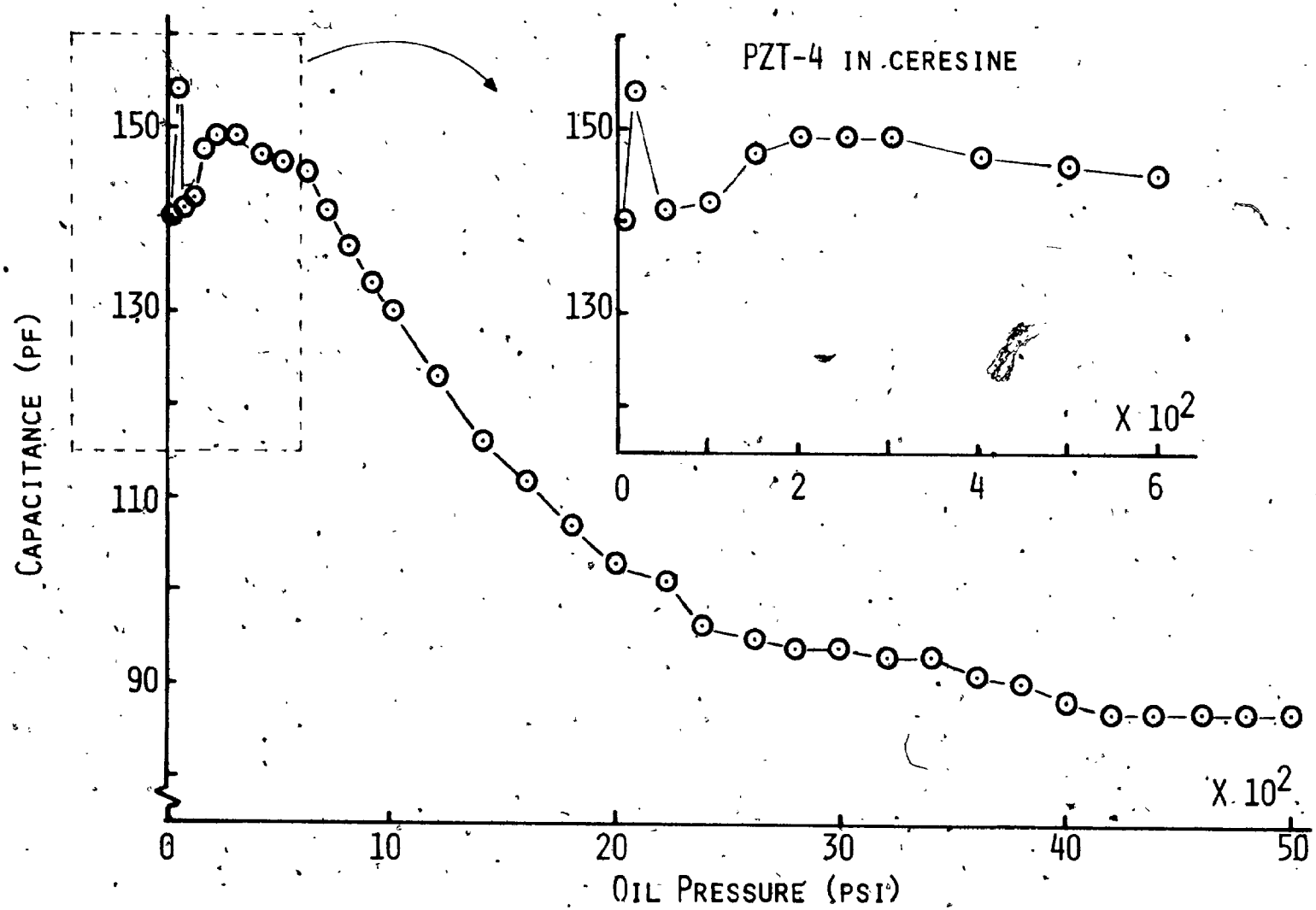

Figure 6.3 : Graph of the change in capacitance of ceramic PZT-4 in ceresine versus the hydraulic oil pressure. An oil pressure of 5,000 psi in the rams corresponds to a central cell pressure of 49 kbar.

there was a sharp increase in the capacitance on initial loading! This was followed by a gradual decrease to a constant value for oil pressures above 4,000 psi (~42 kbar). The low pressure behaviour in this case was exactly the opposite of that observed for a pyrophyllite matrix. Evidently, therefore, the nature of the matrix material can drastically influence the dielectric response of the ceramic to the applied external pressure. Undoubtedly, not the loading characteristics of the press but the pressure generation and its transmission in the vicinity of the sample are different for the two cases. For a pure pyrophyllite matrix, the response of the ceramic suggests that in the initial phase of pressure generation, the sample experiences a two-dimensional planar stress perpendicular to the axis of the disc. Based on Brown's (1961) experimental results, the magnitude of this stress is estimated to be on the order of 3-5 kbar. Interpretation of the results for a ceresine matrix (Figure 6.3) on the other hand, indicates that in this case, the sample initially experiences a net compressive stress along the disc axis which gradually gives way to a planar stress perpendicular to this direction. A stress of this type seems similar to that generated in a tetrahedral press at pressures of the same order of magnitude (Lees and McCartney, 1968).

The dielectric response of a PZT-5A ceramic disc, snugly fitted into a pure boron nitride matrix, was monitored as a function of the externally applied load (Figure 6.4). For this matrix, the dielectric constant decreased slightly to a ram oil pressure of ~150 psi. With further increase in pressure, however, the capacitance dropped abruptly as the matrix yielded by plastic flow. This was accompanied by loud crackling noises as small particles of boron nitride were flung from

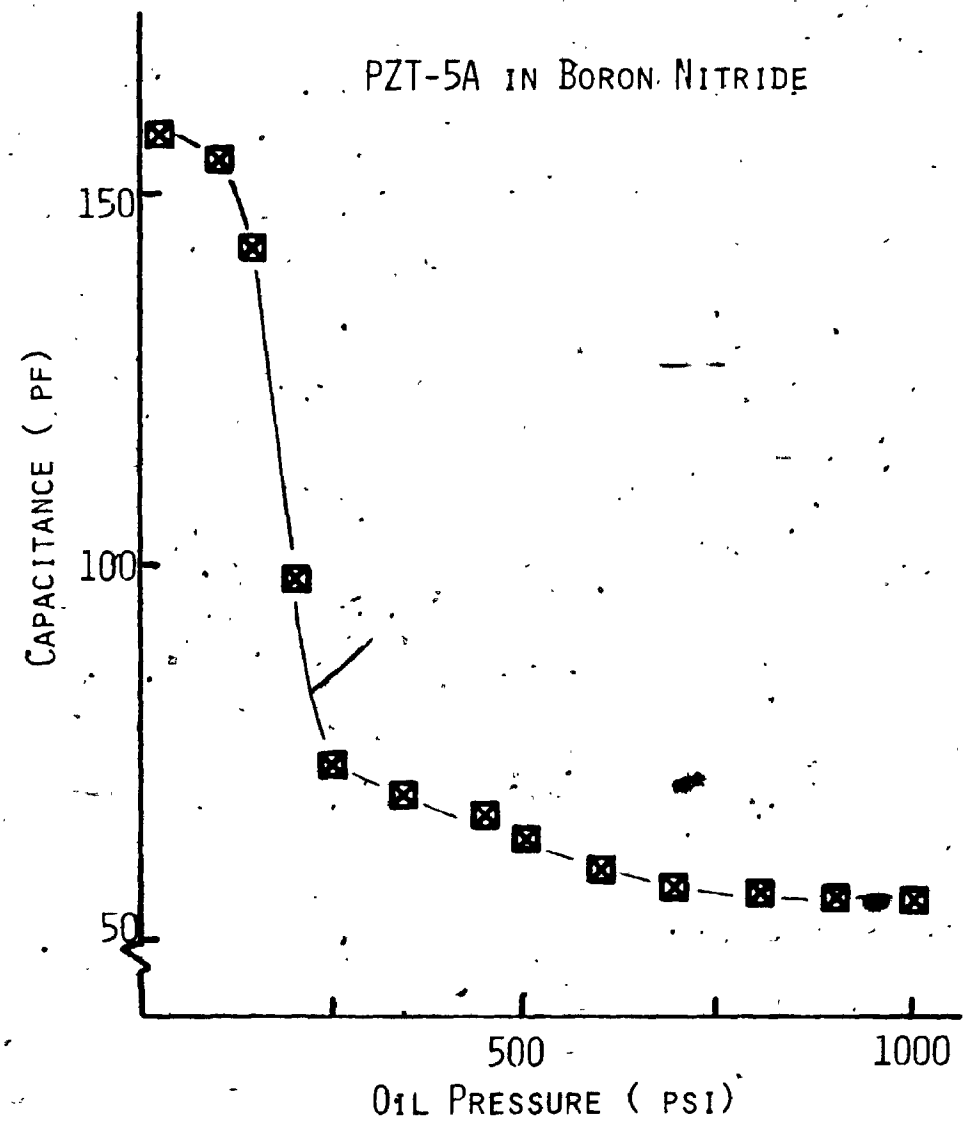

Figure 6.4 : Graph of the change in capacitance of ceramic PZT-5A in boron nitride versus the hydraulic oil pressure during initial loading of the press.

the press. As far as the sample is concerned, the basic behaviour in this case is quite similar to that observed for a pure pyrophyllite matrix.

6.3 Isovalent-Doped Ceramic PZT-4

PZT-4 was the first ceramic of the $Pb(Zr,Ti)O_3$ system to be investigated. This ceramic is a member of the 'unmodified' group (Gerson, 1960) in that it has neither donor nor acceptor doping. It does, however, have isovalent substitution of some Pb^{2+} by Sr^{2+} ($(Pb_{.94}Sr_{.06})Ti_{.47}Zr_{.53}O_3$). The strontium lowers the Curie point by ~9.5°C for every atom-% added, thereby raising the dielectric constant at room temperature. This composition is similar to the unmodified ceramic whose physical properties have been detailed by Gerson (1960). The room pressure Curie temperature T_c^o for PZT-4 is ~325°C.

Figure 6.5 shows the variation of the temperature of maximum dielectric constant, T*, with pressure for all of the PZT-4 samples investigated. Within experimental accuracy, T* decreases linearly with pressure at rates of -4.4, -4.6 and -4.8 °C/kbar for the samples shown in Figure 6.5. This linear decrease with pressure is similar to that observed for $BaTiO_3$ ceramics (Figure 5.6). The reason for the decrease in T* with pressure for this PZT compound is the same as that previously discussed in detail for BT ceramics (section 5.3).

Figure 6.6 shows the temperature variation of the real part of the dielectric constant for various pressure settings for one of the PZT-4 samples investigated. It is apparent that, similar to that found for BT ceramics (section 5.2), the dielectric constant - temperature peak

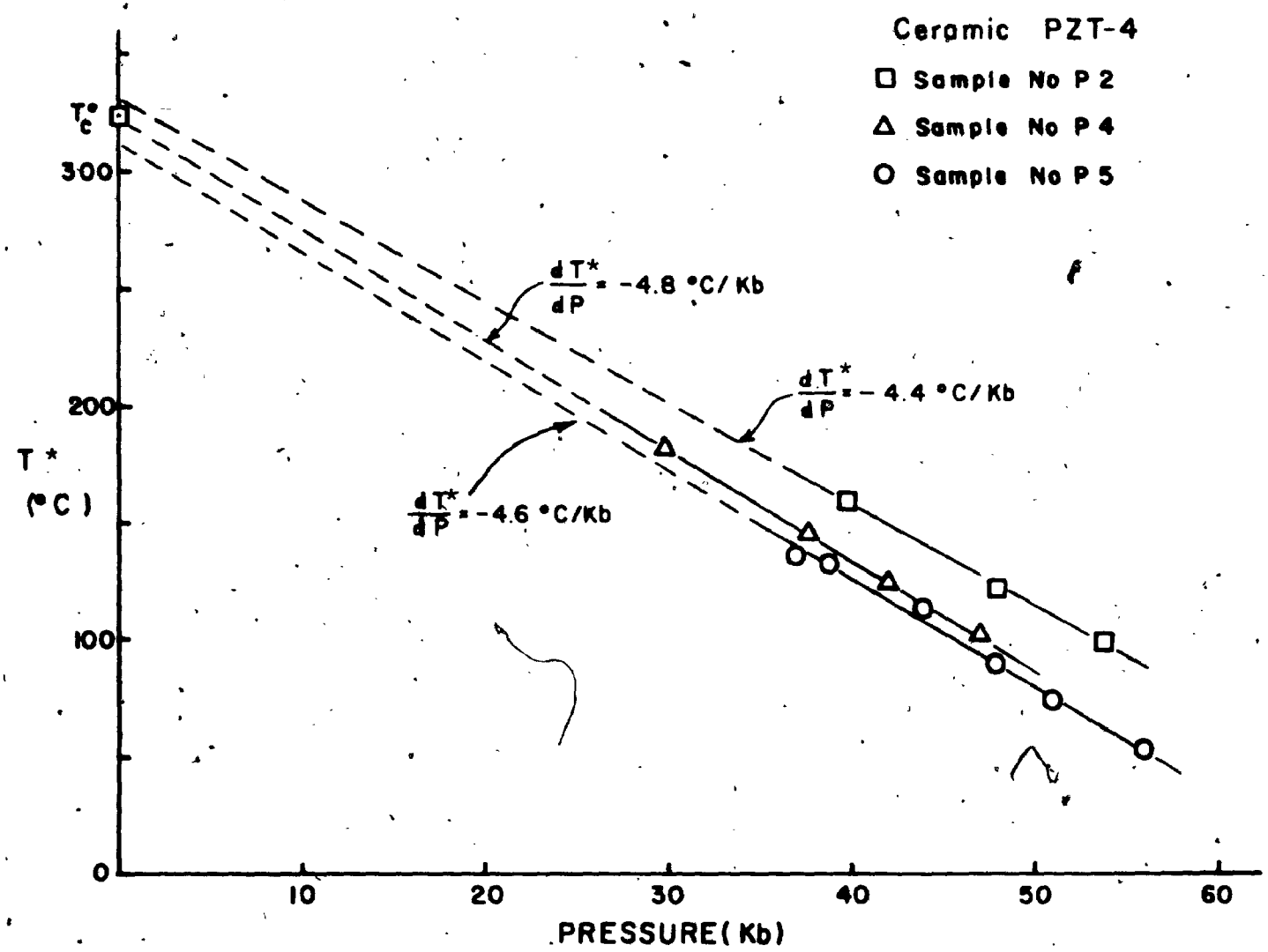

Figure 6.5 : Graph of the change in T* with pressure for each of the PZT-4 samples investigated.

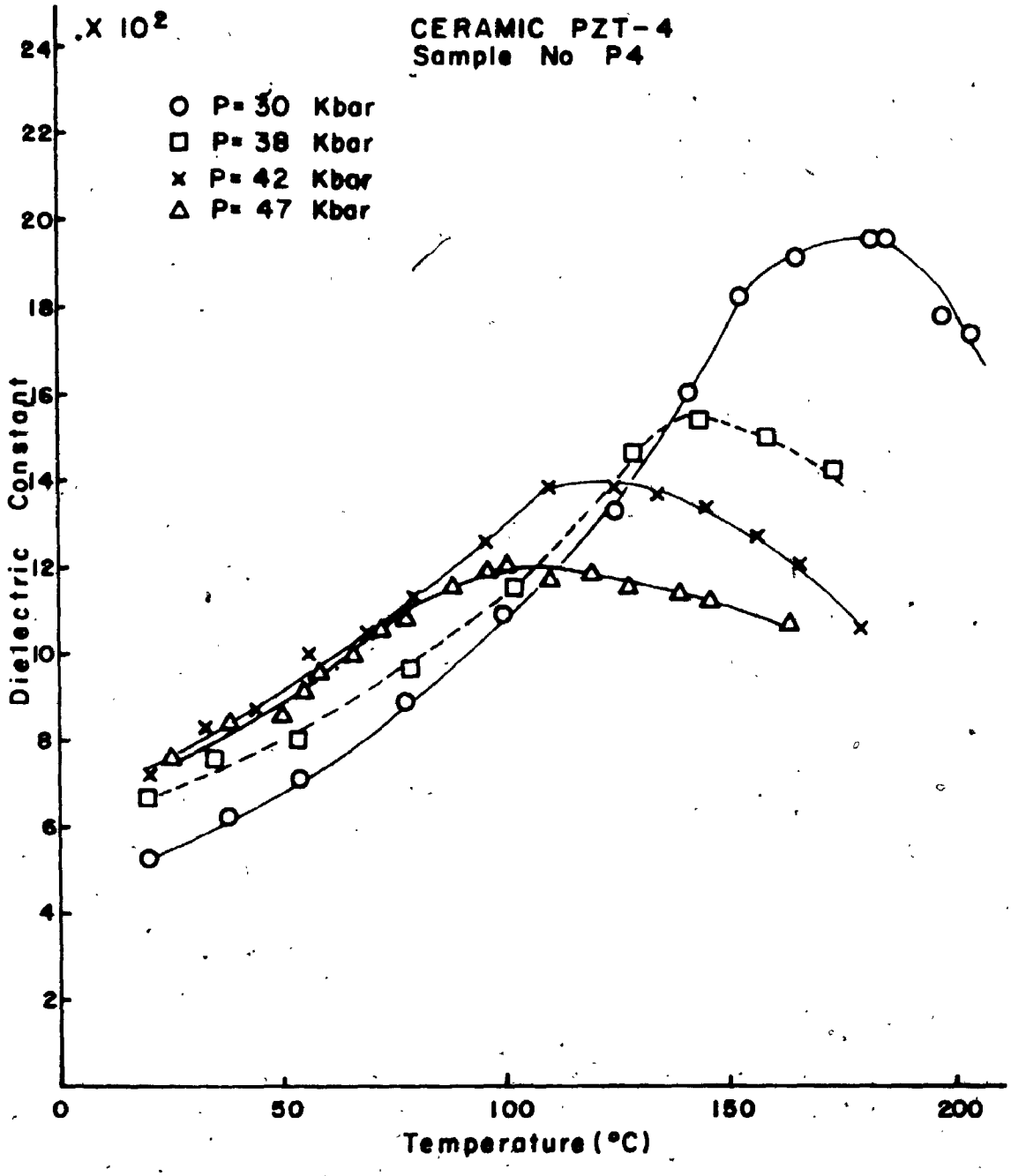

Figure 6.6 : Graph of the temperature dependence of the dielectric constant at various pressures for one of the PZT-4 samples (P4).

broadens with increasing values of pressure. For this sample, the isobaric profiles at pressures of 30, 38 and 47 kbar were obtained on initial pressure increase; whereas, the curve for p = 42 kbar was obtained on release of pressure from p = 47 kbar. The excellent fit of the 42 kbar profile suggests that whatever property influences the FE transition of the ceramic behaves elastically in this pressure region.

The observed k-T peak broadening with increasing pressure appears to be typical for these types of ceramics. In addition to the previously mentioned broadening found for BT ceramics, a similar effect has been observed for $Ba(Ti,Sn)O_3$ ceramics to 7.5 kbar (Polandov and Mylov, 1968), $CdTiO_3$ to 4.5 kbar (Martin and Hegenbarth, 1973), PZT-5A to 2.8 kbar (Martirena and Burfoot, 1974a, 1974b) and PZT-5H to 40 kbar (Timco and Schloessin, 1976b, 1976c). This broadening is somewhat similar to that found in perovskite ceramics owing to either decreasing grain size (Okazaki and Nagata, 1973; Keizer and Burggraaf, 1974; Martirena and Burfoot, 1974a, 1974b) or substitution of various amounts of isovalent ions (Clarke and Burfoot, 1974; Burns, 1976). In these cases, the observed broadening could be attributed to either the influence of local residual microstresses or compositional inhomogeneities in these ceramics.

A feature which is evident from the dielectric constant-temperature curves for PZT-4 (Figure 6.6) is that the Curie-Weiss law is macroscopically not obeyed. This is reminiscent of the situation found in studies on the influence of changes in grain size (Martirena and Burfoot, 1974b) or composition (Clarke and Burfoot, 1974) on the dielectric properties of perovskite ceramics. To describe the temperature dependence of the dielectric constant above T*, Martirena and Burfoot (1974a,

1974b) have proposed an emperical law of the form

$$\frac{1}{k} = \frac{1}{k_{max}} + \beta(T - T^*)^m \qquad (6.2)$$

where k is the dielectric constant at temperature T, k_{max} is the maximum dielectric constant, and β and m are constants. When m = 1, this reduces to the Curie-Weiss law; whereas, when m = 2, the equation is that used to describe diffuse phase transitions (Smolensky, 1970).

It was of interest to inquire whether an empirical relationship such as equation (6.2) would yield a linear fit when applied to the results of polycrystalline FE ceramics under the constraint of a matrix. The reasoning for this was based on the possibility that microstresses would be related to grain size, and that the changes in microstresses with both applied pressure and changes in grain size would follow similar types of distribution curves. The applicability of equation (6.2) was examined by drawing smooth curves through the experimental points determined for $(T - T^*) > 10^0C$ for PZT-4 (Figure 6.6) and using the values of k along these curves in the equation. As evident in Figure 6.7, this kind of relationship is reasonably well obeyed in the high pressure region.

6.4 Donor Doped (A Vacancy) Ceramic PZT-5A

PZT-5A is a member of the donor doped series of $Pb(Zr,Ti)O_3$ ceramics. In this series, some of the ions are replaced by ions that are more positive (or less negative) in valence. Since the lead oxide (PbO) is volatile and can leave the ceramic, these additives cause A-position vacancies. Thus, for each two atoms of 3+ or 5+ valancy

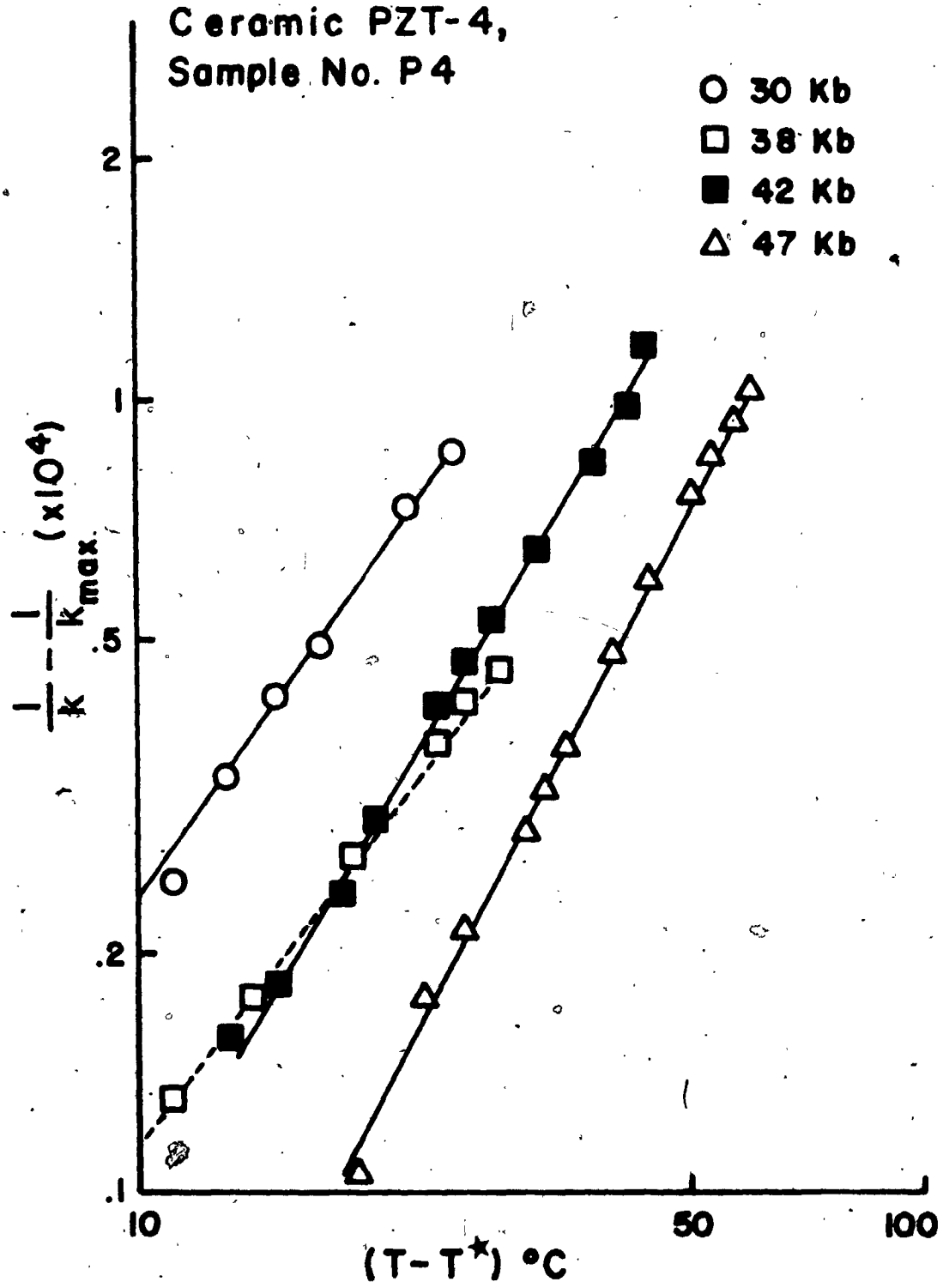

Figure 6.7 : Log-log graph of equation (6.2) using the curves of figure 6.6. For p=30 kbar, m=1.5; p=38 kbar, m=1.3; p=42 kbar, m=1.6; p=47 kbar, m=1.9.

introduced into the lattice, one Pb vacancy occurs (Jaffe et al, 1971). This modification increases the dielectric constant, piezoelectric coupling factor and elastic compliance, thereby improving some of the properties relevant to their use as piezoelectric transducers. This results since the A-vacancies facilitate the motion of domain boundaries and thereby greatly enhance the initial stress relief (Gerson, 1960). In a sense, therefore, the additives make the ceramic 'softer', both mechanically and electrically. In this case, the addition of Nb_2O_5 (1% by weight) to the basic $Pb(Zr_{.52}, Ti_{.48})O_3$ composition yields the well known PZT-5A ceramic (Gerson, 1960; Martirena and Burfoot, 1974b). The room pressure Curie temperature for PZT-5A is ~365°C.

Figure 6.8 shows the variation of the temperature of maximum dielectric constant, T*, with pressure for PZT-5A as an inhomogeneous inclusion in a pyrophyllite matrix. Similar to BT and PZT-4, T* decreases with increasing pressure but, in this case, the equilibrium line is non-linear with an apparent point of inflection at p ~ 30 kbar. With increasing pressure above 40 kbar, $dT^*/dp \rightarrow 0$. Non-linear phase boundaries for ferroelectrics have also been observed for $CdTiO_3$ ceramics (Martin and Hegenbarth, 1973) and $PbTiO_3$ single crystals (Samara, 1971). The excellent agreement between T* - p values obtained on the initial and second run of sample no. 5P2 suggests that whatever the mechanism for the change in T* is, it must be reversible with p and T. T* was not frequency dependent in the range 1 - 10 kHz for any of the ceramics studied (see Figure 6.9).

Figure 6.10 shows the temperature dependence of the dielectric constant for PZT-5A for various pressures. All samples, including the

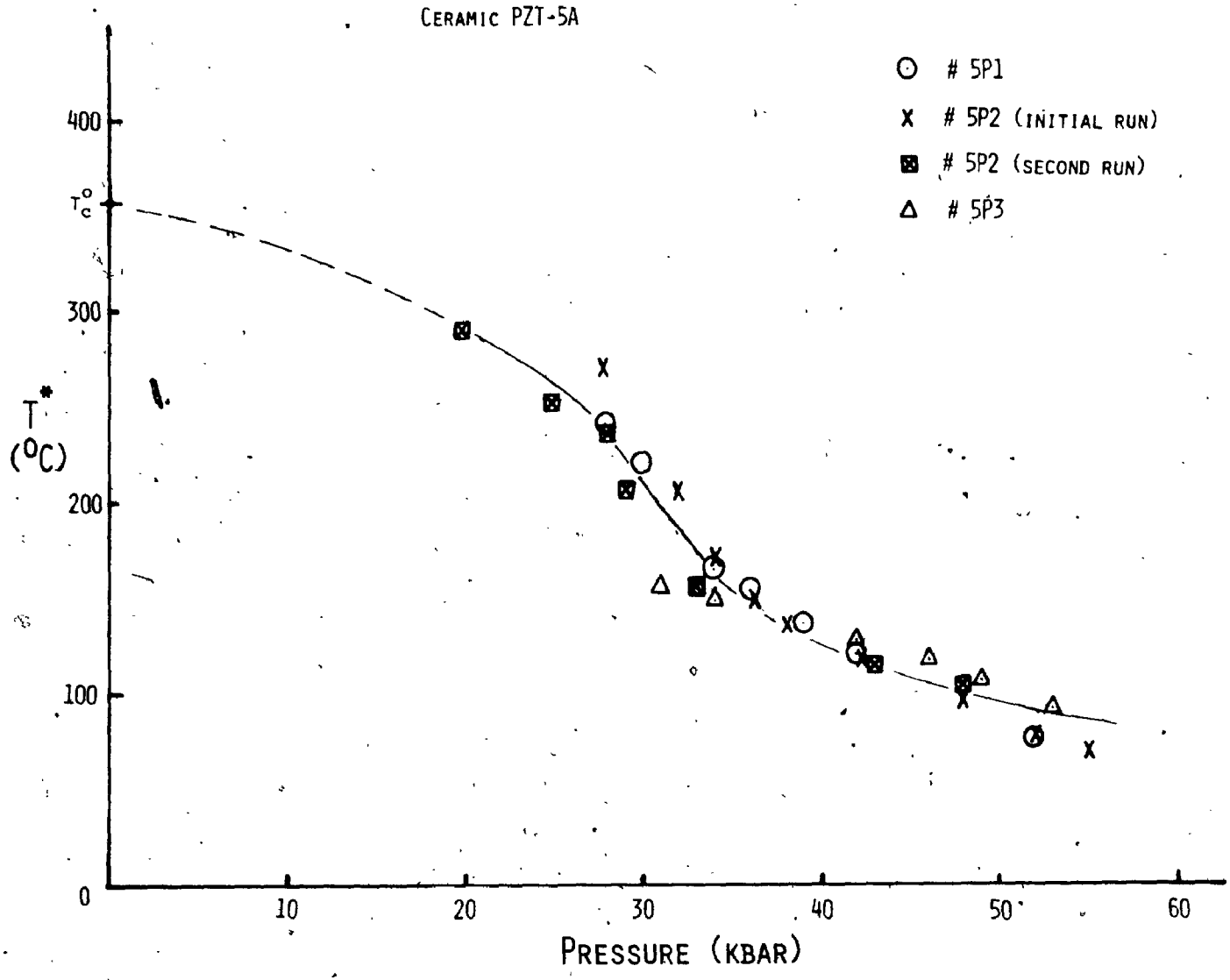

Figure 6.8 : Graph of the change in T* with pressure for each of the PZT-5A samples investigated.

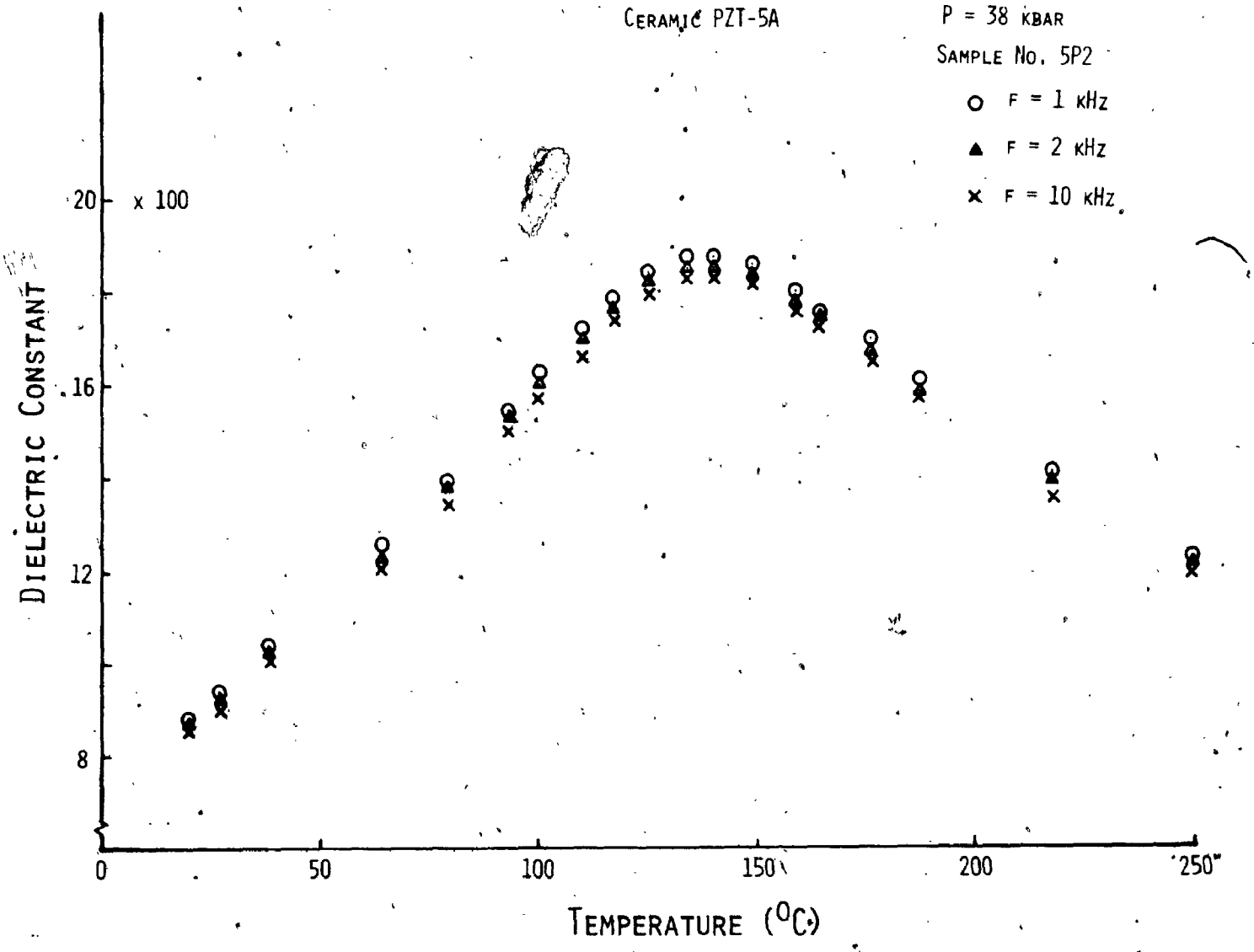

Figure 6.9 : Graph of the dielectric constant versus temperature and frequency for PZT-5A ceramic (5P2) at p=38 kbar. Note that T* is independent of frequency in the range 1-10 kHz.

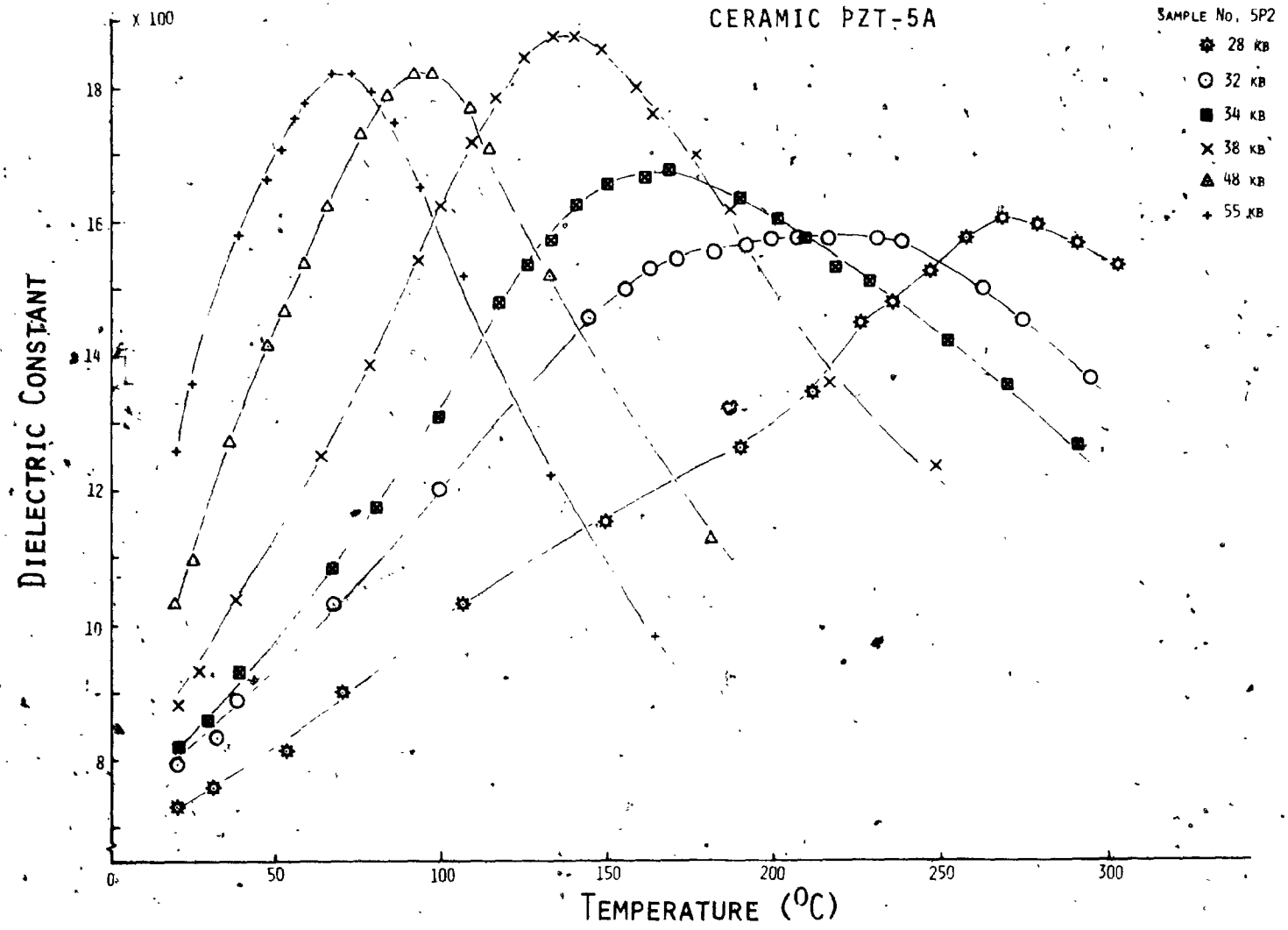

Figure 6.10 : Graph of the temperature dependence of the dielectric constant at various pressures for one of the PZT-5A samples (5P2).

second pressure excursion on no. 5P2 showed qualitatively the same behaviour. The dielectric values for the second run no. 5P2 (Figure 6.11), however, were typically ~25% larger than those measured on the first run (Figure 6.10). In the pressure region around 30 kbar, the peak is extremely broad and, with increasing pressure, the peak shape 'sharpens' showing little pressure dependence above ~40 kbar. Unfortunately, attempts to obtain isobaric profiles in the lower pressure region (below ~25 kbar) were thwarted by the increased high temperature electrical conductivity of the pyrophyllite surrounding the sample. Nevertheless, it is evident that for pressures above 30 kbar, PZT-5A behaves as if it was mechanically 'hard' and, as evidenced by the rather similar dielectric curves for pressures of 38, 48 and 55 kbar (Figure 6.10), as well as the relatively small change in T* in this pressure region (Figure 6.8), much more insensitive to the externally applied pressure.

The behaviour of PZT-5A ceramics for pressures above ~30 kbar is very different from that observed for PZT-4 (Figure 6.6) and other perovskite ceramics previously mentioned. However, measurements to 2.8 kbar on PZT-5A in a fluid-media press (Martirena and Burfoot, 1974a, 1974b) have indicated that the "typical" peak broadening does occur in this ceramic in the lower pressure region. This observation combined with the present results for PZT-5A (Figure 6.10) suggests that the peak broadens with increasing pressure to ~30 kbar whereupon the peak re-sharpens and, at pressures ~40 kbar, becomes relatively insensitive to pressure. The reason for this apparently anomalous peak sharpening is not known.

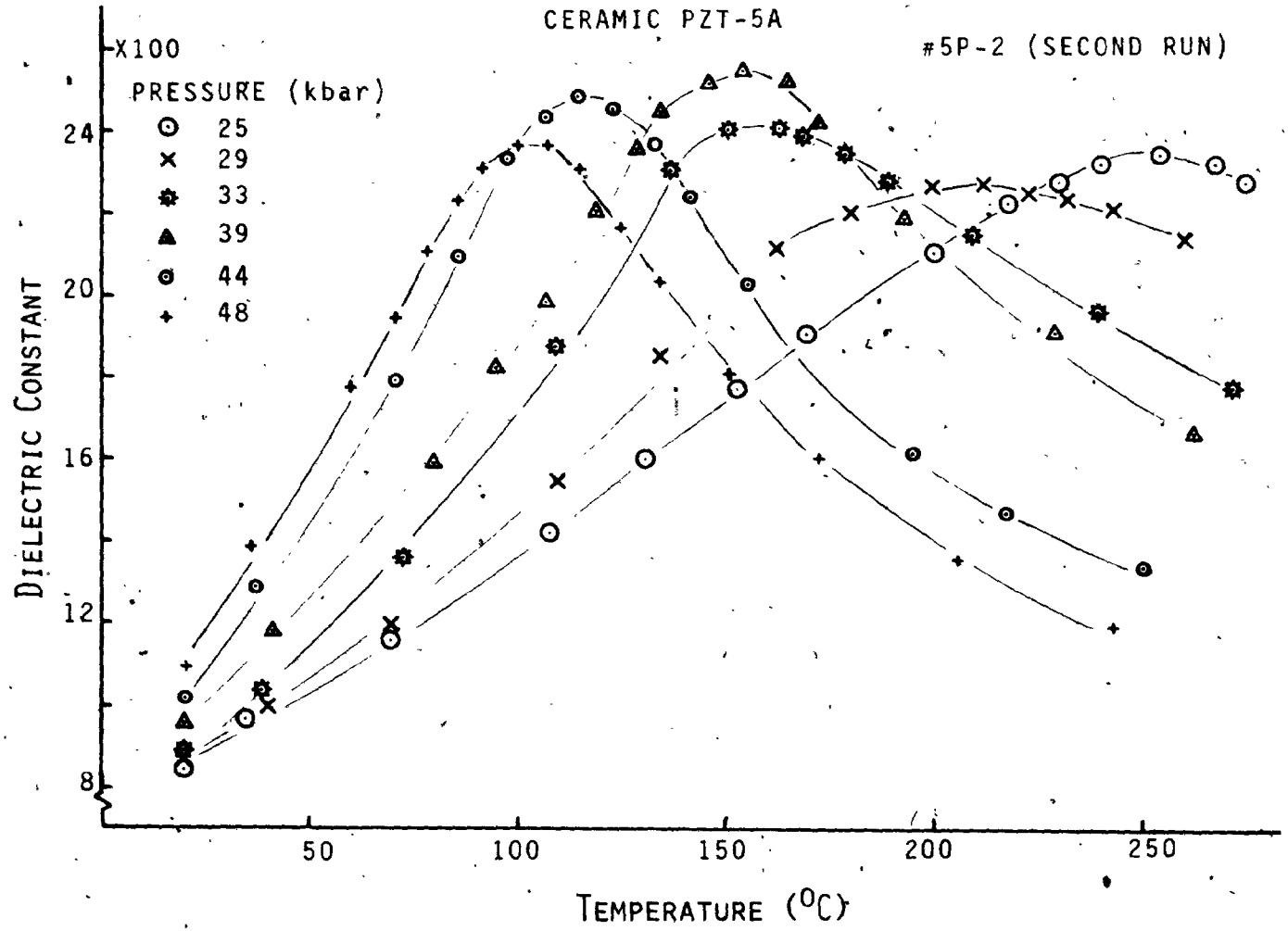

Figure 6.11 : Graph of the temperature dependence of the dielectric constant at various pressures for the second run on PZT-5A ceramic 5P2.

One can speculate, however, on the cause of the peak sharpening exhibited by the 5A ceramic by extending the basic ideas of Diamond's distribution model (section 5.2) to these results. This, then, would suggest that the dielectric peak sharpening observed in this pressure region is due to the relaxation of the microstress level in the ceramic. This may be accomplished by a partial release of the stresses built up at grain boundary contacts, possibly by plastic flow. The fact that the dielectric constant values on the second run of sample no. 5P2 (Figure 6.11) were typically ~25% larger than those obtained on the first run (Figure 6.10) indicates that some stress adjustment took place during the course of the first high pressure excursion. The qualitatively similar behaviour of the k-T curves for both runs would then imply that the peak shape is essentially determined by the now-elastic contact stresses. Moreover, the excellent correlation of the T* - p curves for these runs (Figure 6.8) implies that T* is predominately dependent upon the externally applied pressure, and not on the internal stress system.

If the proposed hypothesis of stress release were to be correct, one would assume that at some pressure this relaxation should occur for all perovskite ceramics. Consequently, one must explain why this stress adjustment occurs at much lower applied pressures in the case of PZT-5A ceramics than, say, for ceramic PZT-4. At this stage, however, difficulties arise due to the unknown (at least to the author) differences in manufacturing processes, firing times and temperatures, etc. for these ceramics. It is known, however, that the grains in the 5A ceramic are more angular than those in the 4 ceramic (Gerson, 1960; Jaffe et al, 1971). If, then, one employs the suggestion of Timco and Schloessin

1976a) that Hertzian-like contact formation between adjacent grains is the chief cause of the increase in the level of microstresses with pressure, one might reasonably expect relaxation by plastic deformation. One could argue that the corresponding redistribution of microstresses would take place at a much lower applied pressure for a ceramic with angular, pointed grains.

Figures 6.12 and 6.13 show the temperature dependence of the dissipation factor with pressure and frequency respectively for the PZT-5A sample shown in Figure 6.10. With increasing temperature, the dissipation values gradually decrease around the transition temperature, then rise sharply, thereby producing a minimum in the curve. A somewhat similar minimum has been observed for $PbTiO_3$ single crystals (Samara, 1971). The reason for the decrease in D is the same as that previously discussed for $BaTiO_3$ ceramics (section 5.2), and the steep rise can probably be attributed to both a decrease in the charging current and an increase in conductivity in the higher temperature region. With increasing pressure, the depth of the minimum increases and the half-width decreases. This pressure dependence is simply a reflection of the pressure dependent behaviour of the real part of the dielectric constant (Figure 6.10).

6.5 Donor Doped (A Vacancy) Ceramic PZT-5H

Since the high pressure behaviour of ceramic PZT-5A was vastly different than that observed for BT and PZT-4 ceramics, a second ceramic of the A-vacancy series was chosen for study in order to see if the anomalous 5A behaviour was characteristic of all A-vacancy ceramics.

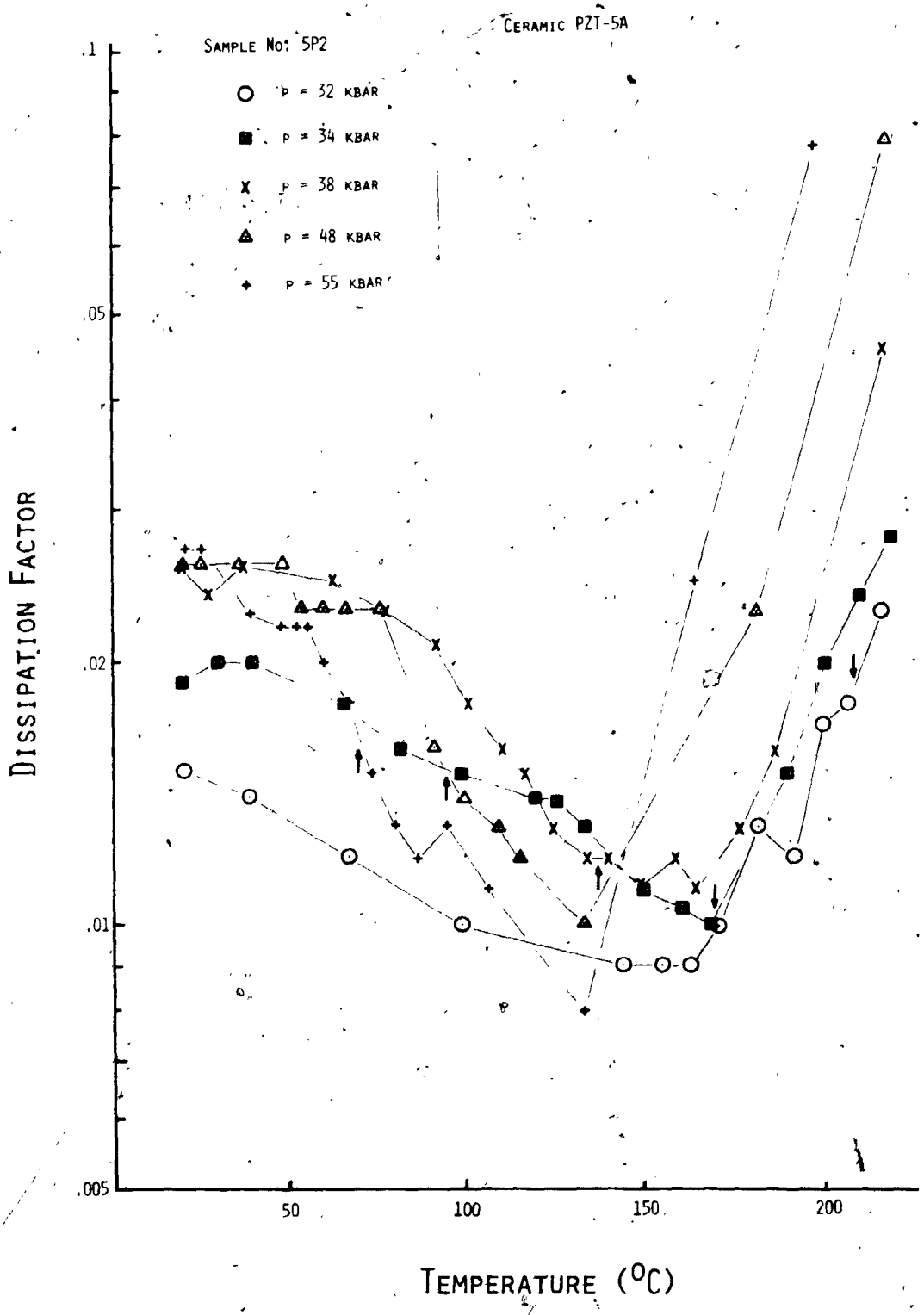

Figure 6.12 : Graph of the isobaric variation of the dissipation factor, D, with temperature for ceramic PZT-5A (#5P2). The arrows indicate T* determined from the dielectric constant curves of figure 6.10.

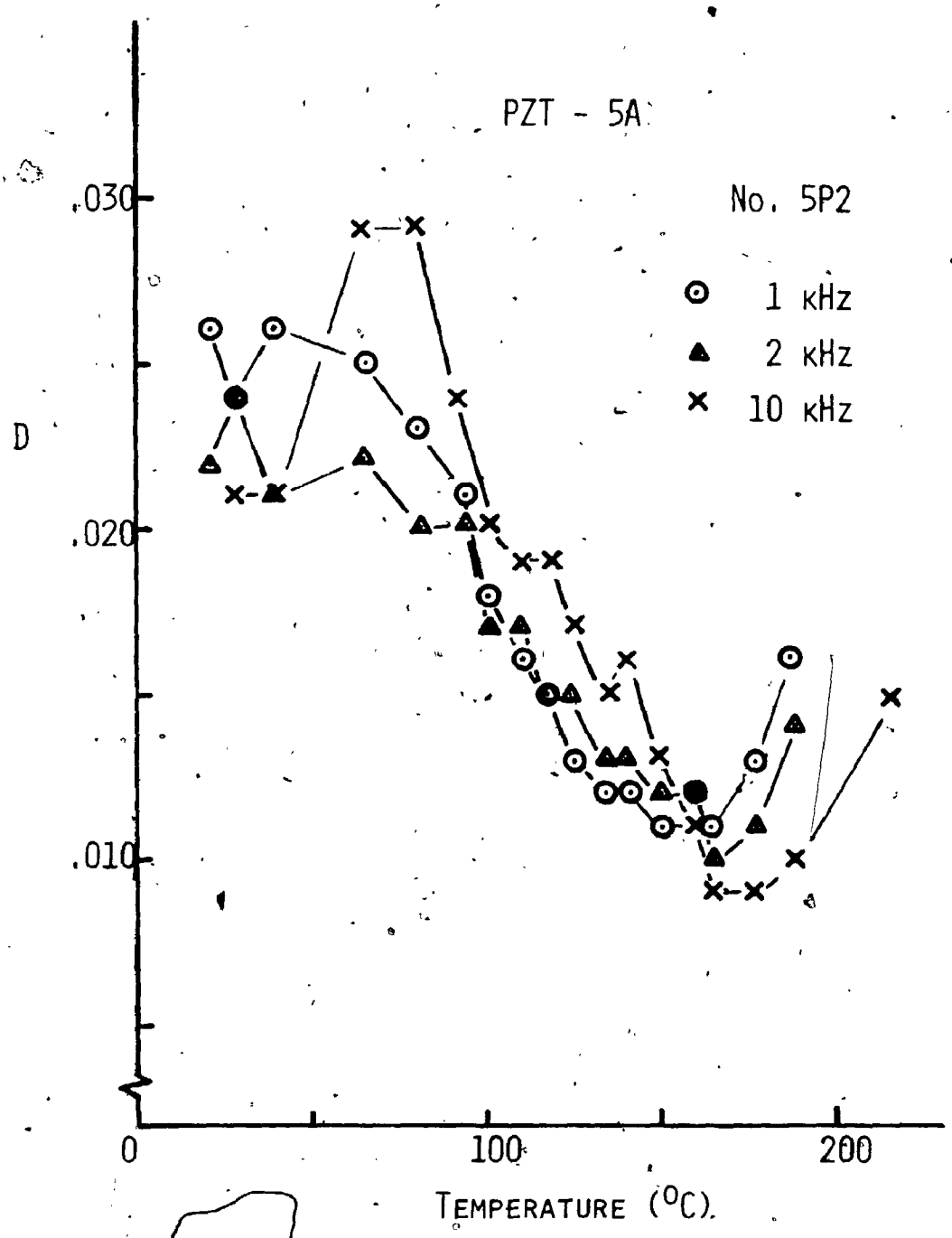

Figure 6.13 : Graph of the temperature dependence of the dissipation factor, D, for various measuring frequencies for ceramic PZT-5A (#5P2) at p=38 kbar.

Consequently, several experiments were performed on PZT-5H, a donor doped ceramic which, although more heavily doped than PZT-5A, is also on the tetragonal side of the $Pb(Zr,Ti)O_3$ tetragonal-rhombohedral phase boundary. The exact chemical composition of this material is not known by the author. Although PZT-5H has the highest dielectric constant at room temperature and pressure ($k \sim 3,400$) of all the PZT ceramics investigated (Table 6T-1), it also has the lowest room pressure Curie temperature ($\sim 195^{o}C$).

Figure 6.14 shows the variation of T* with pressure for PZT-5H for all of the samples investigated. Within experimental accuracy, T* decreases linearly with pressure at rates of -4.6, -4.1 and -3.9 $^{o}C/kbar$ for the three samples studied. This linear decrease is similar to that observed for $BaTiO_3$ (Figure 5.6) and PZT-4 (Figure 6.5) ceramics. The reason for the decrease in T* with pressure, as well as the spread in dT*/dp values has previously been discussed in section 5.3.

Figure 6.15 shows the temperature variation of the real part of the dielectric constant for various pressure settings for one of the PZT-5H samples investigated. All samples showed similar behaviour. It is apparent from this graph that, with increasing values of pressure, the maximum value of the dielectric constant decreases, and the half-width of the k-T curve increases. This peak broadening with increasing pressure is similar to that observed for both $BaTiO_3$ and PZT-4 ceramics, but not for PZT-5A ceramics. This behaviour indicates that the anomalous peak broadening (Figure 6.10) and non-linear T* - p curve (Figure 6.8) of ceramic PZT-5A is not characteristic of all A-vacancy ceramics of the $Pb(Zr,Ti)O_3$ system. Clearly, PZT-5H behaves in a manner which appears to be typical for most perovskite ceramics subjected to high pressure.

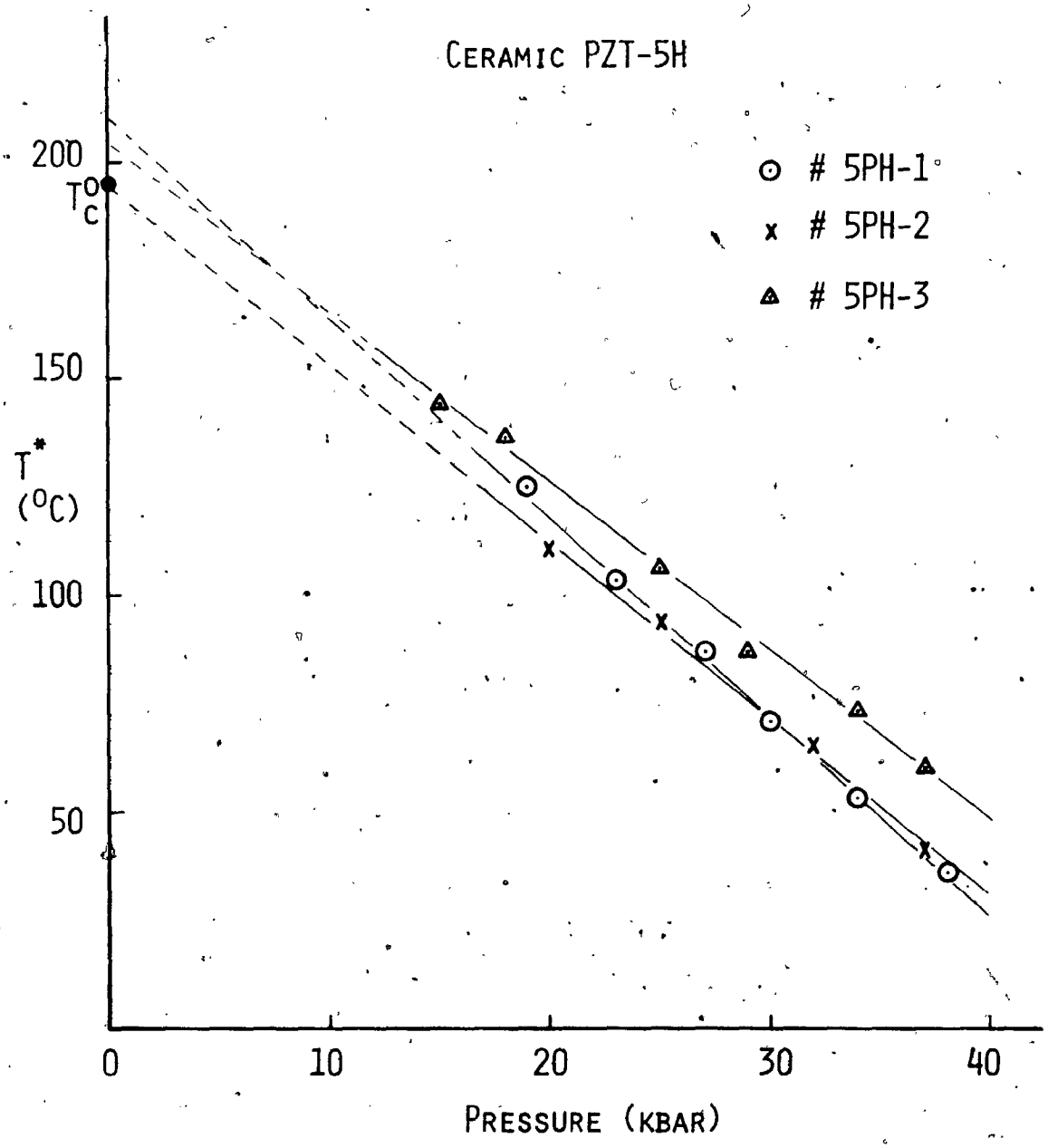

Figure 6.14 : Graph of the change in T* with pressure for each of the PZT-5H samples investigated.

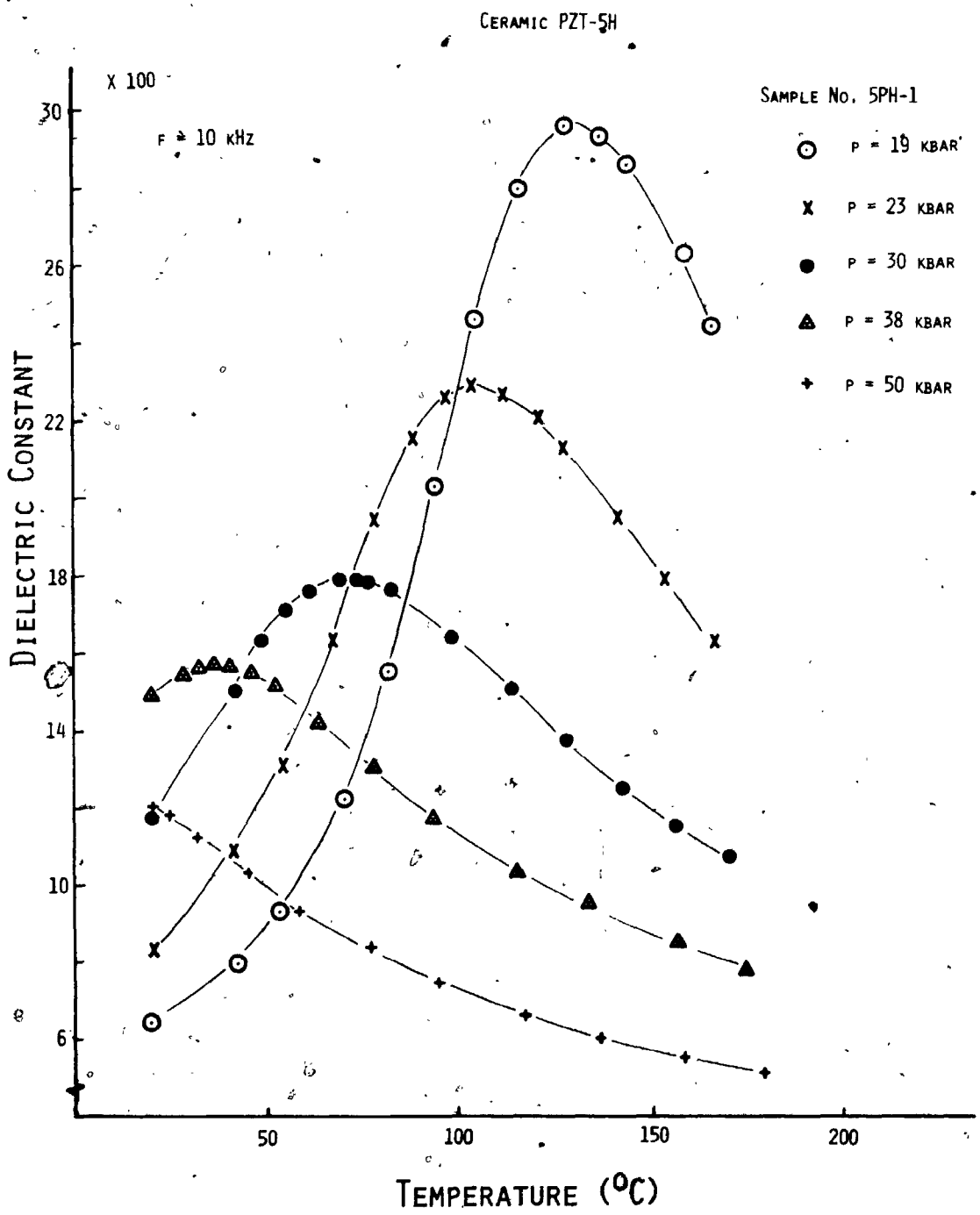

Figure 6.15 : Graph of the temperature dependence of the dielectric constant at various pressures for one of the PZT-5H samples (5PH-1).

One can get a good pictorial representation of the overall behaviour of the dielectric constant with both temperature and pressure by representing the dielectric constant in a k, T, p diagram. Figure 6.16 shows the dielectric constant surface for one sample (5PH-1) of ceramic PZT-5H. This conveys a good overall idea of the nature of the change in phase transition with pressure and temperature, in addition to its aesthetic appeal.

Figure 6.17 shows the temperature dependence at various constant pressure settings of the dissipation factor, D, for the same PZT-5H sample and experimental conditions shown in Figure 6.15. In general, with increasing pressure at constant temperature, D decreases, and with increasing temperature at constant pressure, D values decrease gradually towards a constant value. In this case, the decrease is not a sudden drop as found for $PbTiO_3$ single crystals under pressure (Samara, 1971), but is spread over a temperature interval.

6.6 Acceptor Doped (O Vacancy) Ceramic PZT-8

In the acceptor doped series of ceramics, a lower valence ion is substituted in place of either the Pb^{2+} or $(Zr,Ti)^{4+}$ ion. This type of subsitution results in O-position vacancies which cause relatively low dielectric constants and losses (Jaffe et al, 1971). In addition, the ceramics are known to be less sensitive to small applied stresses than any of the other ceramics investigated. Although the detailed chemical formula for PZT-8 is not known by the author, it is known that it has 5 - atom% Sr^{2+} substitued for Pb^{2+}, as well as acceptor doping 3+ in the B^{4+} position (Krueger, 1967). The room pressure Curie temperature

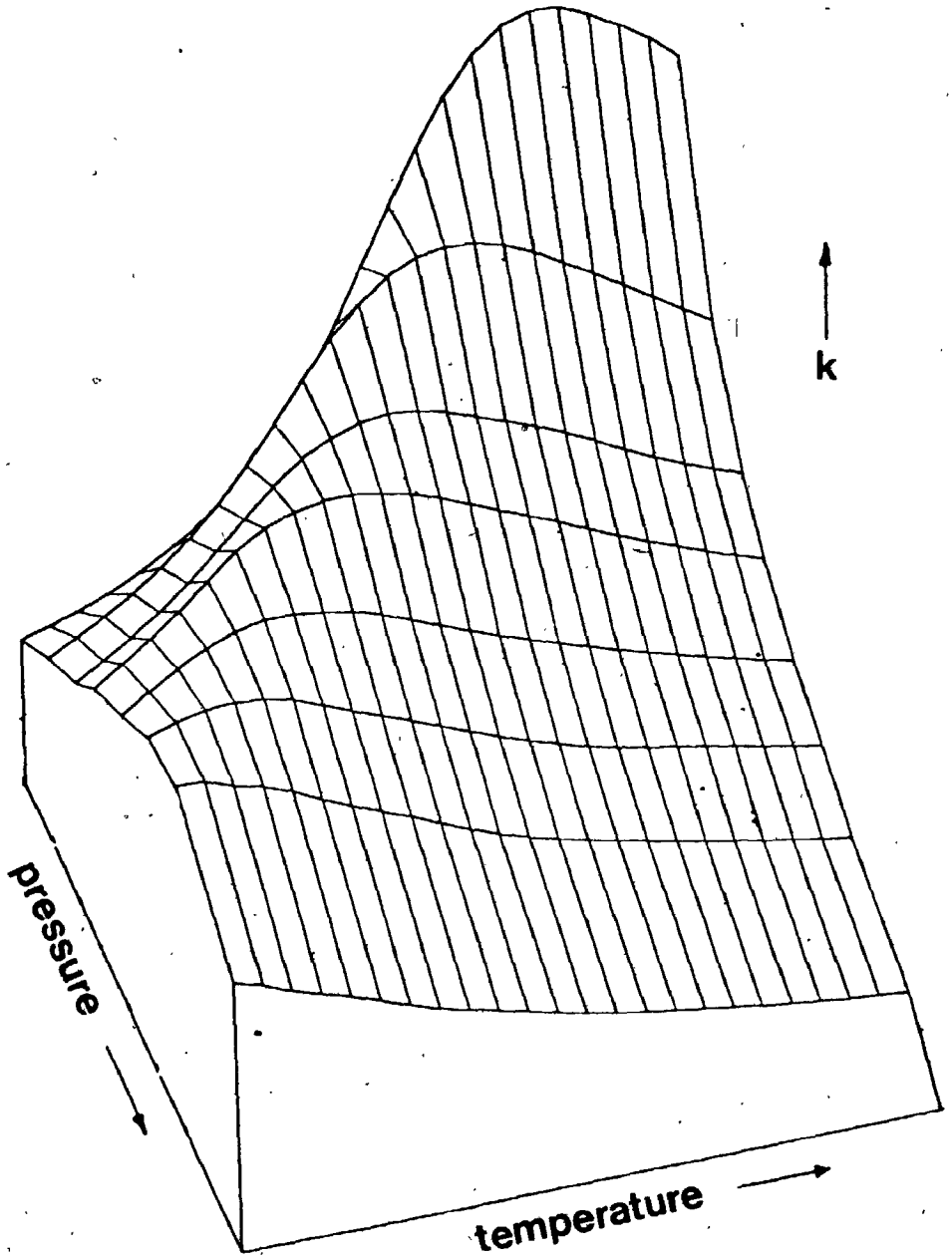

Figure 6.16 : Representation of the changes in the dielectric constant, k, in terms of a k, T, p diagram for the same PZT-5H sample shown in figure 6.15 (5PH-1).

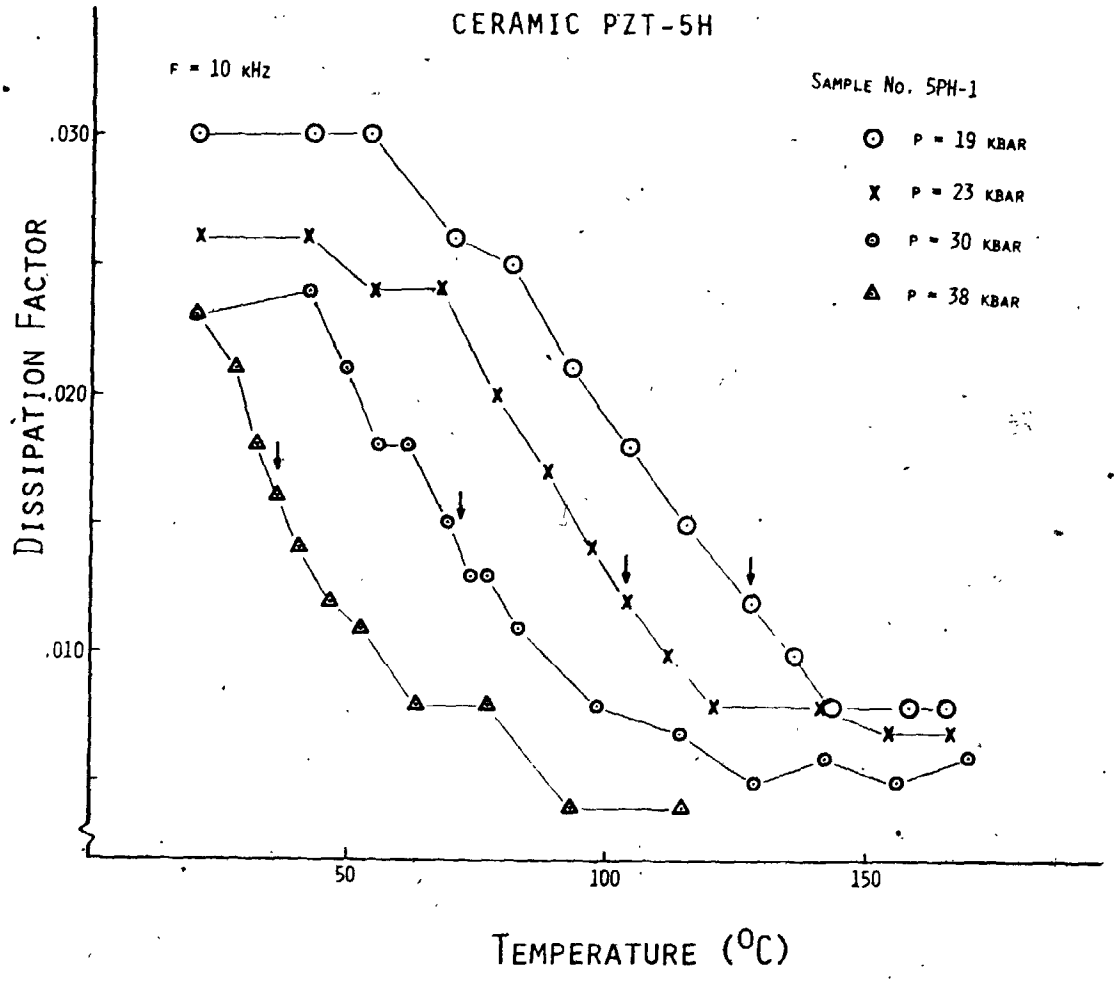

Figure 6.17 : Graph of the isobaric variation of the dissipation factor, D, with temperature for ceramic PZT-5H (#5PH-1). The arrows indicate T* determined from the dielectric constant curves of figure 6.15.

of PZT-8 is ~300°C.

Two samples of PZT-8 were investigated. Within experimental accuracy, the transition temperature decreased linearly with pressure at rates of -5.5 and -5.7 °C/kbar for these samples (Figure 6.18). This linear behaviour is similar to that observed for BT, PZT-4 and PZT-5H ceramics.

Figure 6.19 shows the temperature dependence of the dielectric constant for one of the PZT-8 samples investigated. Both samples exhibited similar behaviour. Clearly, PZT-8 shows the same type of k-T peak broadening as $BaTiO_3$, PZT-4 and PZT-5H and, as such, indicates that this member of the O-vacancy series exhibits the behaviour which is apparently typical of most FE perovskite ceramics.

It is of interest to note that compared with members of the donor doped 5 series, the response time for changes in pressure was much longer for the PZT-8 acceptor doped ceramics. In fact, one felt that one was taking measurements in 'slow motion' on these ceramics. This is caused by the relative lack of stress sensitivity of the O-vacancy series (Jaffe et al, 1971). Clearly, if one were going to use a PZT-type transducer in a situation of low superimposed hydrostatic stress conditions (as, for example, on ocean floor seismic studies) this compound would be a wise choice.

6.7 General Discussion

The present high pressure investigation of the dielectric properties of the $Pb(Zr,Ti)O_3$ system of ceramics has exposed several important features. It appears that the typical high pressure behaviour

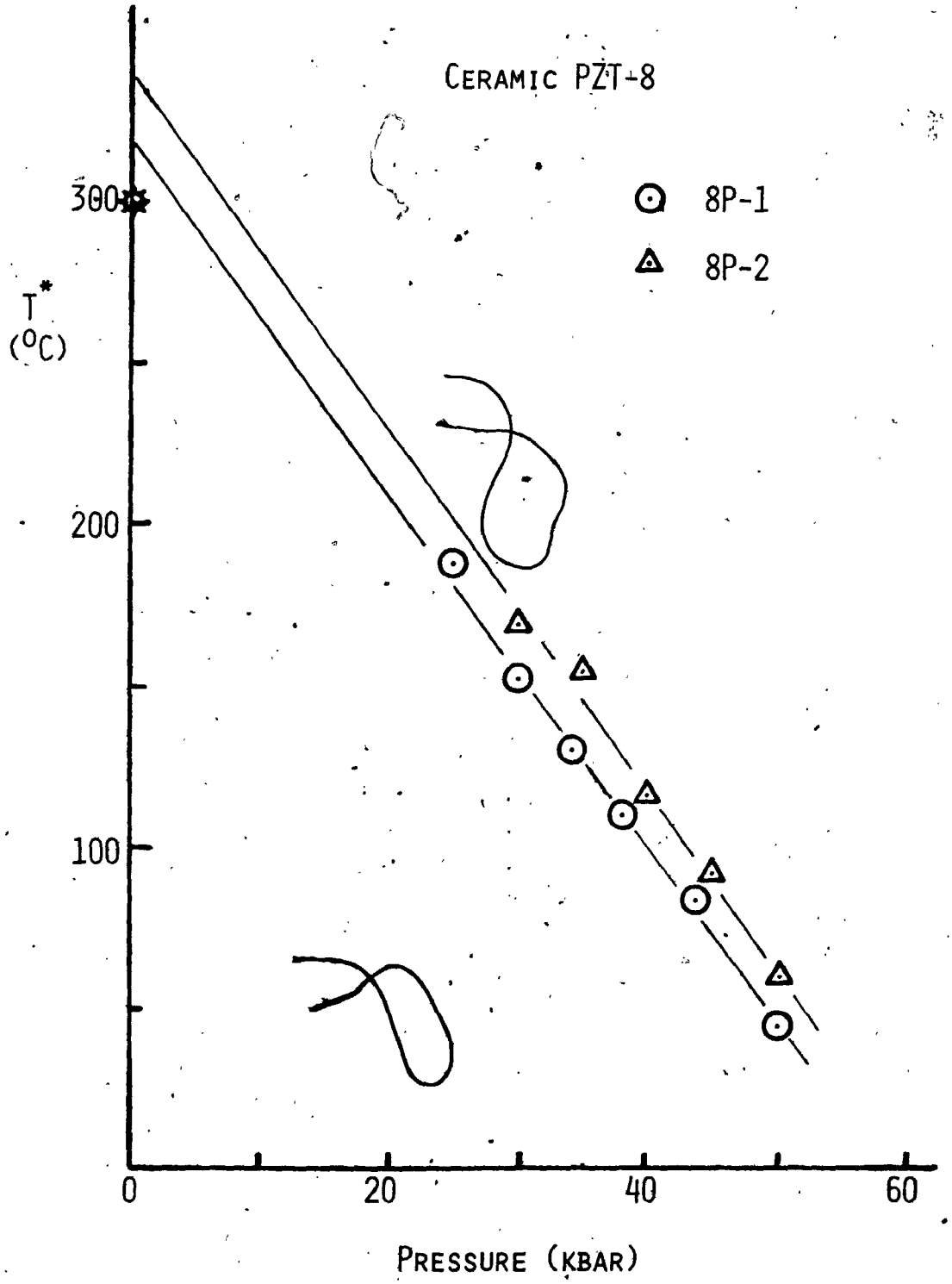

Figure 6.18 : Graph of the change in T* with pressure for both of the PZT-8 samples investigated.

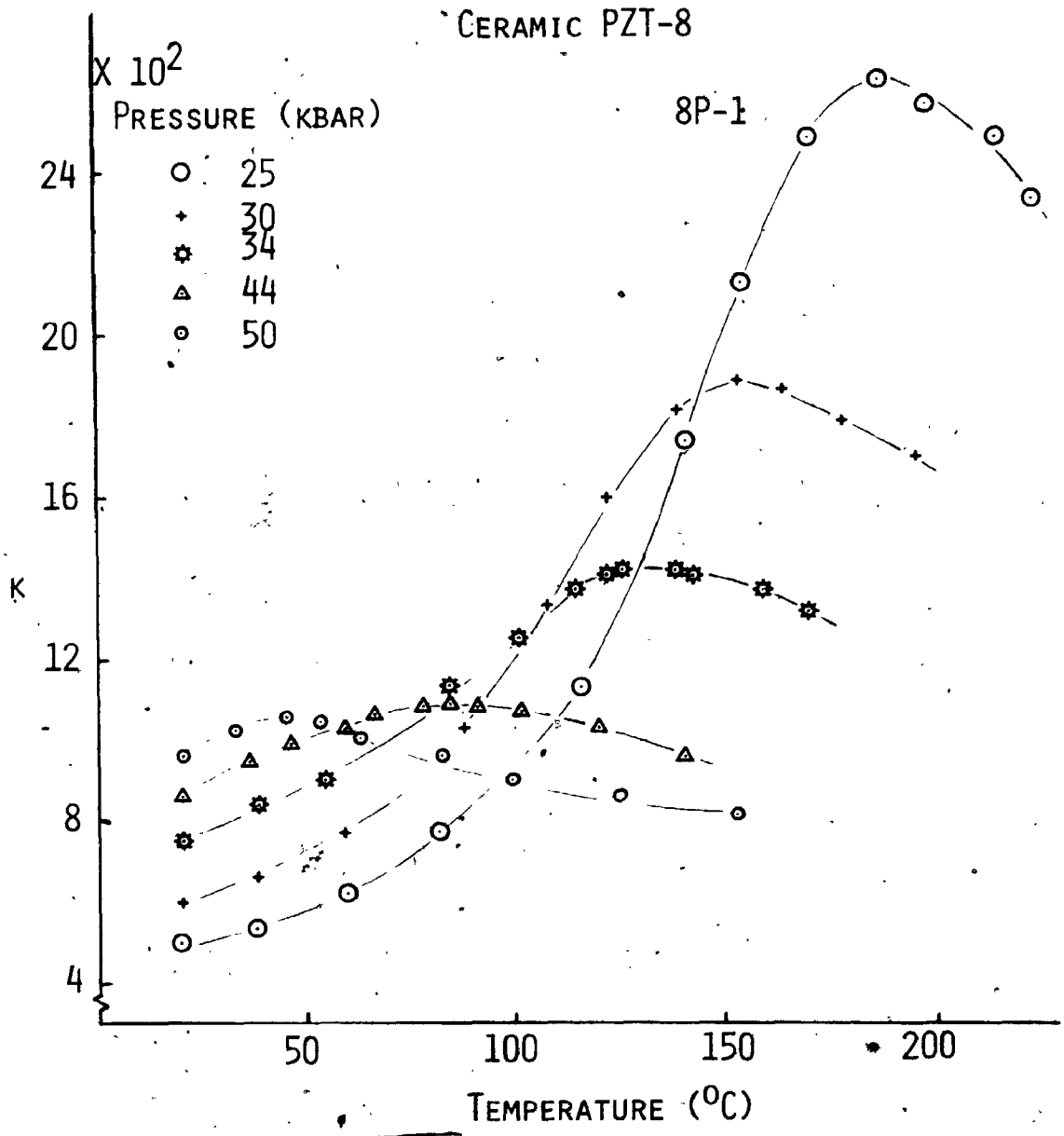

Figure 6.19 : Graph of the temperature dependence of the dielectric constant, k, at various pressures for one of the PZT-8 samples (8P-1).

of these ceramics consists of a linear decrease in the transition temperature with pressure at a rate on the order of 4 - 6 ^{o}C/kbar (Table 6T-2). This result, although of importance to material scientists working on the PZT system, should be applied cautiously to perovskite structures in the earth's mantle. That is, the fact that dT*/dp is found to be negative for all perovskite ceramics in the present experiments is expected, since this represents the change in the tetragonal - cubic phase boundary which is known to decrease with pressure (Samara, 1969, 1970; Samara et al, 1975). If, however, this trend of negative dT/dp values also occurs for the solid-solid transformations in silicate perovskites, this could have important geophysical implications. In particular, this would be of importance in relation to the recent theories on the role of phase transitions in the earth's mantle as the mechanism for regulating and driving the lithospheric plates (see, for example, Ringwood, Chap. 15, 1975). However, in light of the absence of measurements on silicate perovskite materials themselves, it would be misleading to emphasize this effect. Clearly, experimental studies on silicate perovskites which either confirm or refute this finding would be desirable.

A second feature of note is that the peak in the variation of the dielectric constant with temperature remains prominent to the highest investigated pressures (>50 kbar). With increasing values of pressure, however, the peak shape is found to broaden and shift towards lower temperatures. The details of broadening depends upon both the composition of the ceramic and the pressure range investigated. In general, however, the typical behaviour of FE perovskite ceramics consists of a phase transition which, although it remains prominent even at high

Table 6T-2

Ceramic	Sample No.	(dT*/dp) (°C/kbar)
PZT-4	P2	-4.4
PZT-4	P4	-4.8
PZT-4	P5	-4.6
PZT-4	Average	-4.6
PZT-5A	5P-1	non-linear
PZT-5A	5P-2	non-linear
PZT-5A	5P-3	non-linear
PZT-5H	5PH-1	-4.6
PZT-5H	5PH-2	-4.1
PZT-5H	5PH-3	-3.9
PZT-5H	Average	-4.2
PZT-8	8P-1	-5.5
PZT-8	8P-2	-5.7
PZT-8	Average	-5.6

pressures, is "smeared out" with increasing pressure (Figure 6.16). Clearly, the dielectric constant - temperature curves for these ceramics yield information not only on the change in T* with pressure, but also on the change in the nature and general behaviour of the phase transition with pressure. One can reasonably apply the results from the PZT ceramics to predict the behaviour of a mineral which undergoes a phase transition (not necessarily ferroelectric) in the earth's crust or upper mantle. Under these pressure conditions, a crystallographic change in a mineral in a polycrystalline form would not occur abruptly at the depth z which corresponds to the pressure - temperature equilibrium point for the transformation. Instead, the transformation would take place over a much larger radial interval in the earth's interior.

CHAPTER VII

SINGLE CRYSTAL CALCIUM TITANATE

7.1 General Properties

Calcium titanate ($CaTiO_3$) is a naturally occurring mineral which is found in several localities including Magnet Cove (Arkansas), Hot Springs (Arkansas) and Alno (Sweden). Although the perovskite-structured materials derive their name from the mineral form of $CaTiO_3$, the latter has a distorted perovskite structure and, at room temperature and pressure is orthorhombic (Kay and Bailey, 1957). In addition, both natural and synthetic crystals are highly twinned. Calcium titanate, which is not ferroelectric, is thought to be a paraelectric material with a "negative" (<0K) Curie temperature (Rupprecht and Bell, 1964). The frequency of the soft mode in this material never becomes small enough for lattice instability to cause a FE transition.

To date the temperature and frequency dependence of the dielectric properties of both synthetic crystals and ceramics have been reasonably well investigated. Linz and Herrington (1958), who investigated the dielectric and optical properties of synthetic $CaTiO_3$ found that with increasing temperature the dielectric constant decreases, whereas the loss tangent increases. No anisotropy effects or frequency dependence were observed. They report, however, on a crystallographic transition which was observed optically at ~0°C although no details of the transition were given. Rupprecht and Bell (1964) measured the dielectric

properties of $CaTiO_3$ at microwave frequencies and report that the dielectric constant accurately obeys a Curie-Weiss law of the form $k = k_L + C/(T - T_c)$ over a wide temperature range up to ~1000 K. Tsykalov and Poplavko (1969) investigated polycrystalline specimens of $CaTiO_3$ and found little temperature dependence for the dielectric constant in the temperature range 0 - 1000°C. In addition, no dispersion was observed in the frequency range of 37-77 GHz. Finally, Knyazev et al (1974) measured the dielectric properties of polycrystalline calcium titanate at 37 GHz, and found a decrease in the dielectric constant with increasing temperature. All of the above mentioned investigations on either synthetic crystals or ceramics indicate that the dielectric constant decreases with increasing temperature, and that little or no dispersion is observed in this material. To the author's knowledge, no detailed pressure or temperature investigations of the dielectric properties have been undertaken on natural perovskite single crystals.

7.2 Dielectric Measurements

The crystals investigated in the present study were from Magnet Cove, Arkansas. All specimens were black in colour with a dull metallic lustre. Although some samples showed cubic and dodecahedral faces, their external shapes were mostly octahedral with several well defined crystal faces. They appeared to be, however, quite weathered with several small cracks, and in some cases contained light brown or whitish inclusions. The best specimens were chosen and ground into platelets of ~1 - 1.5 mm thickness parallel to a (100) plane. These faces were silver painted with a thin wire attached, and surrounded by ceresine in the

high pressure cell. As in the case of the barium titanate single crystals, several experiments were unsuccessful due to the wire shearing on initial loading of the press. Experimentally, one has little control over this situation. Thus, of the seven experiments attempted, only three were successful.

The results of these experiments are presented in Figures 7.1 to 7.6 such that Figures 7.1 and 7.2 indicate the results for sample no. CT-1, Figures 7.3 and 7.4 for sample no. CT-2 and Figures 7.5 and 7.6 for sample no. CT-3. Note that the (measured) capacitance is plotted in these figures instead of the dielectric constant. This was done since an accurate area determination which is required to calculate the dielectric constant was not possible due to the irregular shape of the sample platelets. Nevertheless, approximate areas are given in Table 7T-1 along with a brief summary of some of the results.

Figure 7.1 shows the temperature dependence of the capacitance and dissipation factor for sample CT-1 for various frequencies (1, 2, 5, 10 kHz) under isobaric (p = 30 kbar) conditions. In general, for constant pressure, the capacitance increases with both increasing temperature and decreasing frequency; whereas, the dissipation factor decreases with increasing temperature and increasing frequency. Note the minimum in D observed with a measuring frequency of 1 kHz.

Figure 7.2 shows the temperature dependence of both the capacitance and dissipation factor for sample CT-1 at various pressures (25, 40, 50 kbar) and measuring frequencies (1, 10 kHz). In general, with increasing temperature, the capacitance increases with increasing pressure and decreasing frequency. The dissipation factor decreases

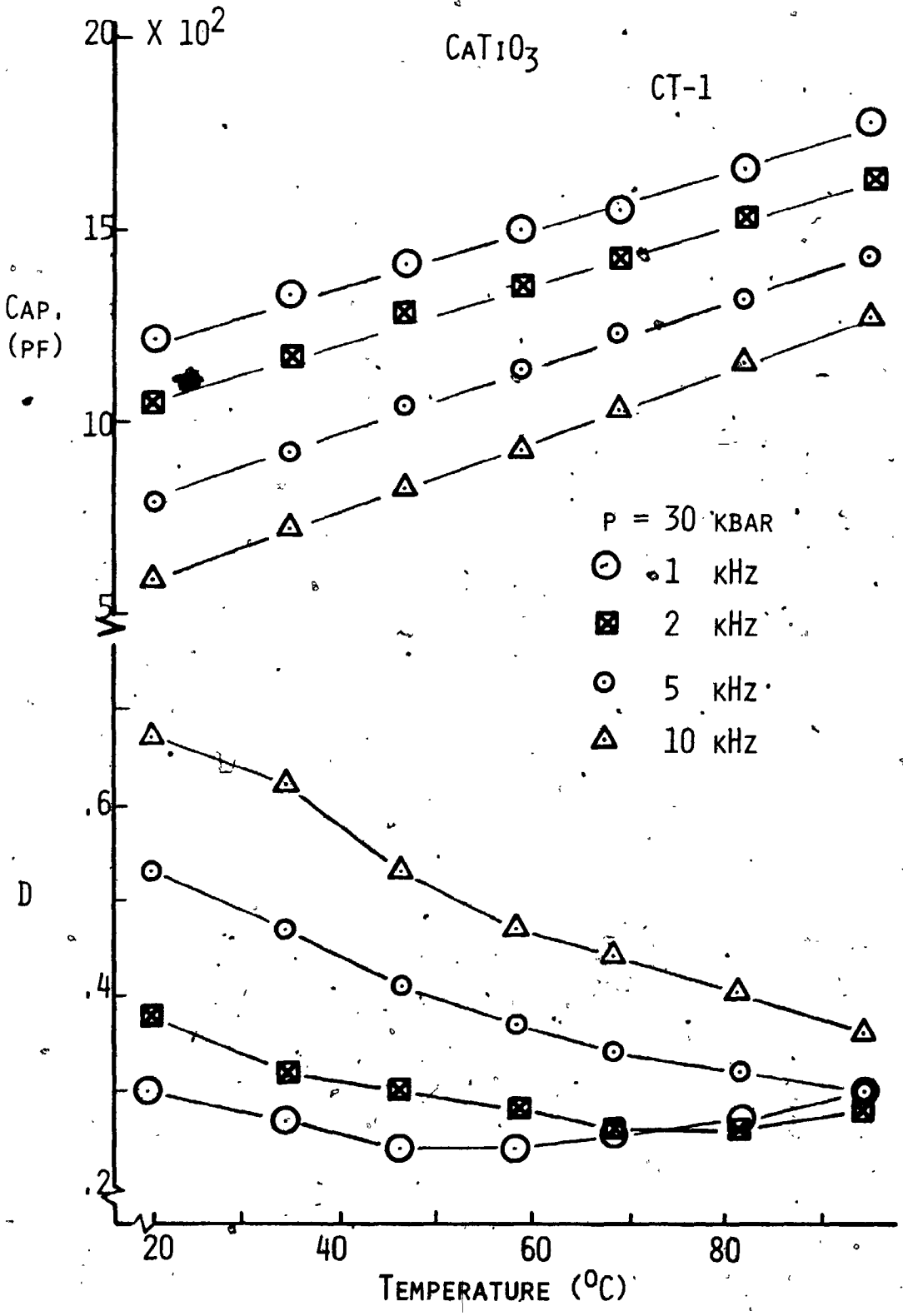

Figure 7.1 : Graph of the temperature and frequency dependence of the capacitance and dissipation factor for CT-1 at p=30 kbar.

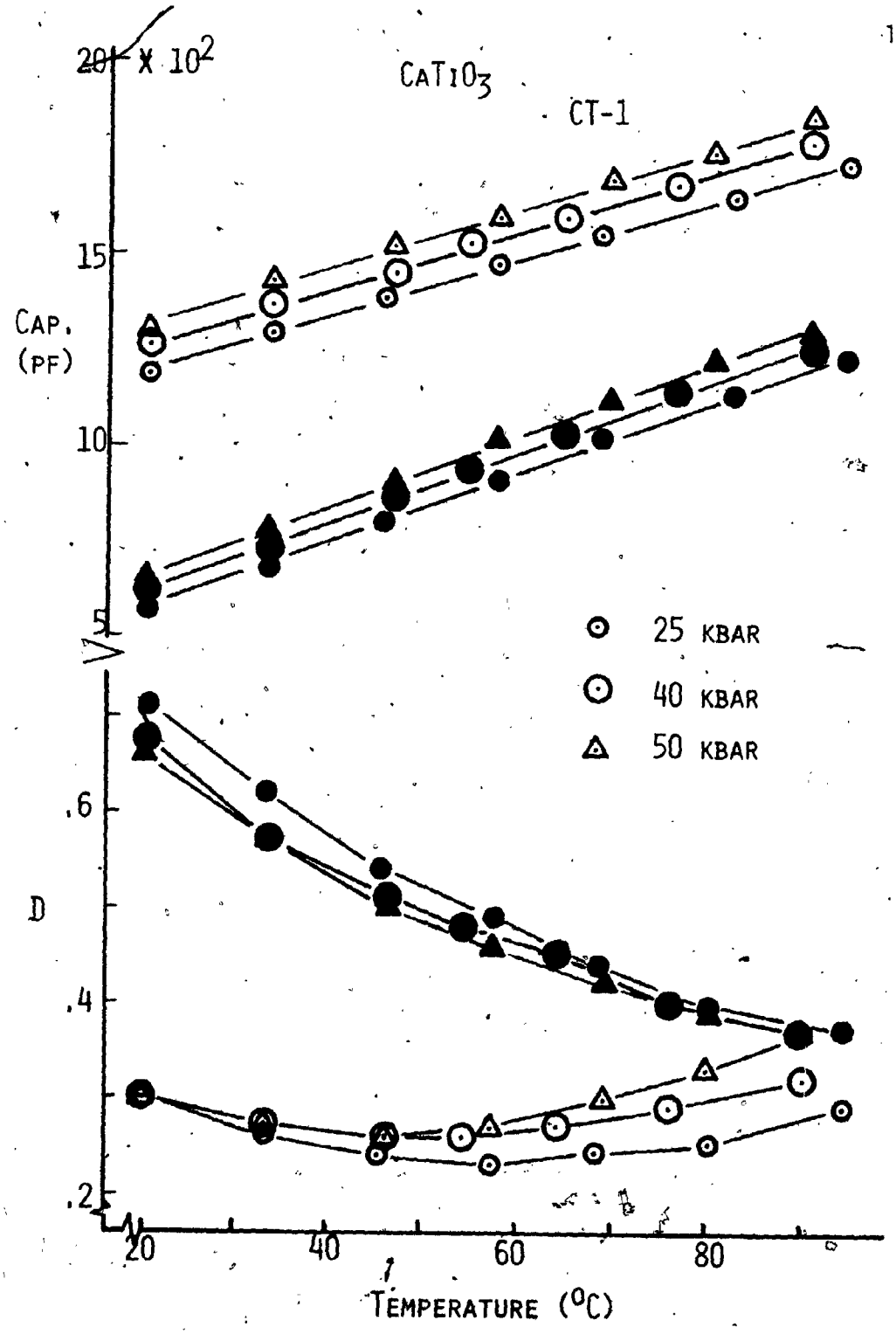

Figure 7.2 : Graph of the temperature and pressure dependence of the capacitance and dissipation factor for CT-1 for 1 kHz (open symbols) and 10 kHz (shaded symbols).

with increasing pressure for f = 10 kHz but increases for f = 1 kHz. In addition, the minimum exhibited in D for f = 1 kHz is shifted to higher D values and lower temperatures with increasing pressure.

Figure 7.3 shows the temperature and frequency dependence of the capacitance and dissipation factor for sample CT-2 for p = 30 kbar. Similar to sample CT-1, the capacitance increases with increasing temperature and decreasing frequency. The behaviour of the dissipation factor, however, is completely different than that observed for CT-1. In this case, a minimum in the curve is exhibited for frequencies of 2, 5 and 10 kHz such that with increasing frequency, the minimum is shifted to higher D values and higher temperatures. Also, no minimum is observed for f = 1 kHz - it simply increases with increasing temperature.

Figure 7.4 shows the temperature dependence of the capacitance and dissipation factor of sample CT-2 for various pressures (25, 40 and 50 kbar) for two measuring frequencies (1 and 10 kHz). The capacitance increases with increasing temperature, pressure and decreasing frequency. Similar to the minimum in the D curve for CT-1 for f = 1 kHz, the minimum in D for f = 10 kHz in this case is shifted to higher D values and lower temperatures with increasing pressure. Similar behaviour was observed for frequencies of 2 and 5 kHz. For f = 1 kHz, however, D increases with increasing temperature and increasing pressure.

Figure 7.5 indicates the temperature and frequency dependence of the capacitance and dissipation factor for sample CT-3 under isobaric (p = 30 kbar) conditions. As with the other samples investigated, the capacitance increases with increasing temperature and decreasing frequency. In this case the dissipation factor increases with increasing

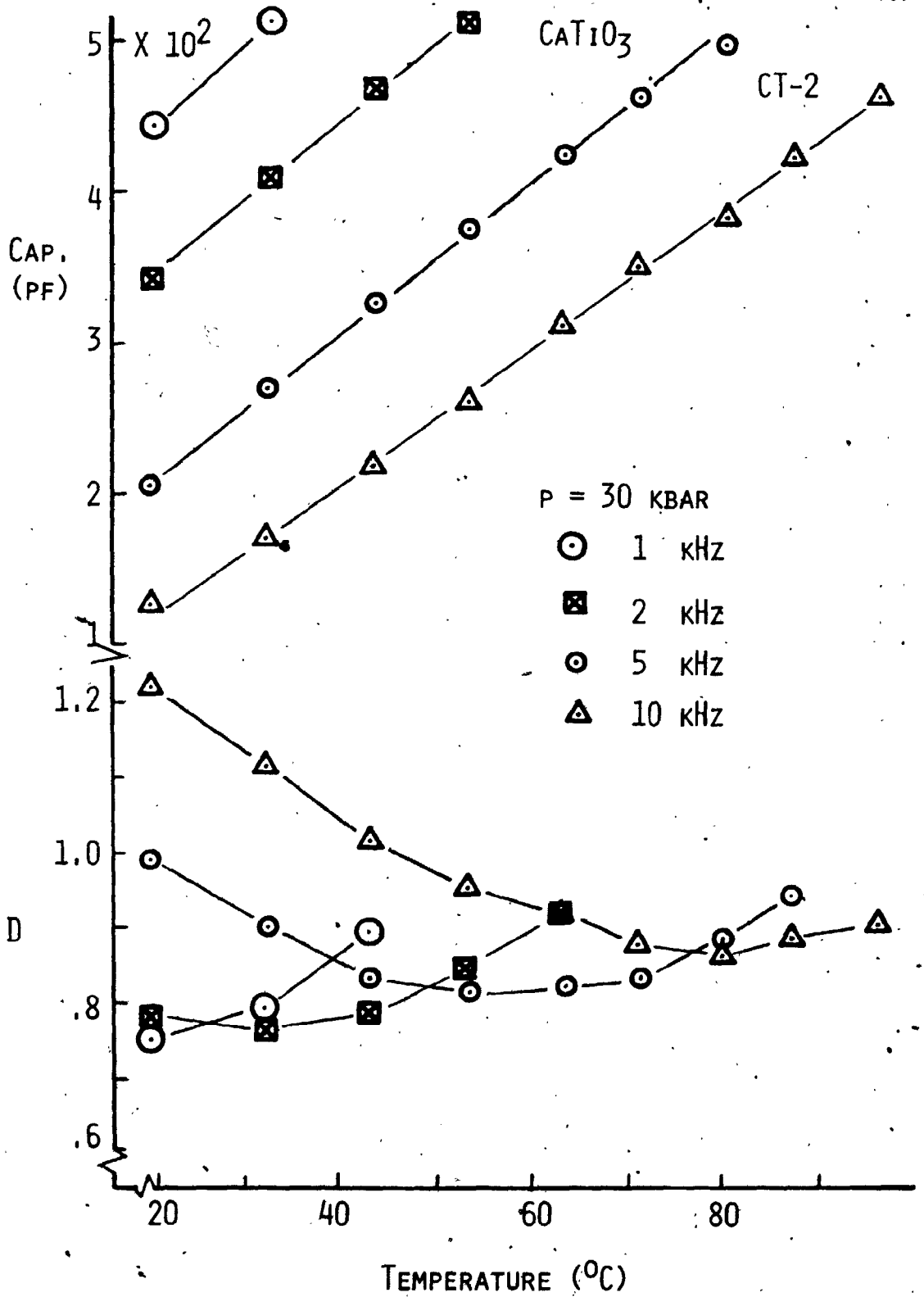

Figure 7.3 : Graph of the temperature and frequency dependence of the capacitance and dissipation factor for CT-2 at p=30 kbar.

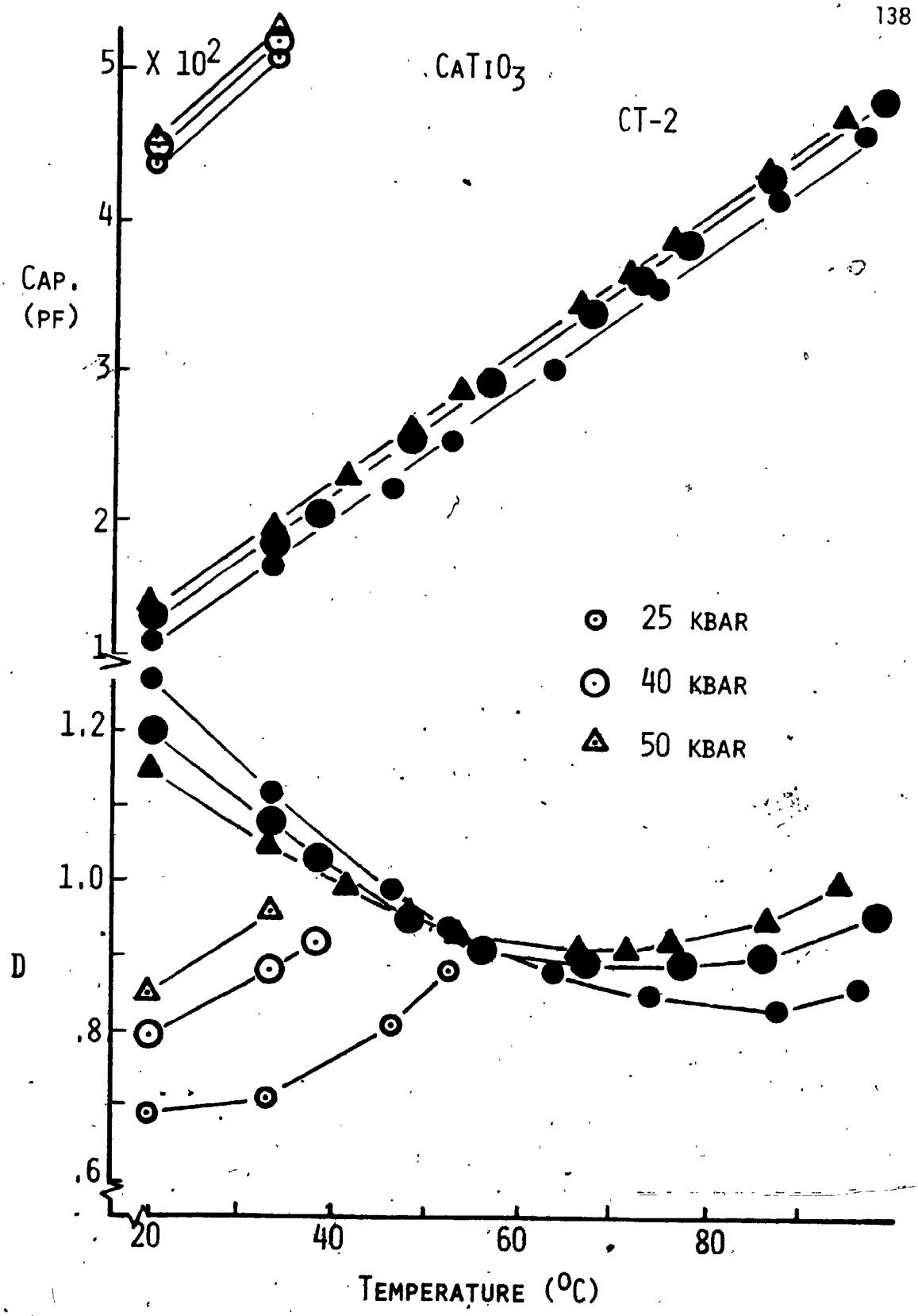

Figure 7.4 : Graph of the temperature and pressure dependence of the capacitance and dissipation factor for CT-2 for 1 kHz (open symbols) and 10 kHz (shaded symbols).

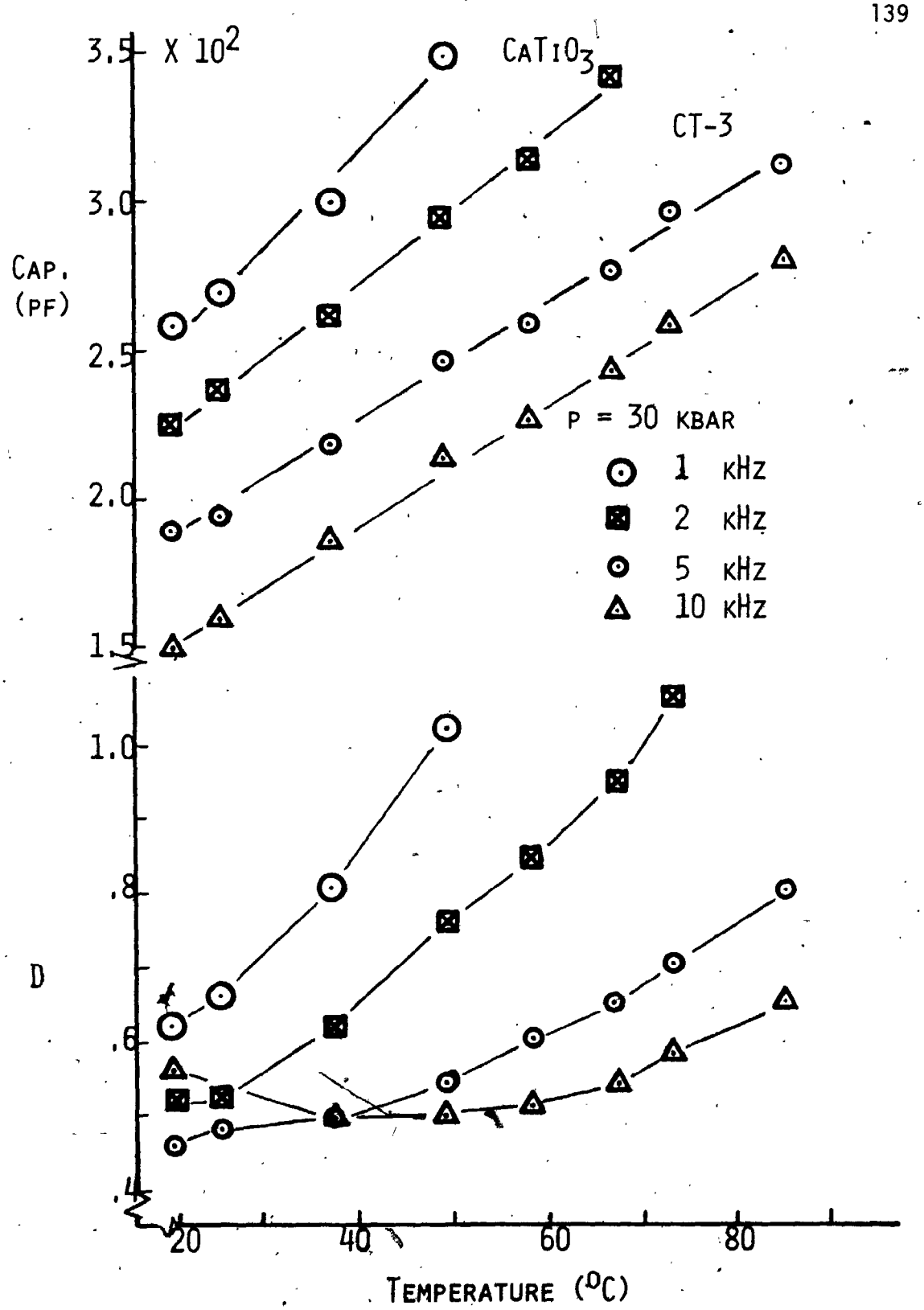

Figure 7.5 ; Graph of the temperature and frequency dependence of the capacitance and dissipation factor for CT-3 at p=30 kbar.

temperature for measuring frequencies of 1, 2 and 5 kHz. For f = 10 kHz, however, a broad minimum is observed.

Figure 7.6 shows the temperature dependence of the capacitance and dissipation factor for sample CT-3 for various constant pressures (25, 40 and 50 kbar) and frequencies (1, 10 kHz). In general, with increasing temperature and pressure the capacitance increases. This behaviour is similar to that observed for the other two samples. The dissipation factor increases with increasing pressure for both measuring frequencies, and the minimum in D for f = 10 kHz is shifted to higher values and lower temperatures with increasing pressure.

7.3 Discussion of $CaTiO_3$ Results

A calculation of the dielectric constant, k, for each of the three samples (see Table 7T-1) indicates that there is not only a large difference among the samples (k ~ 2200, CT-1; k ~ 1500, CT-2; k ~ 1100, CT-3; all at p = 30 kbar, f = 10 kHz, T = 22°C), but that the dielectric constant for each sample is well above that previously reported for pure synthetic calcium titanate (k ~ 170, Linz and Herrington, 1958). In addition, these values are considerably larger than those observed for non-perovskite naturally occurring single crystals (k ~ 8, calcite $CaCO_3$; k ~ 25, hematite Fe_2O_3; k ~ 4.5, quartz SiO_2; k ~ 34-81, ilmenite $FeTiO_3$; Parkhomenko, 1967). In fact, the dielectric constant values measured for these crystals are enormous for a material which is not ferroelectric. Part of the polarizability arises due to the perovskite structure of the minerals. That is, the perovskite structure itself generates an internal electric field which increases both the polarization and the dielectric

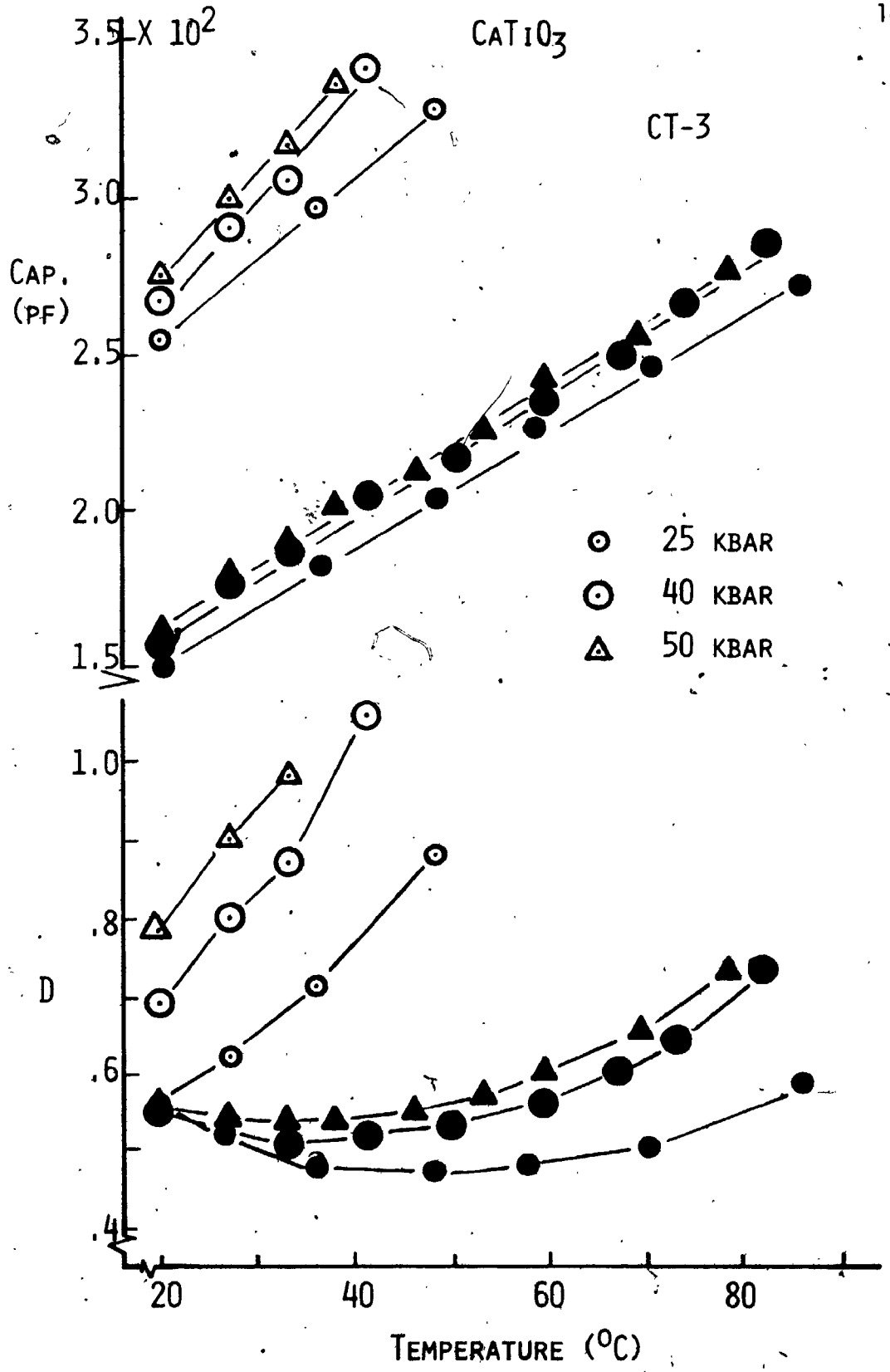

Figure 7.6 : Graph of the temperature and pressure dependence of the capacitance and dissipation factor for CT-3 for 1 kHz (open symbols) and 10 kHz (shaded symbols).

Table 7T-1

Sample No.	~t (cm)	~A (cm^2)	C (pf)	~k	(dC/dT) (pf/^oC)
CT-1	.10	.30	590	2200	9.1
CT-2	.14	.13	126	1500	4.4
CT-3	.10	.16	150	1100	2.0

All samples are (100) orientation. Values for C are for p = 30 kbar and room temperature (22^oC). Both C and (dC/dT) are for a measuring frequency of 10 kHz at 30 kbar. Values for (dC/dT) were determined by a linear regression analysis for the temperature range 20-80^oC.

constant. Nevertheless, it is evident that some other polarization mechanism is responsible for the values of the observed order of magnitude. Certainly the most likely candidate is some form of relaxation polarization caused by impurities in the sample. As evidenced from the previous discussion on the $Pb(Zr,Ti)O_3$ system (Section 6.1), even minor amounts of chemical additives to perovskite structure materials can drastically alter their physical properties. Thus the large numerical discrepancies found from sample to sample in the present experiments could simply be attributed to differing amounts and/or kinds of sample impurities. In addition, both the large temperature dependence of the dielectric constant and the observed dispersion could readily be attributed to impurity related polarization (Parkhomenko, 1967).

An examination of the temperature dependence of the dissipation factor for the three samples (Figures 7.1, 7.3, 7.5) clearly shows that in the investigated temperature range, the behaviour of the dissipation factor with temperature at constant pressure differs from sample to sample. In brief, for CT-1 (Figure 7.1) the dissipation factor decreases with increasing temperature for frequencies of 2, 5 and 10 kHz, but exhibits a relative minimum for a measuring frequency of 1 kHz. For CT-2 a relative minimum is observed for frequencies of 2, 5 and 10 kHz, but not for a frequency of 1 kHz. For the latter frequency, D monotonically increases with increasing temperature. For CT-3, a minimum is observed for a measuring frequency of 10 kHz, and, for the other three measuring frequencies, D values are seen to increase with temperature. These observed differences among samples simply reflect the fact that one is looking in a different part of the total D-T curve for each sample. One

can readily combine the results of the three experiments to make a composite picture of the behaviour of the dissipation factor with temperature for $CaTiO_3$ (see Figure 7.7). Clearly, the temperature at which the minimum occurs simply represents that at which the predominent loss mechanism for the sample changes. One might expect that the decrease in D observed in the lower temperature region is the tail of a still lower temperature relaxation peak associated with the impurity content of the sample. From Table 7T-1 and Figures 7.1, 7.3, 7.5, 7.7, it can be seen that, for constant pressure and frequency, the temperature of the minimum is higher for samples with larger dielectric constant and (dC/dT) values. If one makes the reasonable assumption that both of these values increase with increasing impurity content, then the qualitative differences observed in the D values between different samples can easily be explained. Obviously, the loss associated with the relaxation mechanism remains predominant to higher temperatures for samples with higher impurity content. The observed increase in the dissipation factor for each sample in the higher temperature region is undoubtably merely caused by an increase in the frequency dependent electrical conductivity of the sample. This frequency dependence of the minimum in D may be explained as being caused by an increase in the relaxation frequency with increasing temperature (R.K. Chan, personal communication, U.W.O., 1976).

The dielectric measurements as such give little clue as to the type of impurity content in the sample. There are, however, several types of impurities which may play a role. One might expect, for example, that the samples are highly non-stoichiometric, having probably

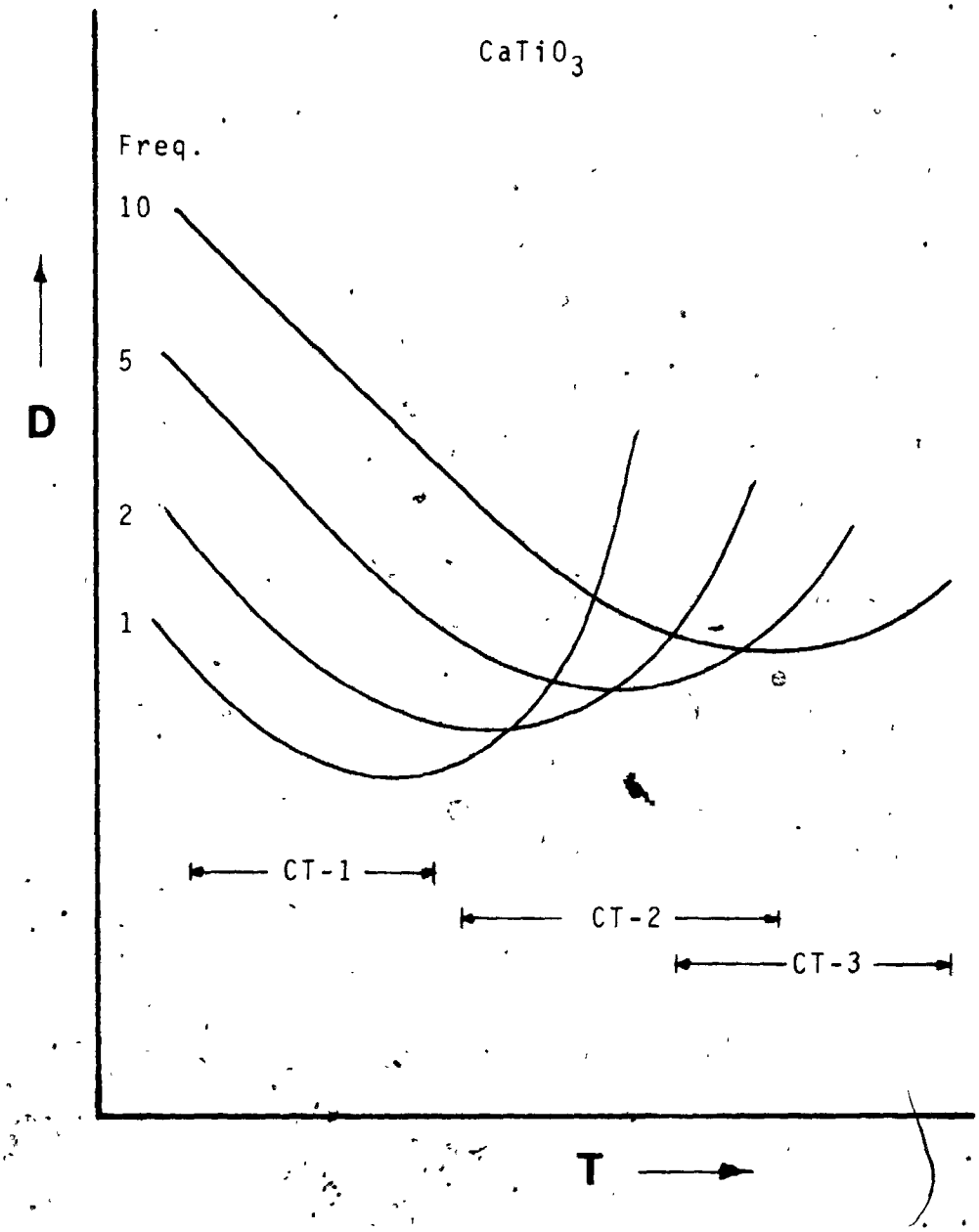

Figure 7.7 : Schematic composite representation showing the overall isobaric temperature and frequency dependence of the dissipation factor for a natural crystal of $CaTiO_3$. The portion of these curves detailed by each of the three samples investigated is shown at the bottom of the figure. Note that since k(CT-1) > k(CT-2) > k(CT-3), and the investigated temperature range is the same for each sample (20-100°C), the actual temperature of the minimum is higher for a sample with a larger dielectric constant.

a large number of oxygen vacancies. Alternatively, atoms in substitutional or interstitial lattice sites may be thermally activated and thereby affect the dielectric properties of the crystal. If the crystal itself is inhomogeneous, interfacial polarization of the Maxwell-Wagner type may occur (von Hippel, 1954). In this case, if the crystal contains small inclusions or pockets of a conductor or semi-conductor, substantial accumulation of charge would be found at the interfaces. This would lead to a large frequency dependent dielectric constant which would decrease with increasing frequency. In any event, the experiments on calcium titanate single crystals indicate that extremely large dielectric constant values can be obtained for perovskite structured materials, even for those which are not ferroelectric.

CHAPTER VIII

SUMMARY AND CONCLUSIONS

(1) On the basis of independent experimental evidence, the suggestion and possible role of ferroelectric phases in planetary interiors, with a particular emphasis on perovskite structures in the earth's interior has been put forward. By implication, it was reasoned that, if present, FE phases in the earth's mantle would affect the attenuation of electromagnetic radiation, space charge distributions, electrical current flow, radiative heat transfer, diffusion of charged particles and the propagation of elastic seismic waves. The present experiments have clearly demonstrated that FE hysteresis is possible in perovskite ferroelectrics which are under high pressure conditions of deviatoric stresses and strains in which the FE phase forms part of a composite system; that is, under the conditions it would encounter if it formed part of a planetary interior. Moreover, the experiments have shown that, depending upon the dielectric and elastic compatibility between matrix and inclusion, the stability field for the ferroelectric phase may be extended into p-T regions which, under normal circumstances are outside the FE stability range for the material.

(2) The concept of the inhomogeneous (transforming) inclusion embedded in a solid matrix has been applied to experiments performed with solid-media high pressure devices. In particular, the Gibbs free energy change for a ferroelectric inclusion undergoing the paraelectric-ferroelectric transition in the presence of an (isotropic) constraining

matrix was determined. It was found that extra energy terms arise due to the elastic energy of the transformed inclusion, as well as the interaction energy of the inclusion with the applied stress field. This theoretical treatment suggests that suitable matching of the elastic contrast between matrix and inclusion with the applied stress field can (a) stabilize an existing FE phase in a p-T region which is outside its normal stability field, and (b) lead to a FE state in a material which is not ordinarily FE under high pressure conditions.

(3) A general technique was developed for measuring the pressure dependence of the dielectric properties of large dielectric constant materials in solid-media pressure devices. The technique has two distinct advantages over the method used previously by three independent research groups. First of all, the electrical leads to the crystal need not be brought through the pyrophyllite gaskets. This makes the pyrophyllite cube both easier and faster to assemble, and increases the number of successful runs. Secondly, the impairing effects of the high pressure cell on the capacitance and dissipation factor can be conveniently accounted for. In particular, it was found that the edge corrections are relatively small provided that the measurements are made with a high (~10 kHz) measuring frequency, and that the water content of the pyrophyllite is low.

(4) High pressure hysteresis loop studies on barium titanate single crystals has shown that FE hysteresis is possible in perovskite structure materials in single crystal form under high pressure constraint. The existence of the ferroelectric hysteresis loop at a pressure of 49 kbar and room temperature corresponds to the highest

pressure at which FE hysteresis has been observed. It would appear that the persistence of hysteresis under pressure, as well as the relative values of polarization and coercive field depend not only on the orientation and dimensions of the sample, but also on the elastic and plastic properties of the surrounding matrix.

(5) A high pressure investigation to pressures greater than 50 kbar on the dielectric properties of polycrystalline barium titanate and four members of the perovskite $Pb(Zr,Ti)O_3$ system has detailed the behaviour of these materials in a pressure region well above that previously reported. In general, four of the five ceramics investigated ($BaTiO_3$, PZT-4, PZT-5H, PZT-8) exhibited behaviour which seems to be typical for perovskite ceramics. This behaviour consists of a linear decrease with pressure in the ferroelectric-paraelectric transition temperature at average rates of $-4.4^{o}C$/kbar ($BaTiO_3$), $-4.6^{o}C$/kbar (PZT-4), $-4.2^{o}C$/kbar (PZT-5H) and $-5.6^{o}C$/kbar (PZT-8). In addition, plots of the temperature dependence of the dielectric constant for various isobaric pressure settings has indicated that with increasing values of pressure, the maximum value of the dielectric constant decreases, and the peak half-width, i.e. its extent in temperature increases. This finding was tentatively explained in terms of the difference in magnitude and distribution of residual microstresses in the ceramic compact. For the other ceramic investigated, PZT-5A, the transition temperature also decreases with increasing pressure, but exhibits a point of inflection in the T*-p curve at ~30 kbar. In this case, the dielectric constant - temperature peak is extremely broad in this region, and with increasing values of pressure, 'sharpens' to a relatively pressure independent shape for

pressures above ~40 kbar. For all of the FE ceramics investigated, the initial application of pressure results in a large decrease in their dielectric constant. This decrease was attributed to 90^0 domain re-orientation relative to the direction of maximum deviatoric (planar) stresses during the initial stage of non-hydrostatic stress distribution.

(6) The interpretation of the experimental results in terms of the deviatoric stresses present in a solid-medium high pressure apparatus has indicated that during the initial loading of the press, the sample experiences a predominately two-dimensional deviatoric stress perpendicular to the axis of the sample disc of 3-5 kbar in magnitude. In the higher pressure region, the results suggest that the same type of deviatoric stress is present, but of magnitude on the order of 1 kbar.

(7) The pressure and temperature dependence of the dielectric properties of natural single crystals of calcium titanate indicated a wide variance in the dielectric values from sample to sample. Moreover, the large dispersion in both the dielectric constant and dissipation factor is in contrast to that previously reported for synthetic crystals and ceramics. With increasing temperature, for constant pressure, the dielectric constant values increase, whereas the dissipation factor values exhibit a frequency dependent minimum. In general, the temperature of the minimum is higher for samples with larger dielectric constant and (dC/dT) values. This difference is attributed to differing amounts and kinds of sample impurities in these naturally occurring specimens. These experiments clearly show that extremely large dielectric constant values ($k \sim 10^3$) can be obtained even for non-ferroelectric perovskite structure materials.

APPENDIX A

Dielectric Definitions

The definitions of the parameters measured in these experiments follow that of von Hippel (1954), ASTM (1970) and Collett and Katsube (1973).

When a sinusoidal voltage V of angular frequency ω is connected across a capacitor which has vacuum as its dielectric, the capacitor stores a charge

$$Q = C_o V \tag{A.1}$$

and draws a charging current I_c which leads the voltage by 90°. C_o is the vacuum (or geometrical) capacitance. When filled with an insulating material, the capacitor increases its capacitance to

$$C = k C_o \tag{A.2}$$

where k is the (relative) dielectric constant of the material. For a disc shaped sample, the dielectric constant is given by

$$k = \frac{C t}{\varepsilon_o A} \tag{A.3}$$

where t is the sample thickness, A is the area of the plate and ε_o is the permittivity of free space. In addition to the charging component of the current, there may simultaneously appear a loss current component, I_ℓ, in

phase with the voltage such that

$$I_\ell = G\,V, \tag{A.4}$$

where G is the conductance of the dielectric. The dissipation factor, D, or loss tangent, tan δ, is the ratio of the loss current to charging current, i.e.

$$D = \tan\delta = \frac{I_\ell}{I_C} \tag{A.5}$$

Since the loss current can contain an inphase component which can be due to any loss mechanism, it is customary to express this by the introduction of a complex permittivity:

$$\varepsilon^* = \varepsilon' - i\,\varepsilon'' \tag{A.6}$$

where ε^*, ε' and ε'' are the complex permittivity, real permittivity and loss factor, respectively. Alternatively, the relative complex permittivity, k^*, can be defined as

$$k^* = \frac{\varepsilon^*}{\varepsilon_o} = k' - i\,k''. \tag{A.7}$$

Then the dissipation factor becomes

$$D = \tan\delta = \frac{\varepsilon''}{\varepsilon'} = \frac{k''}{k'} \tag{A.8}$$

The dielectric conductivity, σ, is

$$\sigma = \omega\varepsilon'' = \omega\varepsilon' \tan\delta. \tag{A.9}$$

All of the results obtained in the present experiments are presented in terms of the real dielectric constant, k, and the dissipation factor, D. Knowing these and the above equations, any other dielectric quantity (ε', ε'', σ, etc.) can readily be calculated.

APPENDIX B

Technique for Bringing Electrical Leads Through the Pyrophyllite Gasket

In order to ensure that the "backing insulation" capacitances (B, C, Figure 4.4) were effectively eliminated from the measuring circuit by the grounding techniques described in Section 4.3, an experimental procedure was devised to by-pass these large capacitances. This involved bringing the electrical leads out through the pyrophyllite gaskets between the anvil faces. In this section, the basic experimental procedure for doing this will be outlined. The features of this technique are shown in Figure B.1 and may be summarized as follows:

(1) The wires should be brought out through any of the (1, 1, 1) directions of the pyrophyllite cube (i.e. the cube corners) since the flow of pyrophyllite appears to be less in these regions than along the cube edges.

(2) Since a bare wire immediately breaks on loading of the press, the wire must necessarily be protected by a stainless steel tube. For the 1000 ton capacity press, syringe tubes of both 22 and 17 gauge proved successful.

(3) The tube has to be completely immersed into the cube until it is almost touching the sample. Gluing it with a paste of Elmer's white glue mixed with pyrophyllite powder is effective in securing it there.

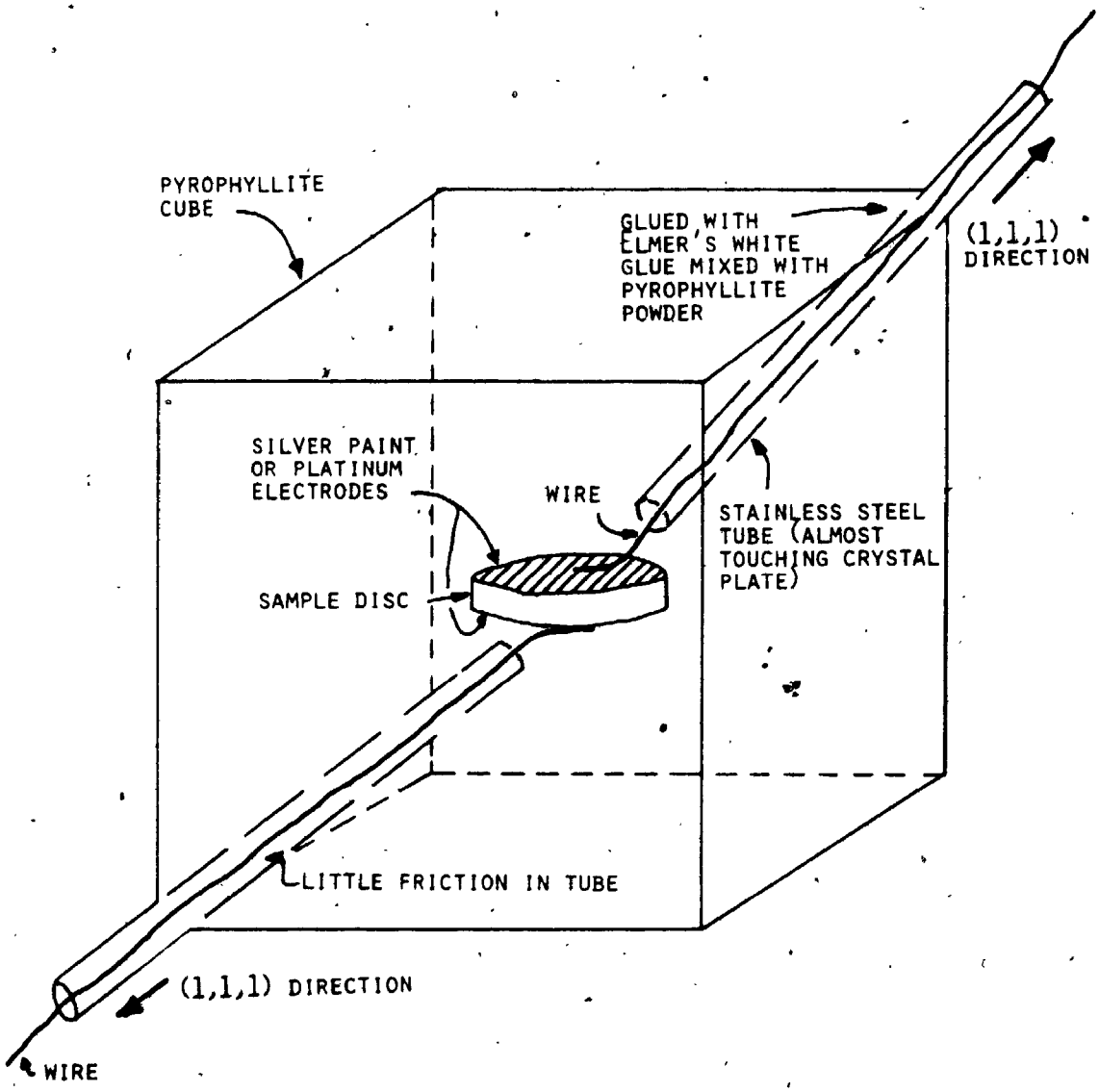

Figure B.1 : Schematic representation of the experimental proceedure for bringing electrical leads through the pyrophyllite gaskets.

(4) The inner wire should be loose fitting with little or no internal friction in the tube.

(5) The wires should not be touched once the gasket forms.

APPENDIX C

Edge Correction Data and Sample Calculation

Figures C.1 and C.2 show the temperature and frequency dependence of the edge capacitances (C_e) and conductances (G_e) which are present in a pyrophyllite cell in the 1,000 ton capacity press. These results were used in equations (4.1) - (4.3) to correct for the capacitances (D, E, Figure 4.4) and electrical leakage paths (F, G, Figure 4.4) shunting the sample in the high pressure cell (see Section 4.3). The application of these figures in equations (4.1) - (4.3) is straightforward. For example, for sample no. 5P2 (PZT-5A) at a temperature of 142°C and a pressure of 42 kbar, the measured capacitance (C_x) for a measuring frequency of 1 kHz was 179 pf. From Figure C.1, the edge capacitance (C_e) for this temperature and measuring frequency is 3 pf. Thus, the sample's capacitance (C) is (equation 4.1)

$$C = C_x - C_e$$

$$= 179 - 3$$

$$= 176 \quad \text{pf.}$$

Similarly, for the correction of the measured dissipation factor ($D_x = .020$), the measured conductance ($G_x = 22 \times 10^{-9}$ ohm^{-1}) and (from Figure C.2) the edge conductance ($G_e \simeq 10.5 \times 10^{-9}$ ohm^{-1}) need to be known. Then the sample's dissipation factor is (equation 4.3)

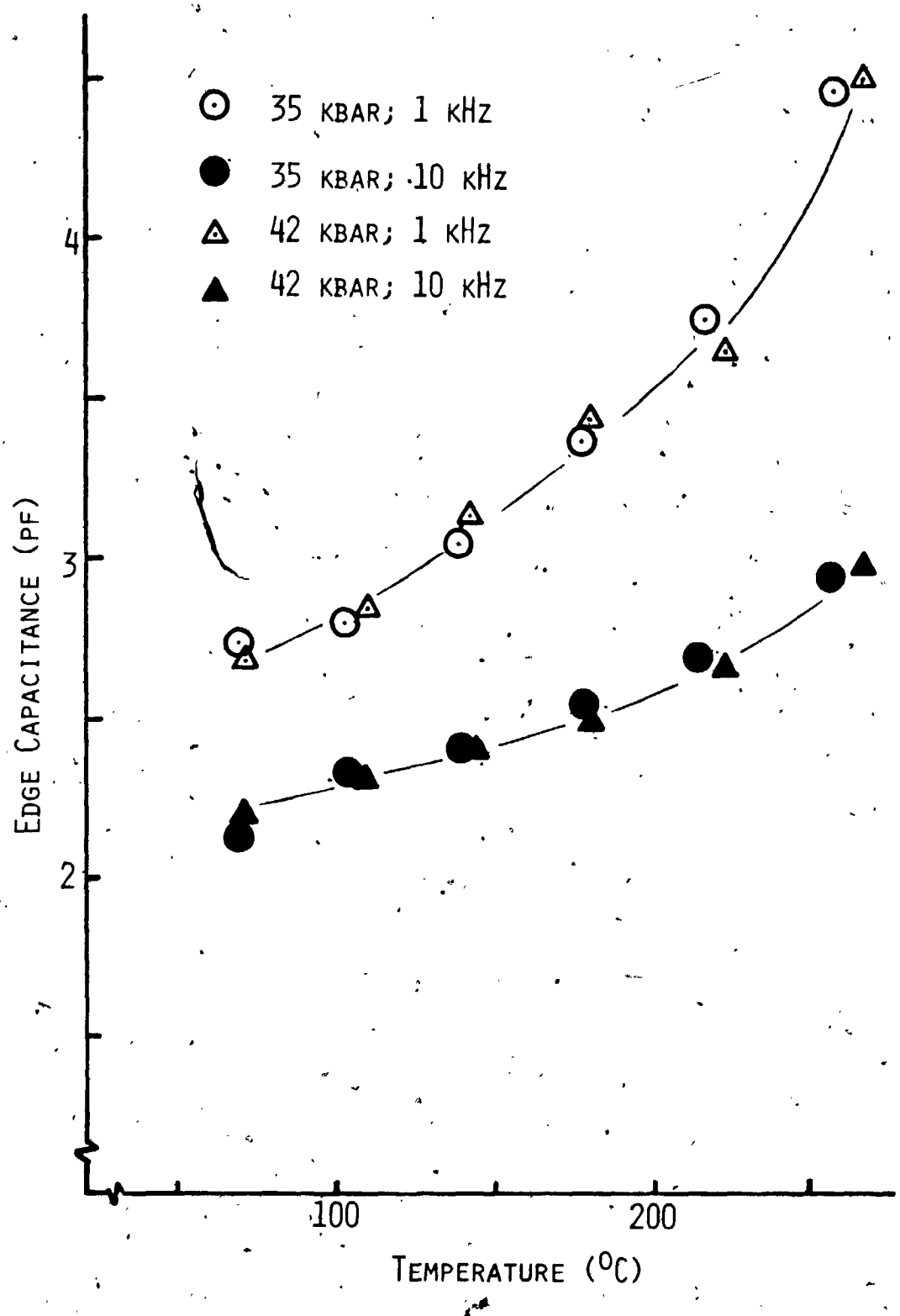

Figure C.1 : Graph of the edge capacitance versus temperature for measuring frequencies of 1 and 10 kHz.

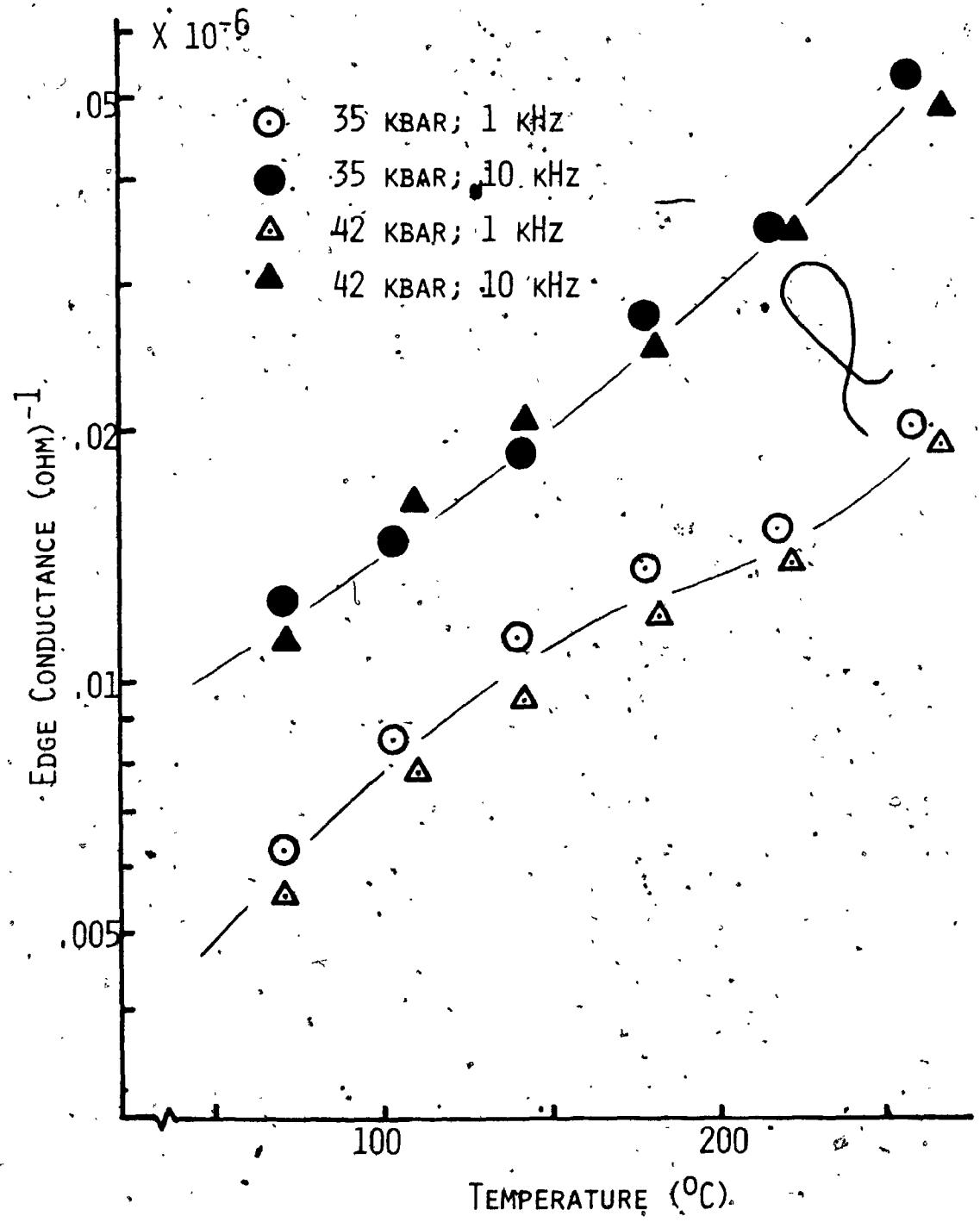

Figure C.2 : Graph of the edge conductance versus temperature for measuring frequencies of 1 and 10 kHz.

$$D = D_X \frac{1 - (G_e/G_X)}{1 - (C_e/C_X)}$$

$$= (.020) \frac{1 - (10.5/22)}{1 - (3/179)}$$

$$= .011$$

These values are shown in Figure 4.6.

APPENDIX D

Dielectric Properties of Pyrophyllite as a Function of Water Vapour Pressure and Frequency

To gain some quantitative information of the factors affecting the dielectric properties of pyrophyllite, an experiment was designed to measure its dielectric properties as a function of both frequency (0.05-10 kHz) and water vapour pressure (0 - 70%) at constant temperature. The results of this experiment are presented here.

Silver paint electrodes were applied in a three-terminal arrangement (ASTM, 1970) to a pyrophyllite disc of diameter 2.50 cm, thickness .103 cm, and effective electroded measuring surface 2.72 cm^2, which was cut from a bar of pyrophyllite obtained from the American Lava Corp. (grade A unfired lava). The sample was mounted in a vacuum chamber of the B.E.T. type as shown in Figure D.1. Care was taken to ensure that both the chamber and the active lead were completely shielded. Since a three-terminal arrangement was employed, the effects of the lead capacitance are eliminated, and therefore the measured capacitance is simply that of the sample under study. The sample chamber was evacuated to better than 10^{-7} Torr, sealed off and thereafter the water vapour pressure was increased in small increments. The pressure was measured by means of a differential manometer and cathetometer, and the whole system was maintained at a constant temperature of 22.4°C by means of a water jacket connected to a Haake Type 113.20 temperature control.

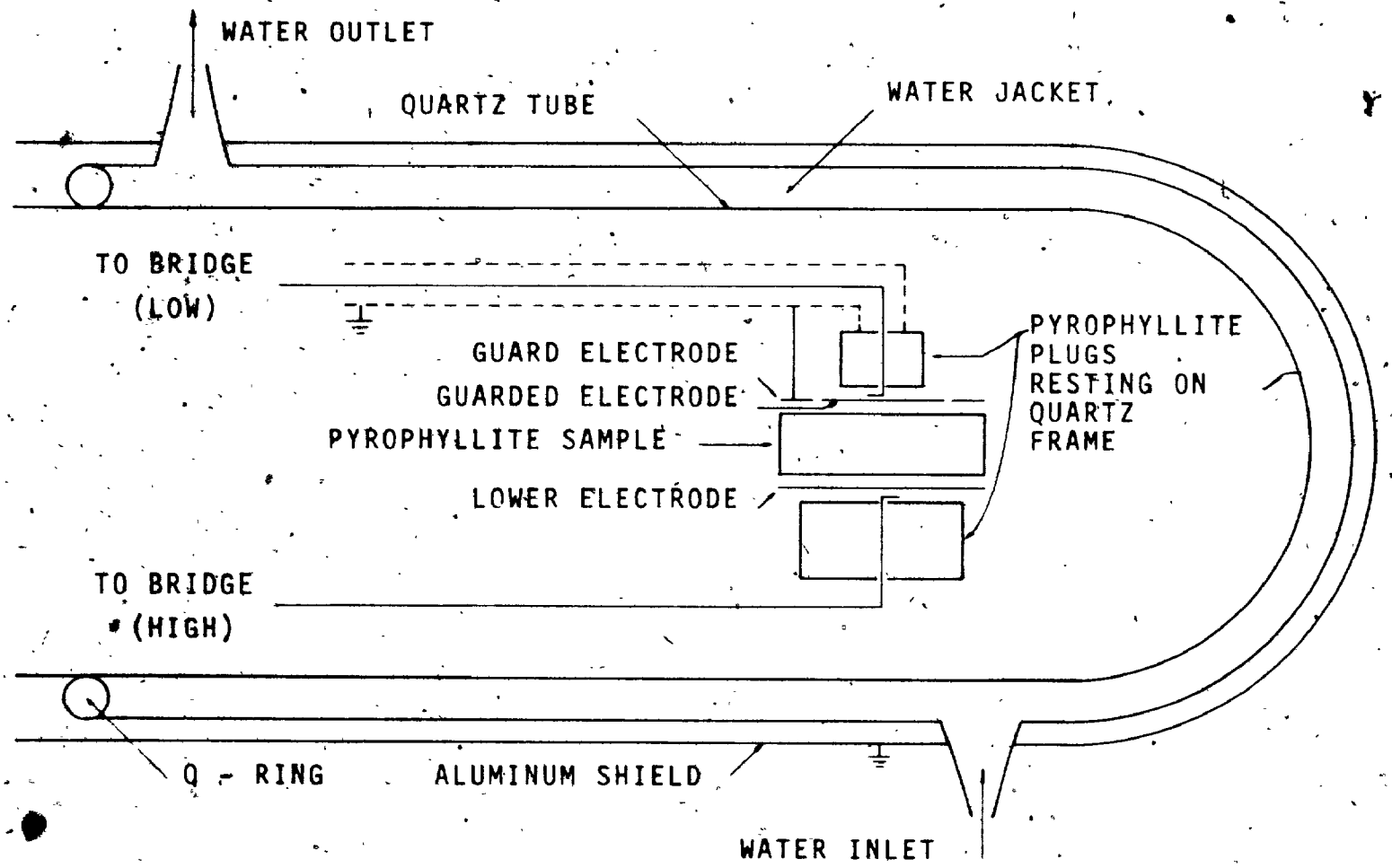

Figure D.1 : Experimental arrangement for three-terminal measurement of the capacitance and dissipation factor of pyrophyllite in vacuum.

Capacitance measurements were taken at least 6 hours after each change in vapour pressure. This time was found to be sufficient for system equilibrium.

Figure D.2 shows the change in capacity with relative water vapour pressure (p/p_o) for various measuring frequencies. In vacuum, ($p/p_o = 0$), the capacitance shows relatively little frequency dependence, changing by only .51 pf between .050 and 10 kHz. With increasing vapour pressure, however, capacitance values rise steeply, especially at low frequencies. For .050 kHz, the total change in capacitance from $p/p_o = 0$ to $p/p_o = 60\%$ amounted to ~350%. At higher frequencies, 10 kHz, the change is only ~43% for this vapour pressure range.

Figure D.3 shows the change in dissipation factor with increasing relative water vapour pressure for various frequencies. In general, for constant vapour pressure, D decreases with increasing frequency, and for constant frequency, increases with increasing water content.

Figure D.4 shows the change in conductance (G) and conductivity (σ) with increasing water vapour pressure for measuring frequencies of .1, 1 and 10 kHz. In the region between $p/p_o = 20\%$ and $p/p_o = 60\%$, log σ increases linearly with increasing p/p_o at a rate of .036 $(\%H_2O)^{-1}$ for .1 kHz, .031 $(\%H_2O)^{-1}$ for 1 kHz and .028 $(\%H_2O)^{-1}$ for 10 kHz.

Figure D.5 shows the effect of frequency on the capacitance and dielectric constant of pyrophyllite for various constant vapour pressure settings. With increasing frequency, the dielectric constant decreases and becomes relatively independent of frequency above ~10 kHz.

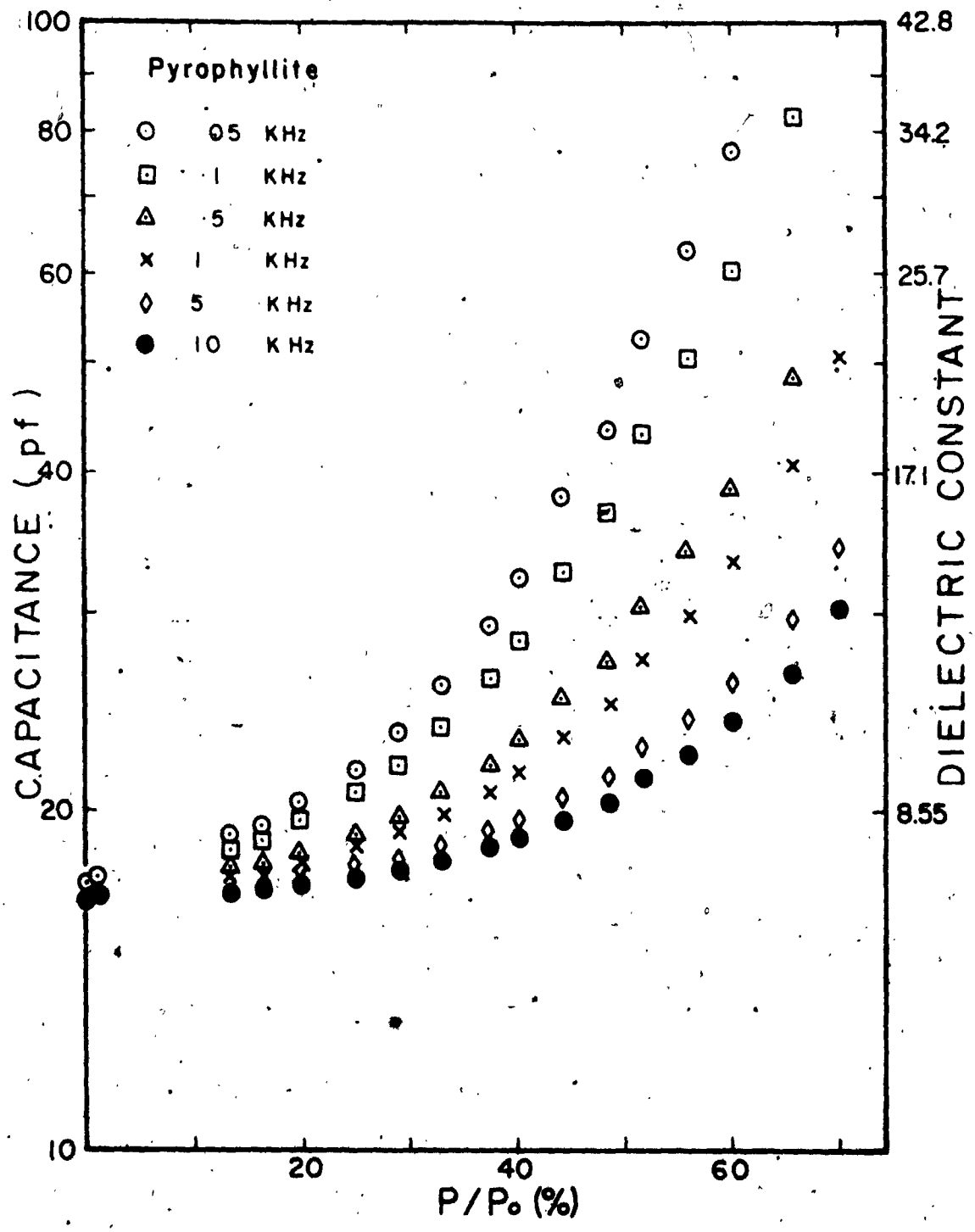

Figure D.2 : Graph of the capacitance and dielectric constant of pyrophyllite as a function of water vapour pressure for various frequencies at T=22.4°C.

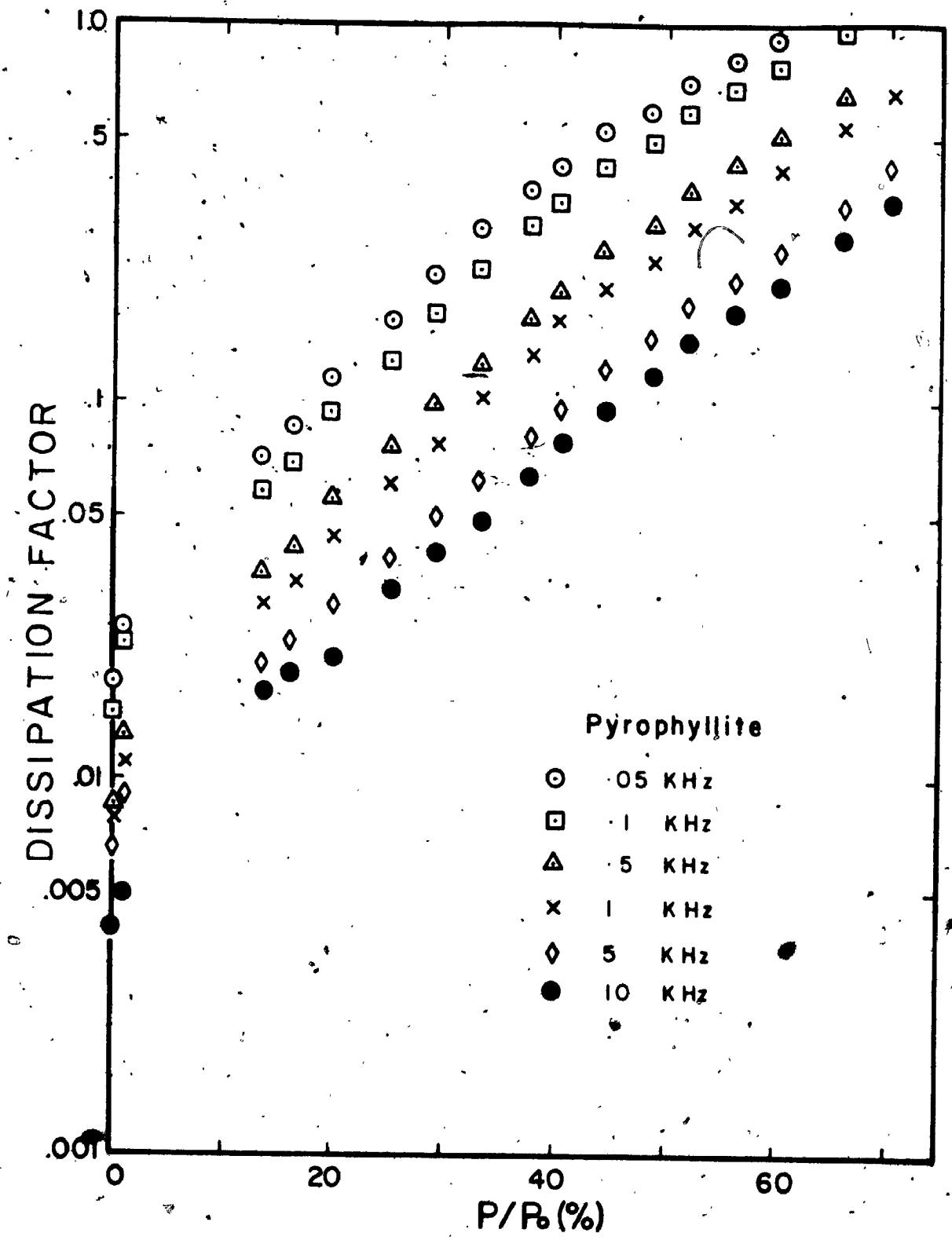

Figure D.3 : Graph of the dissipation factor of pyrophyllite as a function of water vapour pressure for various frequencies at T=22.4°C.

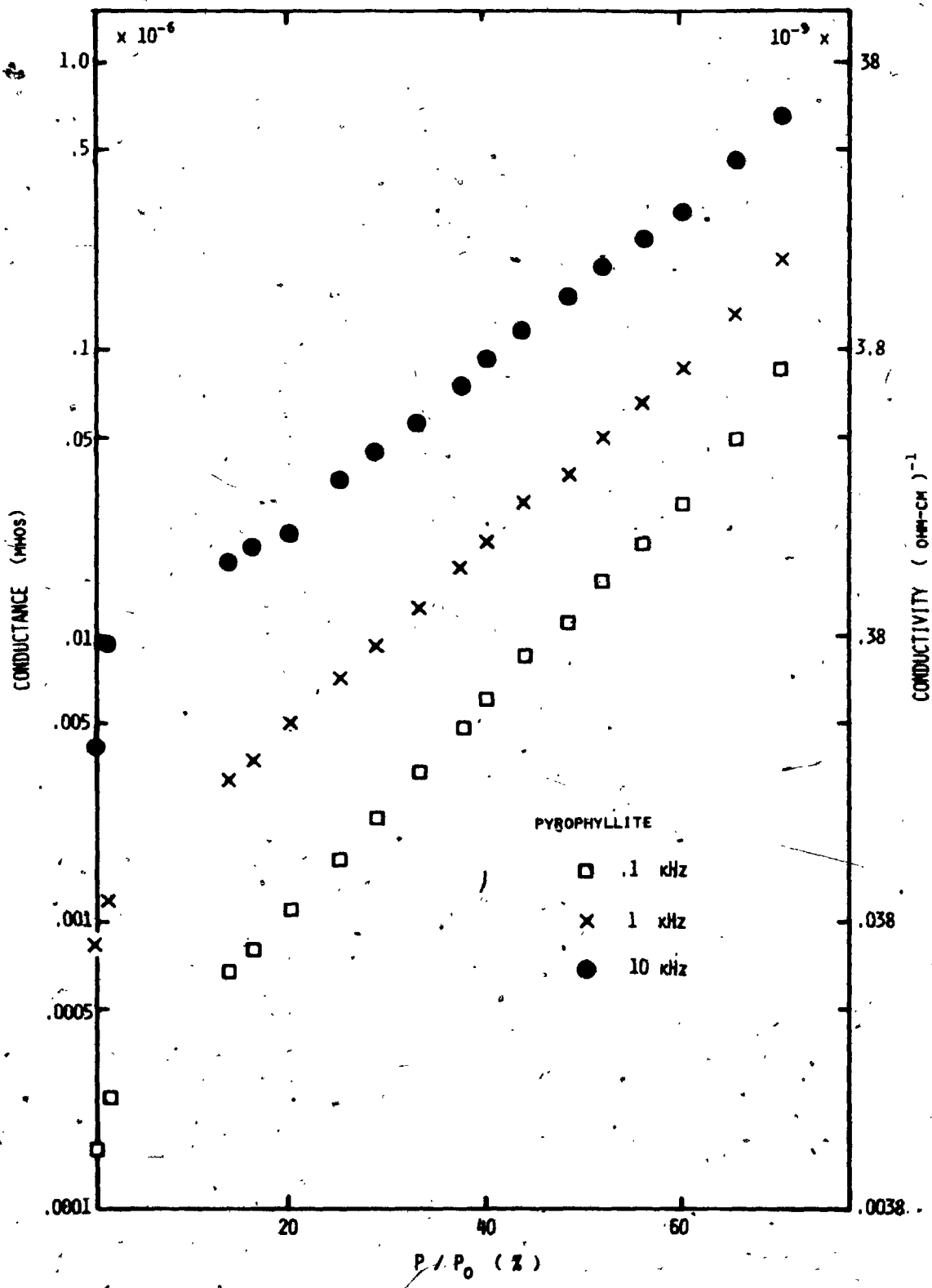

Figure D:4 : Graph of the conductance and conductivity of pyrophyllite as a function of water vapour pressure for various frequencies at T=22.4°C.

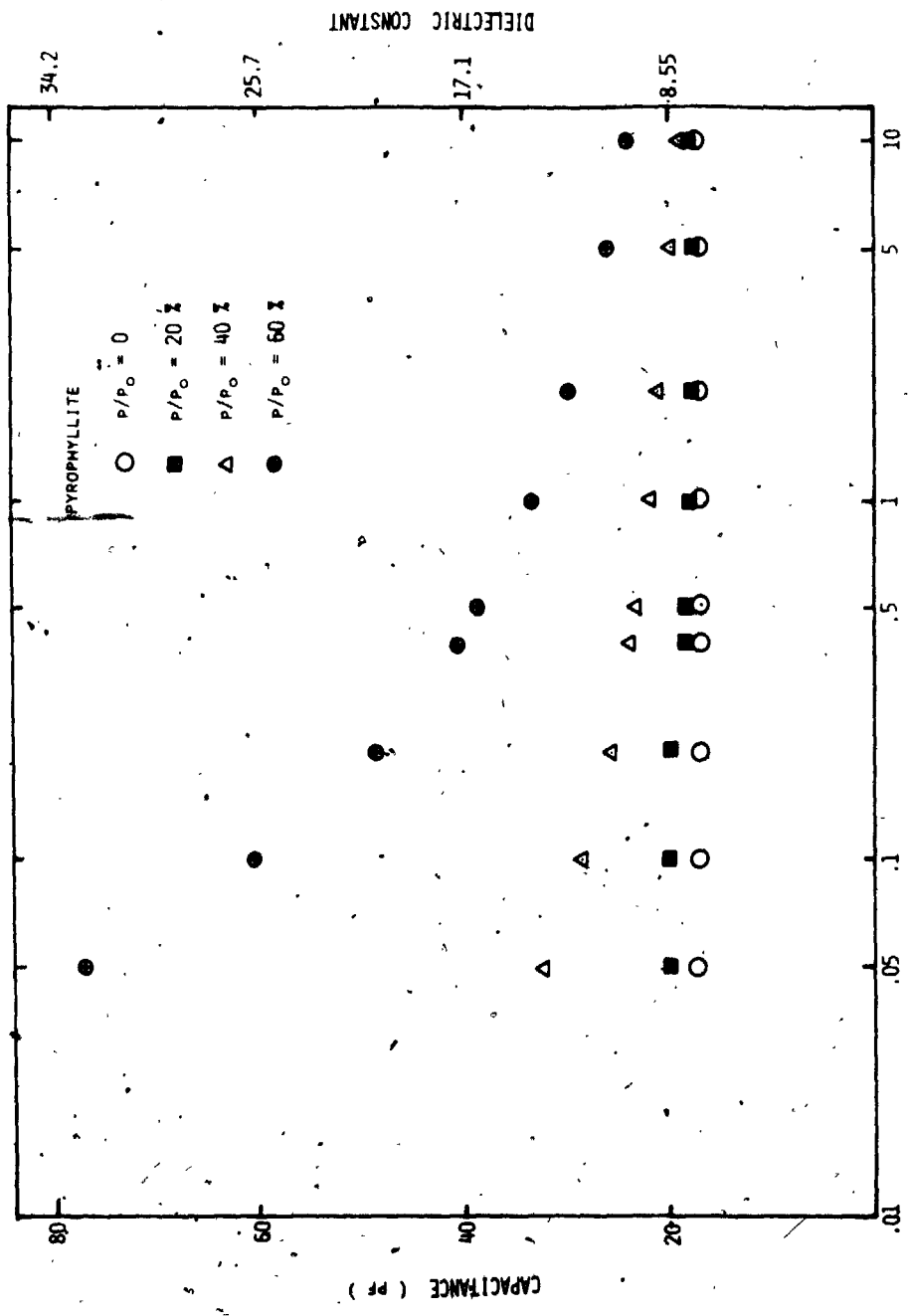

Figure D.5 : Graph of the capacitance and dielectric constant of pyrophyllite versus frequency for various water vapour pressures at T=22.4°C.

Figure D.6 shows the effect of frequency on the dissipation factor for pyrophyllite for p/p_o = 0, 20, 40 and 60%. In general, D decreases with increasing frequency, behaviour which is typical for insulating materials (von Hippel, 1954). An interesting feature of this graph, however, is the apparent "hump" exhibited in the data in frequency range 1 - 10 kHz for the lower (p/p_o = 0) curve. A similar effect has been observed on measurements made on lunar samples (Chung et al, 1970) and earth basalts (Hansen et al, 1973). This effect has been explained in terms of an incomplete drying of the sample in vacuum (i.e. residual water chemically bonded to the surface), and may represent some sort of relaxation mechanism (D.H. Chung, private communication, AGU meeting, Washington, D.C., 1976).

Figure D.7 shows the effect of frequency on the conductance and conductivity of the sample for various constant water vapour pressure settings. In general, the conductivity increases with increasing frequency, an effect commonly observed in insulating earth minerals (Collett and Katsube, 1973).

The results of this experiment clearly show that the dielectric properties of pyrophyllite are strongly dependent upon both the amount of water present and the frequency of measurement. This result, when viewed in terms of electrical conductivity or dielectric studies in pyrophyllite-media high pressure devices, suggests that both the amount of electrical leakage (loss) currents and stray capacitances parallel to the sample through the pyrophyllite gaskets will be greatly influenced by the amount of water absorbed by the gaskets from the air. The present

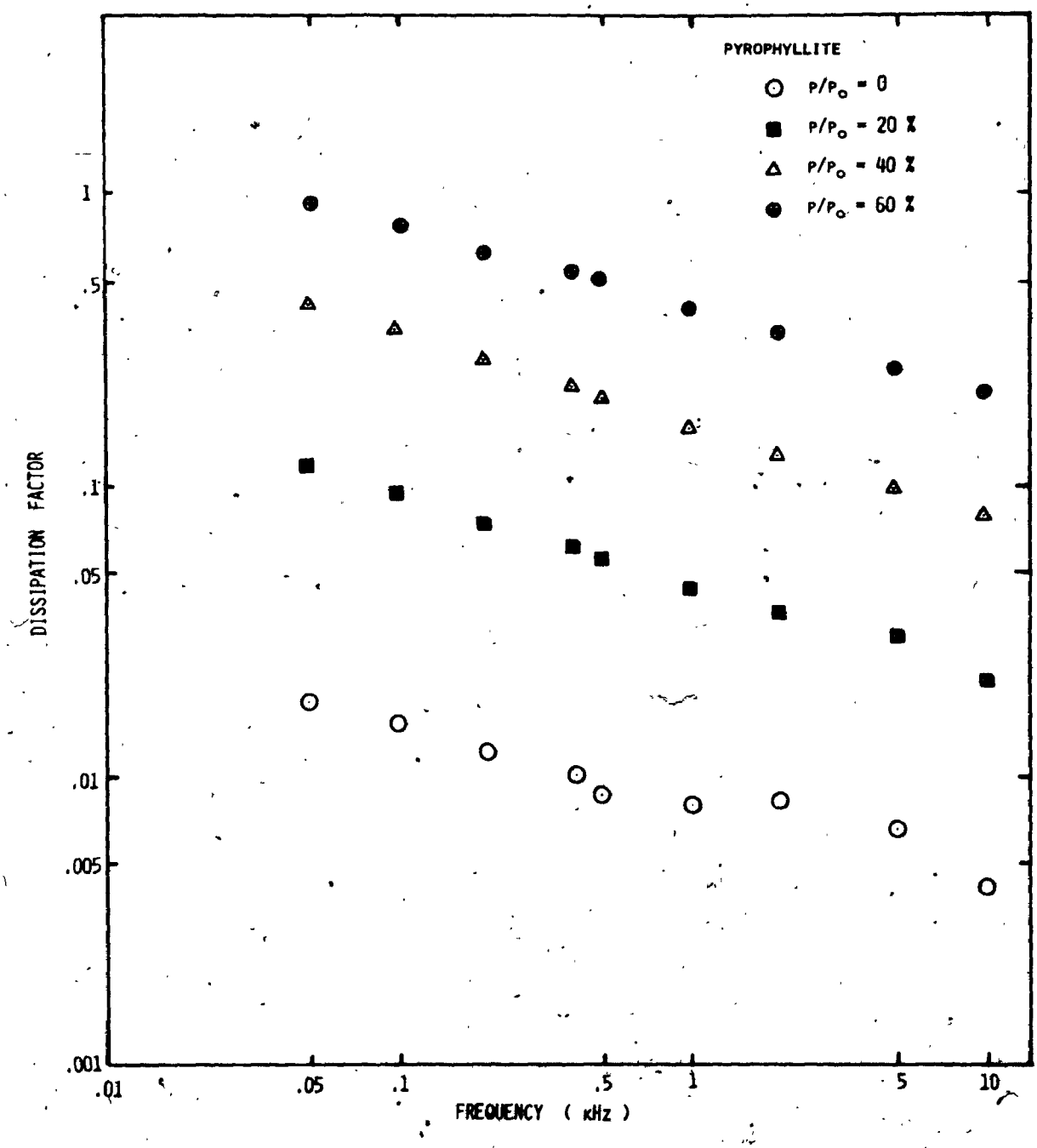

Figure D.6 : Graph of the dissipation factor of pyrophyllite versus frequency for various water vapour pressures at T=22.4^{o}C.

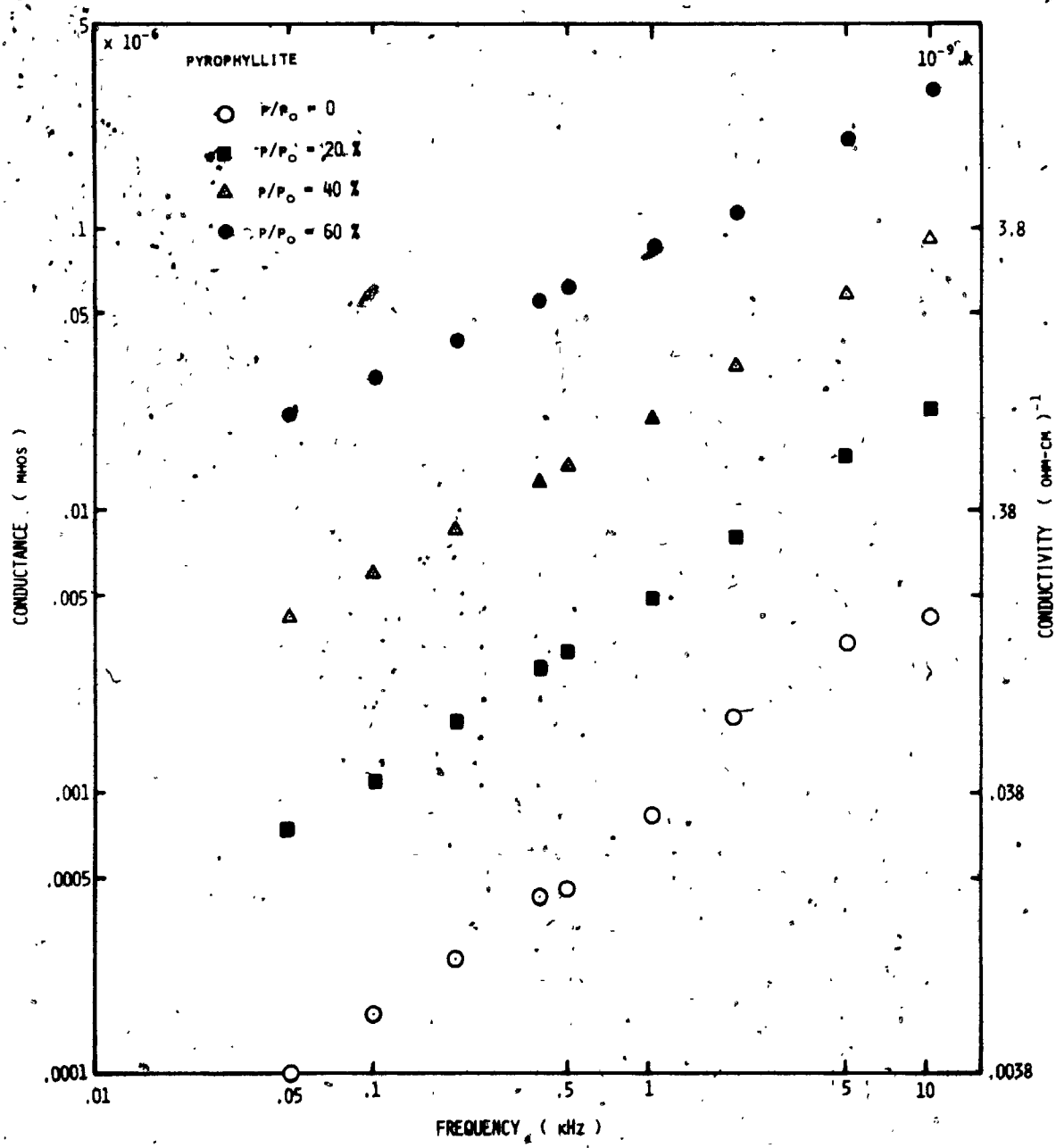

Figure D.7 : Graph of the conductance and conductivity of pyrophyllite versus frequency for various water vapour pressures at T=22.4°C.

experiment indicates that this effect can be substantially reduced by measuring at high frequencies and maintenance of low room humidity.

REFERENCES

ASTM (American Society for Testing Materials), 1970. Standard Methods of Test for AC Loss Characteristics and Dielectric Constant (Permittivity) of Solid Electrical Insulating Materials, ASTM D 150-70, 28-50.

Barnett, J.D., Pack, J. and Hall, H.T., 1969. Structure Determination of a Ferroelectric Phase of Sodium Nitrate above 45 kbar, Am. Cryst. Assoc. Trans. 5, 113-131.

Bassett, W.A., 1976. Mineralogy of the Earth's Lower Mantle, Trans. Am. Geophys. Un. EOS 57, 327 (abstr.).

Berlincourt, D., 1971. Piezoelectric Crystals and Ceramics, in Ultrasonic Transducer Materials, 63-124, ed. O.E. Mattiat. Plenum Press, New York.

Berlincourt, D. and Krueger, H.H.A., 1959. Domain Processes in Lead Titanate Zirconate and Barium Titanate Ceramics, J. Appl. Phys. 30, 1804-1810.

Brown, R.F., 1961. Effect of Two-Dimensional Mechanical Stress on the Dielectric Properties of Poled Ceramic Barium Titanate and Lead Zirconate Titanate, Can. J. Phys. 39, 741-763.

Brown, R.F. and McMahon, G.W., 1962. Material Constants of Ferroelectric Ceramics at High Pressure, Can. J. Phys. 40, 672-674.

Buessem, W.R., Cross, L.E. and Goswami, A.K., 1966. Phenomenological Theory of High Permittivity in Fine-Grained Barium Titanate, J. Am. Cer. Soc. 49, 33-36.

Bundy, F.P., 1961. Effect of Pressure on emf of Thermocouples, J. Appl. Phys. 32, 483-488.

Burfoot, J.C., 1967. Ferroelectrics: An Introduction to the Physical Principles, D. Van Nostrand Co. Ltd., Toronto.

Burfoot, J.C. and Martirena, H.T., 1972. PZT-5 Under Pressure: Dielectric and Piezoelectric Properties, J. De Physique 33, C2-249-C2-250.

Burke, B.F., 1961. Radio Observations of Jupiter. I., in Planets and Satellites, 473-499, ed. G.P. Kuiper, B.M. Middlehurst. University of Chicago Press, Chicago.

Burns, G., 1976. Dirty Displacive Ferroelectrics, Phys. Rev. B 13, 215-226.

Cady, W.G., 1964. Piezoelectricity, Vol. 1 and 2, Dover Publications, Inc., New York.

Chung, D.H., Westphal, W.B. and Simmons, G., 1970. Dielectric Properties of Apollo 11 Lunar Samples and their Comparison with Earth Materials, J. Geophys. Res. 75, 6524-6531.

Clarke, R., 1976. High Pressure Study of $BaTiO_3$ Single Crystals, (unpublished).

Clarke, R. and Burfoot, J.C., 1974. The Diffuse Phase Transition in Potassium Strontium Niobate, Ferroelectrics 8, 505-506.

Cochran, W., 1960. Crystal Stability and the Theory of Ferroelectricity, Adv. in Phys. 9, 387-423.

Cochran, W., 1961. Crystal Stability and the Theory of Ferroelectricity Part II: Piezoelectric Crystals, Adv. in Phys. 10, 401-420.

Cole, R.H. and Gross, P.M., 1949. A Wide Range Capacitance - Conductance Bridge, Rev. Sci. Instr. 20, 252-260.

Collett, L.S. and Katsube, T.J., 1973. Electrical Parameters of Rocks in Developing Geophysical Techniques, Geophys. 38, 76-91.

Costantino, M.S. and Daniels, W.B., 1975. Dielectric Constant of Compressed Solid Methane at Low Temperature, J. Chem. Phys. 62, 764-770.

Cutchen, J.T., 1966. Polarity Effects and Charge Liberation in Lead Zirconate Titanate Ceramics under High Dynamic Stress, J. Appl. Phys. 37, 4745-4750.

Devonshire, A.F., 1954. Theory of Ferroelectrics, Adv. in Phys. 3, 85-130.

Diamond, H., 1961. Variation of Permittivity with Electric Field in Perovskite-Like Ferroelectrics, J. Appl. Phys. 32, 909-915.

Dvorak, Z. and Schloessin, H.H., 1973. On the Anisotropic Electrical Conductivity of Enstatite as a Function of Pressure and Temperature, Geophys. 38, 25-36.

Eshelby, J.D., 1956. The Continuum Theory of Lattice Defects, in Solid State Physics, Vol. 3, 79-144, ed. F. Seitz, D. Turnbull. Academic Press, New York.

Eshelby, J.D., 1957. The Determination of the Elastic Field of an Ellipsoidal Inclusion, and Related Problems, Proc. Roy. Soc. London A 241, 376-396.

Eshelby, J.D., 1961. Elastic Inclusions and Inhomogeneities, in Progress in Solid Mechanics, Vol. 2, 87-140, ed. I.N. Sneddon, R. Hill. North Holland, Amsterdam.

Forsbergh, P.W., 1954. Effect of a Two-Dimensional Pressure on the Curie Point of Barium Titanate, Phys. Rev. 93, 686-692.

Gallet, R.M., 1961. Radio Observations of Jupiter. II., in Planets and Satellites, 500-533, ed. G.P. Kuiper, B.M. Middlehurst, University of Chicago Press, Chicago.

Gerson, R., 1960. Variation in Ferroelectricity Characteristics of Lead Zirconate Titanate Ceramics due to Minor Chemical Modifications, J. Appl. Phys. 31, 188-194.

Gonnard, P., Fetiveau, Y., Bauer, F. and Eyraud, L., 1972. Changement de Phase Induit par une Pression Hydrostatique dans un Materiau Ferroelectrique, C.R. Acad. Sc. Paris 275 B, 633-636.

Hall, H.T., 1964. High Pressure - Temperature Apparatus, in Metallurgical Society Conferences, Vol. 22, 133-179. Gordon and Breach Science Publishers Ltd., London.

Hansen, W., Sill, W.R. and Ward, S.H., 1973. The Dielectric Properties of Selected Basalts, Geophys. 38, 135-139.

Jaffe, B., Cook, W.R. and Jaffe, H., 1971. Piezoelectric Ceramics, Academic Press, New York.

Jaffe, B., Roth, R.S. and Marzullo, S., 1954. Piezoelectric Properties of Lead Zirconate-Lead Titanate Solid-Solution Ceramics, J. Appl. Phys. 25, 809-810.

Jona, F. and Shirane, G., 1962. Ferroelectric Crystals, Macmillan Company, New York.

Kanzig, W., 1957. Ferroelectrics and Antiferroelectrics, Academic Press, New York.

Kay, H.F. and Bailey, P.C., 1957. Structure and Properties of $CaTiO_3$, Acta Cryst. 10, 219-226.

Kay, H.F. and Vousden, P., 1949. Symmetry Changes in Barium Titanate at Low Temperatures and their Relation to its Ferroelectric Properties, Phil. Mag. 40, 1019-1040.

Keizer, K. and Burggraaf, A.J., 1974. Grain Size Effects on the Ferroelectric-Paraelectric Transition, the Dielectric Constant, and the Lattice Parameters in Lanthana-Substituted Lead Titanate, Phys. Stat. Sol. (a) 26, 561-569.

3 3

OF/DE

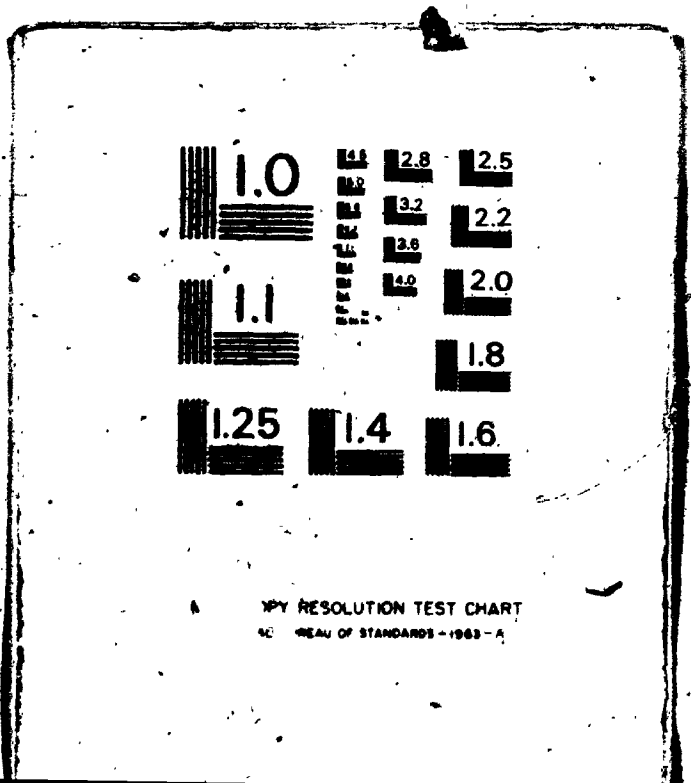
1.0
1.1
1.25
1.4
1.6
1.8
2.0
2.2
2.5
2.8
3.2
3.6
4.0
MPY RESOLUTION TEST CHART
NATIONAL BUREAU OF STANDARDS - 1963 - A

Kennedy, G.C. and La Mori, P.N., 1962. The Pressures of some Solid-Solid Transitions, J. Geophys. Res. 67, 851-856.

Klimowski, J., 1962. Effect of High Hydrostatic Pressure on the Dielectric Properties of $BaTiO_3$ Single Crystals, Phys. Stat. Solidi 2, 456-459.

Knyazev, A.S., Poplavko, Y.M., Zakharov, V.P. and Alekseev, V.V., 1974. Soft mode in the Vibrational Spectrum of $CaTiO_3$, Sov. Phys.-Sol. St. 15, 2003-2005.

Krueger, H.H.A., 1967. Stress Sensitivity of Piezoelectric Ceramics: Part 1. Sensitivity to Compressive Stress Parallel to the Polar Axis, J. Acoust. Soc. Am. 42, 636-645.

Lees, J., 1966. The Design and Performance of U.H.P. Equipment. An Interim Report of the Tetrahedral Anvil Apparatus, in Advances in High Pressure Research, Vol. 1, 1-83, ed. R.S. Bradley. Academic Press, New York.

Lees, J. and McCartney, J.H., 1968. Single Crystal Measurements and Stress Difference in Solid Pressure-Transmitting Media, J. Sci. Instr. (J. Phys. E.) Ser. 2, 1, 911-914.

Leonidova, G.G. and Polandov, I.N., 1962. Transition of Barium Titanate to the Paraelectric State at High Pressures, Sov. Phys. - Sol. St. 4, 1916-1917.

Leonidova, G.G. and Volk, T.R., 1966. Phase Transition in Barium Titanate at High Hydrostatic Pressure, Sov. Phys. - Sol. St. 7, 2694-2696.

Linz, A. and Herrington, K., 1958. Electrical and Optical Properties of Synthetic Calcium Titanate Crystal, J. Chem. Phys. 28, 824-825.

Liu, L., 1974. Silicate Perovskite from Phase Transformations of Pyrope-Garnet at High Pressure and Temperature, Geophys. Res. Lett. 1, 277-280.

Liu, L., 1975a. Post-Oxide Phases of Forsterite and Enstatite, Geophys. Res. Lett. 2, 417-419.

Liu, L., 1975b. High Pressure Phase Transformations and Compressions of Ilmenite and Rutile, I. Experimental Results, Phys. Earth Pl. Int. 10, 167-176.

Liu, L., 1976. Orthorhombic Perovskite Phases Observed in Olivine, Pyroxene and Garnet at High Pressures and Temperatures, Phys. Earth Pl. Int. 11, 289-298.

Lysne, P.C., 1975. Prediction of Dielectric Breakdown in Shock-Loaded Ferroelectric Ceramics, J. Appl. Phys. 46, 230-232.

Lysne, P.C. and Bartel, L.C., 1975. Electromechanical Response of PZT 65/35 Subjected to Axial Shock Loading, J. Appl. Phys. 46, 222-229.

Lysne, P.C. and Percival, C.M., 1975. Electric Energy Generation by Shock Compression of Ferroelectric Ceramics: Normal Mode Response of PZT 95/5, J. Appl. Phys. 46, 1519-1525.

Martin, G. and Hegenbarth, E., 1973. The Influence of Hydrostatic Pressure on the Ferroelectric Phase Transition of $CdTiO_3$ Ceramics, Phys. Stat. Sol. (a) 18, k151-k152.

Martirena, H.T. and Burfoot, J.C., 1974a. Grain Size and Pressure Effects on the Dielectric and Piezoelectric Properties of Hot-Pressed PZT-5, Ferroelectrics 7, 151-152.

Martirena, H.T. and Burfoot, J.C., 1974b. Grain Size Effects on Properties of some Ferroelectric Ceramics, J. Phys. C: Sol. St. Phys. 7, 3182-3192.

Megaw, H.D., 1957. Ferroelectricity in Crystals, Methuen, London.

Megaw, H.D., 1973. Crystal Structures: A Working Approach, W.B. Saunders Co., Toronto.

Merz, W.J., 1949. The Electrical and Optical Behavior of $BaTiO_3$ Single-Domain Crystals, Phys. Rev. 76, 1221-1225.

Merz, W.J., 1950. The Effect of Hydrostatic Pressure on the Curie Point of Barium Titanate Single Crystals, Phys. Rev. 77, 52-54.

Ming, L.C. and Bassett, W.A., 1974. Post-Spinel Phases in Mg_2SiO_4-Fe_2SiO_4 System up to 80% Mg_2SiO_4, Trans. Am. Geophys. Un. EOS 55, 416-417 (abstr.).

Minomura, S., Kawakubo, T., Nakagawa, T. and Sawada, S., 1964. Pressure Dependence of Curie Point and Tetragonal - Orthorhombic Transition Point of $BaTiO_3$, Japan. J. Appl. Phys. 3, 562-563.

Minomura, S., Tanaka, M., Okai, B. and Nagasaki, H., 1970. Pressure Dependence of Transition Temperatures and Electrostrictions in Perovskite $BaTiO_3$, J. Phys. Soc. Jpn. 28 Suppl., 404-406.

Mott, N.F. and Gurney, R.W., 1964. Electronic Processes in Ionic Crystals, Dover Publications, Inc., New York.

Mungall, A.G. and Morris, D., 1963. Precision Capacitance - Conductance Bridge for Dielectric Measurements at Audio and Low Radio Frequencies, Rev. Sci. Instr. 34, 839-843.

Nishi, R.Y. and Brown, R.F., 1964. Behavior of Piezoceramic Projector Materials under Hydrostatic Pressure, J. Acoust. Soc. Am. 36, 1292-1296.

Okazaki, K. and Nagata, K., 1973. Effects of Grain Size and Porosity on Electrical and Optical Properties of PLZT Ceramics, J. Am. Cer. Soc. 56, 82-86.

Parkhomenko, E.I., 1967. Electrical Properties of Rocks, Plenum Press, New York.

Polandov, I.N. and Mylov, V.P., 1968. Investigation of $Ba(Ti,Sn)O_3$ Ferroelectric Ceramics at High Pressures, Sov. Phys. - Sol. St. 9, 1816-1819.

Polandov, I.N., Strukov, B.A. and Mylov, V.P., 1967. Change in the Nature of the Phase Transition in Barium Titanate Single Crystals Under Hydrostatic Pressure, Sov. Phys. - Sol. St. 9, 1153-1156.

Reid, A.F. and Ringwood, A.E., 1975. High Pressure Modifications of $ScAlO_3$ and Some Geophysical Implications, J. Geophys. Res. 80, 3363-3370.

Ringwood, A.E., 1962. Mineralogical Constitution of the Deep Mantle, J. Geophy. Res. 67, 4005-4010.

Ringwood, A.E., 1975. Composition and Petrology of the Earth's Mantle, McGraw-Hill Book Co., Toronto.

Ringwood, A.E. and Major, A., 1967. Some High Pressure Transformations of Geophysical Significance, Earth Pl. Sci. Lett. 2, 106-110.

Ringwood, A.E. and Major, A., 1971. Synthesis of Majorite and Other High Pressure Garnets and Perovskites, Earth Plant. Sci. Lett. 12, 411-418.

Rupprecht, G. and Bell, R.O., 1964. Dielectric Constant in Paraelectric Perovskites, Phys. Rev. 135, A748-A752.

Samara, G.A., 1966. Pressure and Temperature Dependences of the Dielectric Properties of the Perovskites $BaTiO_3$ and $SrTiO_3$, Phys. Rev. 151, 378-386.

Samara, G.A., 1969. The Effects of Hydrostatic Pressure on Ferroelectric Properties, in Advances in High Pressure Research, Vol. 3, 155-239, ed. R.S. Bradley. Academic Press, New York.

Samara, G.A., 1970. The Effects of Hydrostatic Pressure on Ferroelectric Properties, J. Phys. Soc. Jpn. 28 suppl., 399-403.

Samara, G.A., 1971. Pressure and Temperature Dependence of the Dielectric Properties and Phase Transitions of the Ferroelectric Perovskites: $PbTiO_3$ and $BaTiO_3$, Ferroelectrics 2, 277-289.

Samara, G.A. and Giardini, A.A., 1965. Pressure Dependence of the Dielectric Constant of Strontium Titanate, Phys. Rev. 140, A954-A957.

Samara, G.A., Sakudo, T. and Yoshimitsu, K., 1975. Important Generalization Concerning the Role of Competing Forces in Displacive Phase Transitions, Phys. Rev. Lett. 35, 1767-1769.

Sawaguchi, E., 1953. Ferroelectricity Versus Antiferroelectricity in the Solid Solutions of $PbZrO_3$ and $PbTiO_3$, J. Phys. Soc. Jpn. 8, 615-629.

Sawyer, C.B. and Tower, C.H., 1930. Rochelle Salt as a Dielectric, Phys. Rev. 35, 269-273.

Schloessin, H.H. and Timco, G.W., 1975. On the Problem of a Ferroelectric Inclusion in a Matrix Subjected to Pressure, Abstracts - Third European Meeting on Ferroelectricity, 263 (abstr.).

Schloessin, H.H. and Timco, G.W., 1976. On the Problem of the Ferroelectric Inclusion in a Matrix Subjected to Pressure, Ferroelectrics 14, 729-730.

Schloessin, H.H. and Timco, G.W., 1977. The Significance of Ferroelectric Phase Transitions for the Earth and Planetary Interiors, Phys. Earth Pl. Int. (in press).

Smolensky, G.A., 1970. Physical Phenomena in Ferroelectrics with Diffused Phase Transition, J. Phys. Soc. Jpn. 28 suppl., 26-37.

Stacey, F.D., 1969. Physics of the Earth, John Wiley and Sons, Inc., Toronto.

Timco, G.W., 1974. High Pressure Hysteresis Loop Studies of Virtually Clamped Crystals of Ferroelectric Triglycine Sulphate and Rochelle Salt, M.Sc. Thesis, University of Western Ontario, London, Ontario, Canada.

Timco, G.W., 1975. Ferroelectric Phase Transitions in Clamped Systems, Abstr. with Programs 7, 872 (abstr.).

Timco, G.W., Dvorak, Z. and Schloessin, H.H., 1976a. The Effects of H_2O Vapor Pressure and Frequency on the Dielectric Properties of Pyrophyllite, Trans. Am. Geophys. Un. EOS 57, 323 (abstr.).

Timco, G.W., Dvorak, Z. and Schloessin, H.H., 1976b. 'Dielectric Properties of Pyrophyllite as a Function of Water Vapor Pressure, J. Appl. Phys. 47, 2232-2233.

Timco, G.W. and Schloessin, H.H., 1974. Ferroelectric Studies in Solid-Media High Pressure Devices, High Temp. - High Pressures 6, 541-544.

Timco, G.W. and Schloessin, H.H., 1975a. Dielectric Properties of Inhomogeneous Inclusions in a Matrix Subjected to High Pressure, Europhys. Conf. Abstr. 1A, 101 (abstr.).

Timco, G.W. and Schloessin, H.H., 1975b. Pressure and Temperature Studies of the Dielectric Properties of Ceramic PZT-4, Phys. in Can. 31, 20 (abstr.).

Timco, G.W. and Schloessin, H.H., 1976a. The Effects of High Pressure and Temperature on the Dielectric Constant of Ferroelectric Perovskite Ceramic PZT-4, Ferroelectrics 11, 409-412.

Timco, G.W. and Schloessin, H.H., 1976b. High Pressure Dielectric Properties of $Pb(Zr,Ti)O_3$ Ceramics, Phys. in Can. 32, 21 (abstr.); Bull. Am. Phys. Soc. II 21, 782 (abstr.).

Timco, G.W. and Schloessin, G.W., 1976c. Dielectric Properties of Ferroelectric Perovskite $Pb(Zr,Ti)O_3$ Ceramics in a Solid Matrix Sujected to Pressure, High Temp. - High Pressures 8, 73-82.

Tsuzuki, K. and Sakata, K., 1974. Dielectric Properties of Single Crystals of $Pb(Zr_xTi_{1-x})O_3$ Solid Solutions ($x \sim 0.5$), Ferroelectrics 8, 501-503.

Tsykalov, V.G. and Poplavko, Y.M., 1969. Studies of Ferroelectrics in the 50-80 GHz Frequency Range, Bull. Acad. Sci. U.S.S.R., Phys. Ser. 33, 1038-1040.

von Hippel, A.R., 1954. Dielectrics and Waves, John Wiley and Sons; New York.

von Hippel, A., 1970. Do We Really Understand Ferroelectricity?, J. Phys. Soc. Jpn. 28 suppl., 1-6.

Wilhelm, R.V. and McLaren, M.G., 1973. Combined Effects of Hydrostatic Pressure and High Electric Field on Modified Lead Zirconate Titanate Piezoelectric Ceramics, General Motors Corp. Research Publication GMR-1409.